INFORMATION TO USERS

This manuscript has been reproduced from the microfilm master. UMI films the text directly from the original or copy submitted. Thus, some thesis and dissertation copies are in typewriter face, while others may be from any type of computer printer.

The quality of this reproduction is dependent upon the quality of the copy submitted. Broken or indistinct print, colored or poor quality illustrations and photographs, print bleedthrough, substandard margins, and improper alignment can adversely affect reproduction.

In the unlikely event that the author did not send UMI a complete manuscript and there are missing pages, these will be noted. Also, if unauthorized copyright material had to be removed, a note will indicate the deletion.

Oversize materials (e.g., maps, drawings, charts) are reproduced by sectioning the original, beginning at the upper left-hand corner and continuing from left to right in equal sections with small overlaps.

Photographs included in the original manuscript have been reproduced xerographically in this copy. Higher quality 6" x 9" black and white photographic prints are available for any photographs or illustrations appearing in this copy for an additional charge. Contact UMI directly to order.

Bell & Howell Information and Learning
300 North Zeeb Road, Ann Arbor, MI 48106-1346 USA

UMI®
800-521-0600

Study of the Highly Oxidizing Centers in the Metmyoglobin-H_2O_2 Reaction

Craig Fenwick

A Thesis

in

The Department

of

Biochemistry

Presented in Partial Fulfillment of the Requirements
for the Degree of Doctor of Philosophy at
Concordia University
Montréal, Québec, Canada

National Library
of Canada

Acquisitions and
Bibliographic Services

395 Wellington Street
Ottawa ON K1A 0N4
Canada

Bibliothèque nationale
du Canada

Acquisitions et
services bibliographiques

395, rue Wellington
Ottawa ON K1A 0N4
Canada

Your file Votre référence

Our file Notre référence

0-612-39774-2

Canada

NOTE TO USERS

Page(s) not included in the original manuscript are unavailable from the author or university. The manuscript was microfilmed as received.

ii

UMI

Abstract

Study of the Highly Oxidizing Centers in the Metmyoglobin-H_2O_2 Reaction
Craig Fenwick, Ph.D.
Concordia University, 1997.

Metmyoglobin ($MbFe^{III}$) from horse heart forms an oxyferryl heme (Fe^{IV}=O) and an unstable protein radical upon reaction with H_2O_2. Chemical modifications to the globin and heme have been reported as byproducts of the reaction. However, chromatographic and mass spectral analyses followed by peptide mass mapping reveal that Fe^{IV}=O formation and protein radical decay are not responsible for Mb modification. Damage to the polypeptide was found to be linked to the Fe^{IV}=O autoreduction process, with the extent of chemical modification increasing at lower pH. $MbFe^{III}$ was also found to demonstrate catalase-like activity after "priming" with 2 molar equivalents of H_2O_2. FTIR analysis of $MbFe^{IV}$=O and $MbFe^{III}$ over the pH range 7 to 5.4 revealed minor changes in the amide I' and II bands, indicating only small secondary structure changes. Thus, electron transfer pathways through the polypeptide to the heme are not expected to be perturbed by reaction with H_2O_2 nor by pH changes.

Covalent modification of His48 of Mb was performed with three ruthenium complexes (a_4LRu; a = NH_3; L = NH_3, pyridine, isonicotinamide). The derivatives were purified by cation-exchange chromatography and the modification sites confirmed by peptide mass mapping. The reduction potentials ($Ru^{III/II}$) of the Mb-bound complexes were determined by differential pulse voltammetry to be 77, 330, and 400 mV for the a_5Ru, a_4PyrRu, and a_4IsnRu derivatives, respectively.

The kinetics of Fe^{IV}=O heme reduction in Mb by a_4LRu^{II} bound at the surface His48 were investigated using pulse radiolysis. The observed first-order rate constant (k_{obs1}) decreased with increasing pH and reduction potential for the a_4LRu centers. Rate-pD data obtained in D_2O for the a_5Ru derivative revealed the presence of an equilibrium isotope effect, and a pK_a of 5.7 (6.2 in D_2O) was obtained for the acid-base group, which is assigned to the distal His64. A mechanism where protonation *precedes* ET provided a good fit of the kinetic data for the three a_4LRu derivatives. Marcus theory analysis of the k_{ET} (0.74, 1.8, 3.6 s^{-1} for L = Isn, Pyr, NH_3) extracted from the k_{obs1}'s yielded a reorganization energy (λ) of 1.8 eV for $Ru^{II} \rightarrow Fe^{IV}$=O ET in the a_4LRu derivatives, but a λ of 2.1 eV for the a_5Ru derivative. From the latter, it is concluded that ET is strongly gated in the a_5Ru derivative, and this is assumed to be the major reason for the low reactivity of Fe^{IV}=O in Mb at high $-\Delta G^{\circ}$.

The location of protein-based radicals formed in the $MbFe^{III}/H_2O_2$ reaction was investigated by forming stable derivatives at the sites of radical formation. The spin adducts formed between Mb and the spin trap 2-methyl-2-nitrosopropan (MNP) were found to be stable upon reduction with ascorbate. Peptide mass mapping and sequencing by collisionally induced dissociation revealed that Tyr103 and Lys42 were modified in the $MbFe^{III}/H_2O_2$/MNP reaction at neutral pH, and at pH 5 distal His64 was also modified.

Acknowledgements

I would like to thank Dr. Ann English for her encouragement and support throughout my Ph.D. Her energy and enthusiasm, dedicated to research and the learning process of her graduate students contributed greatly to my development as a researcher and her advice will follow me throughout my scientific career.

I would also like to thank my good friend, Dr. George Tsaprailis for the hours (days) of conversation and discussion about science and everything under the sun. You certainly made the more difficult moments bearable as we commiserated over our respective research woes.

I wish to thank Mr. Paul Taslimi for his advice and friendship during my stay at Concordia. Paul was extremely generous with his time in helping anyone who asked him and his contribution to most graduate student's research should not be understated.

I would like to thank Mr. Bernie Gibbs for introducing me to biological mass spectrometry and for his example of dedication to research as a man of science.

I am grateful to all the graduate and undergraduate students that have made my degree at Concordia such a positive experience. In particular, I would like to express my appreciation to Dr. Kelly Millan, Yazhen Hu, Angelo Filoso, Stephen Marmor, Inés Holtzbaur, Greg Huyer, Sue Aitkens and Iolie Bakas.

I would like to thank my parents and sister for their love and finally, I dedicate this thesis to my wife Monique, whose unconditional love and understanding has been a source of constant support and inspiration during the course of my degree.

Table of Contents

List of Figures

List of Tables

LIST OF ABBREVIATIONS

a	NH_3
a_5Ru	pentaammineruthenium
a_4RuPyr	tetraamminepyridineruthenium complex
a_4RuIsn	tetraammineisonicotinamideruthenium complex
Abs	absorbance
ABTS	2,2'-azino-di(3-ethyl-benzthiazoline-6-sulfonic acid)
ABTS(ox)	oxidized ABTS
ARP	*Arthromyces ramosus* peroxidase
CCP	cytochrome c peroxidase
CH_3CN	acetonitrile
CID	collisionally induced dissociation
CIP	*Coprinereus cinereus* peroxidase
$CO_2^{\bullet-}$	formate radical
d^o	distance at van der Waals contact
Da	dalton
DPV	differential pulse voltammetry
E'^o	reduction potential
e^-_{aq}	aqueous electron
E_P	peak potential
EPR	electron paramagnetic resonance
ESI-MS	electrospray mass spectrometry
ET	electron transfer
EXAFS	extended x-ray absorption fine structure
FPLC	fast protein liquid chromatography
FTIR	Fourier-transform infrared spectroscopy
GC-MS	gas chromatography mass spectrometry
G-HCl	guanidine-HCl
H_{AB}	tunneling matrix element
H^o_{AB}	electronic coupling at van der Waals contact
HPLC	high pressure liquid chromatography
HRP	horseradish peroxidase
HRP-II	HRP compound II
k_B	Boltzman constant
k_{ET}	electron transfer rate constant
k_{obs}	observed rate constant
LC-MS	liquid chromatography mass spectrometry
LIP	lignin peroxidase
Mb	Myoglobin
$Mb^{\bullet}$	myoglobin with an unidentified radical
$MbFe^{II}$	ferrous myoglobin
$MbFe^{II}$-CO	ferrous myoglobin with carbon monoxide bound at the heme

$MbFe^{II}$-O_2	ferrous myoglobin with O_2 bound at the heme
$MbFe^{III}$	ferric myoglobin
$MbFe^{III}$-CN	ferric myoglobin with cyanide bound at the heme
$MbFe^{III}$-OH_2	ferric myoglobin with water bound at the heme
$MbFe^{IV}$=O	oxyferryl myoglobin
Mb-MNP	MNP adduct bound to myoglobin
MNP	2-methyl-2-nitrosopropane
MW	molecular weight
NHE	normal hydrogen electrode
$P^{\bullet+}$	protein-based radical center
Pi	phosphate buffer
Q1	first quadrupole
Q2	collision cell
Q3	third quadrupole
RHMb	recombinant human myoglobin
R-MNP-Mb	reduced MNP adduct bound to myoglobin
RP	reversed phase
SKIE	solvent kinetic isotope effect
SSQ	single stage quadrupole
SWMb	sperm whale myoglobin
$t_{1/2}$	half-life
TFA	trifluoroacetic acid
TSQ	triple stage quadrupole
V8	V8 endoproteinase
Zn-Mb	apomyoglobin reconstituted with a zinc substituted porphyrin
β	distance decay factor
ΔG^o	driving force
$\Delta H^{\ddagger}$	activation enthalpy
$\Delta S^{\ddagger}$	activation entropy
λ	reorganizational energy
υ(CO)	stretching vibration of iron bound carbon monoxide

1.0 General Introduction

1.1 Oxyferryl Heme

Myoglobin (Mb) is a small (~17 kDa) heme protein whose physiological function is to reversibly bind dioxygen. It is found in high concentrations in muscle tissue and acts as an oxygen reservoir for oxidative phosphorylation. Although the reduced ferrous (Fe^{II}) heme state is necessary for oxygen binding, oxidized forms of Mb have received much attention because of their similarities to the catalytic intermediates of heme enzymes and their possible role in the oxidation of cellular membranes. Highly oxidized states of Mb are formed on reaction with peroxides and consist of an oxyferryl heme (Fe^{IV}=O) and protein-based radical centers ($P^{\bullet}$).[1,2,3]

Fe^{IV}=O centers are of great interest since it has been found or hypothesized that all heme enzymes involved in redox catalysis use Fe^{IV}=O heme in their catalytic cycles.[4,5] Fe^{IV}=O hemes have oxidizing potentials close to 1 V and their reduction *in vivo* is coupled to a multitude of reactions.[6,7] These include reactions carried out by cytochrome P_{450} in drug metabolism and detoxification in the liver, in the breakdown of lignin by lignin peroxidase, and in the reduction of O_2 to H_2O by cytochrome oxidase. Direct investigation of Fe^{IV}=O centers is difficult in enzymes such as cytochrome P_{450} and cytochrome c oxidase since the Fe^{IV}=O intermediate is highly unstable. In fact, the substrate in cytochrome P_{450}(cam) must be bound close to the heme before the catalytic redox cycle begins to ensure that substrate hydroxylation is coupled to electron transfer.[8]

Fe^{IV}=O centers are best characterized in heme peroxidases where the Fe^{IV}=O species is generated on the rapid reaction ($\geq 10^7$ $M^{-1}s^{-1}$)[9] of the ferric enzyme (Fe^{III},P) with

H_2O_2:

$$Fe^{III},P + H_2O_2 \longrightarrow Fe^{IV}=O,P^{\bullet+} + H_2O \qquad (1.1a)$$

$$Fe^{IV}=O,P^{\bullet+} + 1e^- \longrightarrow Fe^{IV}=O,P \qquad (1.1b)$$

$$Fe^{IV}=O,P + 1e^- + 2H^+ \longrightarrow Fe^{III},P + H_2O \qquad (1.1c)$$

The intermediate formed in reaction 1.1a is termed compound I, where $P^{\bullet+}$ is a cation radical located either on the porphyrin or protein. Compound I is then reduced back to its resting state in two one-electron steps that first reduce the radical species to give compound II (1.1b) and then the $Fe^{IV}=O$ center (1.1c).

A mechanism of compound I formation in peroxidases was first proposed based on the X-ray structure of cytochrome c peroxidase (CCP).[10] This mechanism involved H_2O_2 binding to the ferric heme iron with a concomitant transfer of the α-oxygen proton to the distal His52. The N2 of His52 is maintained in the unprotonated tautomeric form through a H-bond between the side chain oxygen of Asn82 and H-N1 of His52. Thus, the N2 atom of His52 can only act as a H-bond acceptor, which explains why the protonated form of anionic ligands bind preferentially to the heme of CCP.[11] The negative charge that develops on the β oxygen of H_2O_2 was thought to be stabilized by the positively charged side chain of Arg48 through direct ionic interaction. This first proposed mechanism has since been modified after the X-ray structure of the stable O_2 complex of the Trp191→Phe mutant of CCP (W191F) was determined and used as a

model for the unstable Fe^{III}-OOH intermediate.[12] The structure of CCP(W191F)-O_2 revealed that in addition to the predicted H-bond between the protonated His52 and the β-oxygen, the indole N of Trp51 is H-bonded to the α-oxygen, but Arg48 does not directly H-bond to either oxygen (Figure 1.1A). Heterolytic cleavage of the O-O bond is completed by protonation of the β oxygen by His52 (Figure 1.1B), resulting in the formation of Fe^{V}=O and H_2O. In CCP, the Fe^{V}=O is quickly reduced to Fe^{IV}=O through intramolecular transfer of an electron from Trp191, which forms a protein-based cation radical. The stability of the higher oxidation states of CCP is attributed to the H-bond between Asp235 and the proximal His175 ligand (Figure 1.2), which results in increased electron density in the His175-Fe-porphyrin system.[13]

X-ray structures of other members of the peroxidase family [for example, lignin peroxidase (LIP), *Arthromyces ramosus* peroxidase (ARP), and *Coprinus cinereus* peroxidase (CIP)] reveal a high degree of structural similarity with CCP despite <20% sequence homology. The active site residues of CCP (Arg48, His52, Asn82, His175, and Asp235, Figure 1.2) are conserved in other peroxidases,[9] suggesting a similar mechanism for compound I formation. However, most peroxidases, including HRP, have a Phe (Phe41) at the Trp51 position,[14] so the distal arginine may play a more prominent role in compound I formation in these peroxidases than in CCP.

Site-directed mutants of recombinant CCP support the proposed mechanism of compound I formation in Figure 1.1. A His52 →Leu mutation in CCP led to a 10^5-fold decrease in the rate of compound I formation,[15] while Arg48→Lys and Arg48→Leu mutations resulted in only a 2-fold and 200-fold decrease in rate, respectively.[16,17] In HRP

Figure 1.1 Proposed Fe^{III}-OOH complex of CCP and its decay to compound I. (A) The enzyme-substrate complex shows H-bonding between the β-oxygen and His52, and the α-oxygen and Trp51, with the active-site water molecule represented by an asterisk. (B) His52 acts as a proton donor to the β-oxygen, leading to the cleavage of the O-O bond and reorientation of Arg48 to H-bond with the developing oxene ligand. (C) The oxyferryl center of compound I showing the oxene ligand forming H-bonds with Trp51 and Arg48.

A.

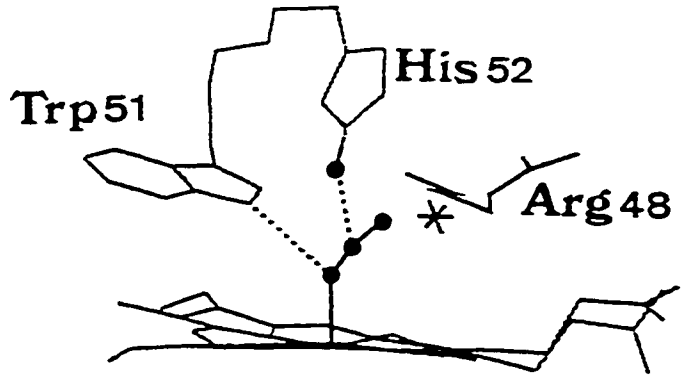

B.

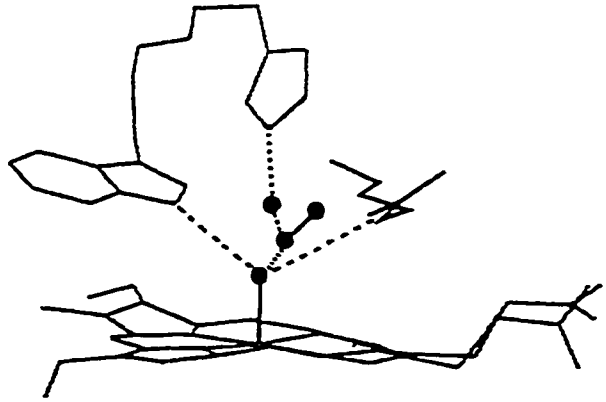

C.

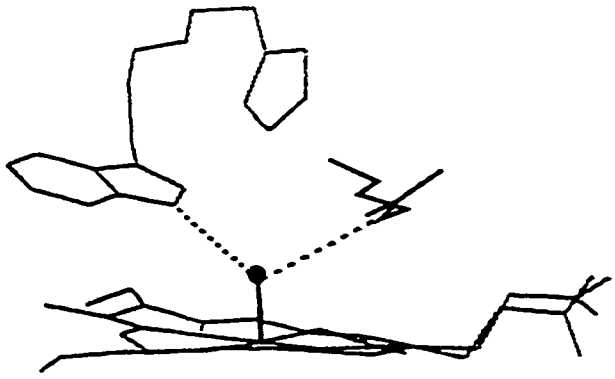

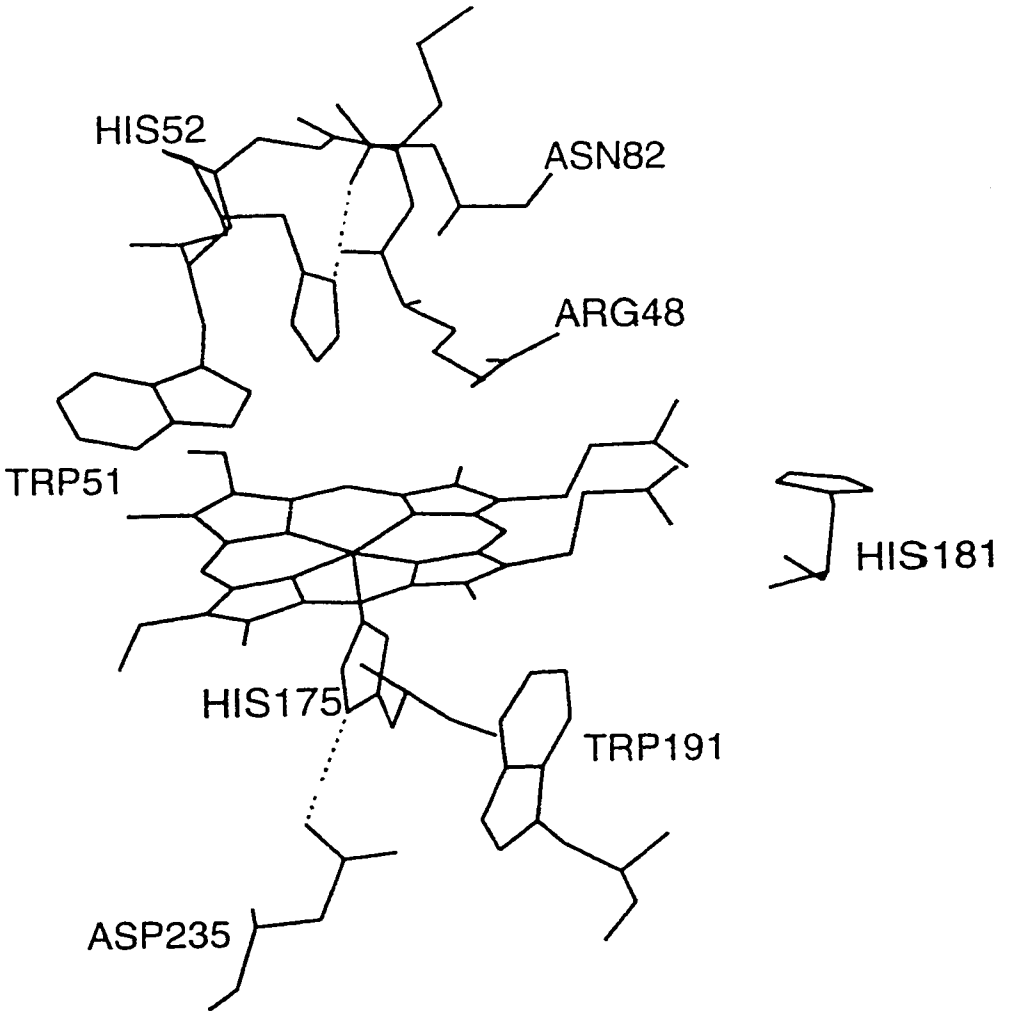

Figure 1.2 Active site structure of yeast cytochrome c peroxidase (CCP). The dashed lines represent H-bonding and the diagram was generated using the X-ray coordinates for the 1.7-Å structure of CCP.[18]

His42→Leu, Arg38→Lys, and Asn70→Val mutations (His42, Arg38 and Asn70 in HRP are equivalent to His52, Arg48 and Asn82 in CCP) led to a 10^5-fold, 500-fold and >10-fold decrease, respectively, in the rate of compound I formation.[19,20,21] A comparison of the CCP and HRP mutant data reveals that the distal histidine plays an essential role in the high reactivity of both peroxidases with H_2O_2. However, the difference in importance of the distal arginine in CCP and HRP, as revealed by the Arg→Lys mutation, indicates that the architecture of the heme pocket is not identical in both peroxidases.

The cation radical ($P^{\bullet+}$: reaction 1.1c) in compound I is either protein- or porphyrin-based depending on the nature of the residues in proximity to the heme. CCP is known to form a protein-based radical and has two tryptophans (Trp51 and Trp191) within 5 Å of its heme. EPR studies of the site-directed mutants, W51F and W191F,[22] and ENDOR studies on CCP containing predeuterated tryptophan residues, confirmed that Trp191 is the location of the protein-based radical.[23] LIP is known to form a porphyrin cation radical on reaction with H_2O_2 and its X-ray structure reveals that Phe46 and Phe193 replace the corresponding Trp51 and Trp191 residues in CCP.[24] Since phenylalanine residues are more difficult to oxidize than tryptophan, the radical center remains on the porphyrin. HRP also forms a porphyrin radical, but replacing Phe172 (which is equivalent to Trp191 in CCP) with tyrosine, results in a compound I with a protein-based radical.[25]

1.2 Oxidation of Metmyoglobin by H_2O_2

Metmyoglobin ($MbFe^{III}$) reacts with H_2O_2 to give an Fe^{IV}=O heme and protein-

based radicals in an analogous fashion to heme peroxidases (reaction 1.1a). However, there are marked differences in reactivity due to the placement and absence of certain residues essential to the peroxidase reaction. The catalytic residues of CCP and the corresponding residues in Mb are shown in Figures 1.2 and 1.3. Arg48 in CCP is replaced by Phe43 in Mb which makes the heme pocket of Mb more hydrophobic than of CCP. Thus Mb has a less favorable environment for charge separation in the splitting of the peroxide O-O bond. The distal His64 in Mb is tautomeric and can act as both a H-bond donor and acceptor to ligands bound to the heme. The importance of the distal histidine as a H-bond acceptor is revealed in the X-ray structure of salicylhydroxamic acid/myloperoxidase (MPO) complex, which was used as a model for the H_2O_2/ peroxidase pre-reaction complex.[26] A H-bond is formed between the distal histidine and peroxide, which presumably leads to deprotonation of the peroxide to yield the anion that binds to the iron.

The distal His64 also isolates the heme pocket from the solvent in Mb, whereas in CCP a water channel connects the heme to the bulk solvent. The proximal His93 in Mb is weakly H-bonded to a carbonyl group of the peptide backbone. The lack of a strong H-bond to the proximal His93 results in a longer Fe-N bond length in Mb compared to peroxidases (2.1 vs 1.9 Å),[27] which affects Fe^{IV}=O stability and favours a 6-coordinate Fe^{III} heme over the 5-coordinate Fe^{III} heme found in peroxidases.[27] The structural differences in Mb compared to the peroxidases result in a much slower bimolecular rate of Fe^{IV}=O formation via reaction 1.1a (210 $M^{-1}s^{-1}$ for HHMb vs 1.4 x 10^7 $M^{-1}s^{-1}$ for CCP).[28,2]

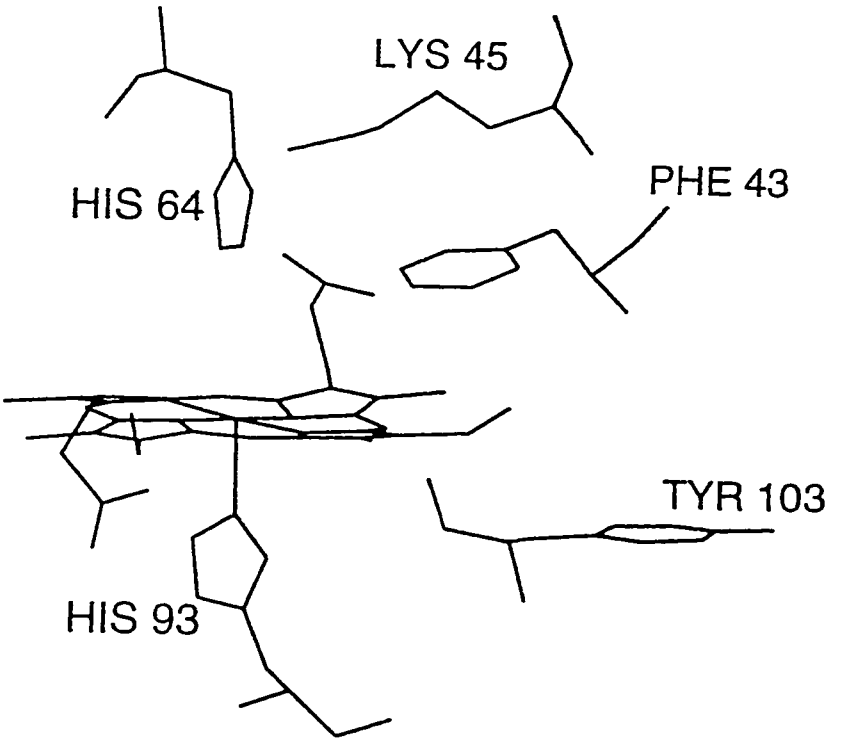

Figure 1.3 Active site structure of horse heart Myoglobin (HHMb). The dashed lines represent H-bonding and the diagram was generated using the X-ray coordinates for the 1.9-Å structure of HHMb.[29]

Tyr103 in Mb is within van der Waals forces of the heme and is believed to be a major site of radical formation on reaction of $MbFe^{III}$ with H_2O_2. However, the stability of the protein-based radical(s) in Mb are significantly lower than that of Trp191 of CCP which has a half-life of ~3 h[30] compared to ~7-30 s for the Mb radical as monitored by EPR.[31,32] The Trp191 radical is believed to be stabilized by the strong negative potential that surrounds the Trp191 side chain,[33] while the solvent exposed Tyr103 in Mb can be readily reduced by exogenous donors.[34] The discovery that sperm whale Mb (SWMb) cleaves peroxides homolytically as well as heterolytically with a 1:2 ratio,[35] suggests that radical formation in Mb may not occur only by intramolecular hydrogen abstraction. Homolytic cleavage of H_2O_2 is analogous to Fenton chemistry and results in the formation of Fe^{IV}=O and the release of a hydroxy radical (OH•). The hydroxy radical has a potential of +2.31 eV (pH 7.0)[36] and abstracts a hydrogen atom from most organic molecules at diffusion controlled rates (>10^9 $M^{-1}s^{-1}$).[37] The abstraction of a hydrogen from residues close to the site of OH• formation may account for the detection by EPR of different protein-based radicals, including Tyr103 in Mb compound I.[38,39]

In vivo, there is no known physiological role for the formation of Fe^{IV}=O or radical centers in Mb. Their main effect is proposed to be the oxidation of neighbouring $MbFe^{II}$ or $MbFe^{II}$-O_2 to $MbFe^{III}$.[40] However, both the Fe^{IV}=O and $P^{\bullet+}$ centers in Mb are potent oxidants (~1 eV) and have been found to oxidize lipids,[41] cause damage and dimerization of proteins,[42] and epoxidize styrene *in vitro*.[43] Antioxidants such as ascorbate,[44] α-tocopherol,[45,46] and thiols[34] can reduce the oxidizing centers in Mb, but there is also an increasing number of compounds that promote oxidative damage such as the

anti-inflammatory drug meclofenamic acid[47] and the antibiotic adriamycin.[48] The oxidation of low density lipoproteins leads to the formation of atherosclerotic lesions[40,49] and Mb's oxidizing centers are thought to have a significant involvement in coronary heart diseases.[50,51] Cardiac tissue is especially susceptible to the peroxide-initiated oxidation due to its high concentration of Mb and the lack of antioxidant enzymes in the heart compared to other tissues.[52]

1.3 Study of MbFe^{IV}=O by Intramolecular Electron Transfer

The Fe^{IV}=O center in Mb presents an opportunity to study Fe^{IV}=O heme reactivity in a protein that was not designed to handle such highly oxidizing species. The porphyrin in Mb and those in most heme enzymes are identical so that the protein structure around the heme is responsible for the characteristic function or activity of a heme protein. As mentioned above, most of our knowledge of Fe^{IV}=O reactivity comes from the study of peroxidases, which has shown that the rate-limiting step in the peroxidase catalytic cycle under optimal conditions is the reduction of the Fe^{IV}=O center (reaction 1.1c).[53,54] Nonetheless, details of how heme peroxidases control the reactivity of Fe^{IV}=O centers is poorly understood. MbFe^{IV}=O was chosen as a model system to elucidate the important elements of Fe^{IV}=O reactivity and to determine how these depend on the architecture of the heme pocket.

Extensive studies of Fe^{IV}=O reduction in heme peroxidases have been performed with a variety of bimolecular reducing agents.[53,55,56,57,58] The steps involved in bimolecular electron transfer are the following:

$$\text{Donor} + \text{Acceptor} \overset{K_D}{\rightleftharpoons} \text{Donor/Acceptor} \overset{k_{ET}}{\rightleftharpoons} \text{Donor}^+/\text{Acceptor}^- \rightleftharpoons \text{Donor}^+ + \text{Acceptor}^- \quad (1.2)$$

$$k_{obs} = K_D\, k_{ET} \quad (1.3)$$

The observed bimolecular rate constant (k_{obs}) is dependent upon the stability (K_D) of the precursor complex (Donor/Acceptor) as well as the rate constant for electron transfer (k_{ET}) within the precursor complex. Since both K_D and k_{ET} can vary with experimental conditions such as pH and ionic strength, it is difficult to determine their individual contributions to k_{obs}.

A method developed to avoid the uncertainties associated with bimolecular electron transfer involves covalently modifying a specific residue on the protein surface with a redox active-reagent. In this way, intramolecular electron transfer can be measured from the donor to acceptor with the observed rate directly related to k_{ET}.

$$\text{Donor}\sim\text{Acceptor} \xrightarrow{k_{ET}} \text{Donor}^+\sim\text{Acceptor}^- \quad (1.4)$$

$$k_{obs} = k_{ET} \quad (1.5)$$

The most established technology involves the attachment of a ruthenium complex, such as ruthenium pentaammine (a_5Ru^{III} where a = NH_3), to a surface histidine residue.[59,60,61]

Using this technology, intramolecular electron transfer has been studied in a large number of ruthenium-modified proteins, including cytochrome c,[62,63] cytochrome b_5,[64] azurin,[59] plastocyanin,[65] myoglobin,[64] and cytochrome c peroxidase.[66] The electron transfer rates can be analyzed using semiclassical Marcus theory (Eq 1.6) for electron transfer within a precursor complex since the donor and acceptor are held at a fixed distance.

$$k_{ET} = (4\pi^3/h^2\lambda k_B T)^{1/2}(H_{AB})\exp[-(\Delta G^\circ + \lambda)^2/4\lambda k_B T] \qquad (1.6)$$

The parameters in this equation are the tunneling matrix element H_{AB}, the nuclear reorganization energy λ, the driving force ΔG°, Planck constant *h* and the Boltzman constant k_B. H_{AB} is a measure of the electronic coupling between the donor and acceptor and depends upon their separation, relative orientation and medium through which the electron has to travel. λ is the energy required to move all of the atoms from their equilibrium position in the pre-electron transfer complex to the post-electron transfer complex without actually transferring the electron. ΔG° is the difference between the reduction potentials of the donor and acceptor in the precursor complex.[67]

The parameters described by the Marcus equation have been thoroughly investigated in SWMb and human Mb modified at His48 with a variety of ruthenium complexes. Changing the ligands coordinated to the bound ruthenium allows for a controlled modulation of the driving force (ΔG°) between the donor and acceptor, and intramolecular electron transfer (ET) rates at various ΔG° values yielded a λ of 1.48 eV for the Fe^{II}/Fe^{III}-OH_2 couple in SWMb. The electronic coupling (H_{AB}) for the path

between ruthenium complexes bound to His48 and the heme was estimated as 0.01 cm^{-1}.[64] The electronic coupling for this pathway is expected to remain unchanged for $MbFe^{IV}$=O reduction so that λ for the Fe^{III}-OH_2/Fe^{IV}=O couple can be calculated from the driving force dependence of the intramolecular ET reaction.

The Fe^{III}/Fe^{IV}=O couple in CCP has been previously investigated by intramolecular electron transfer. However, the surface histidines that are accessible to ruthenium modification are at 20-23 Å away from the heme in CCP. The combination of this long distance and weak electronic coupling[68] resulted in intramolecular ET rates of 3.2 s^{-1} and 1.6 s^{-1} for His60 and His6 derivatives, respectively.[66] Unfortunately, the slow ET rates compared to the maximal turnover rate of 1500 s^{-1} for the CCP peroxidase cycle[69] made it impossible to address the question of whether protonation of the oxene ligand or ET is rate-limiting in Fe^{IV}=O reduction.[66] In addition, driving force dependence experiments were not performed by varying the ruthenium ligands since the rates would have been too slow to measure.[68] Thus, it was impossible to determine the λ value for the Fe^{IV}=O heme in the CCP derivatives prepared. HHMb was chosen here as a model system to study Fe^{IV}=O heme reduction. The results discussed in Chapter 3 include driving force (ΔG°), pH and pD dependence of Ru^{II}→$MbFe^{IV}$=O intramolecular electron transfer rates in ruthenated HHMb derivatives.

1.4 Protein-Based Radical Centers Formed in the $MbFe^{III}/H_2O_2$ Reaction

Unstable protein-based radicals are also formed in the $MbFe^{III}/H_2O_2$ reaction as discussed above. Although these centers have been under investigation over the last 40

years, there is still debate as to the sites of radical formation.[38,39] EPR analysis of both the protein radicals[31,43] and their spin adducts[70,31] have been inconclusive,[38] but the most convincing evidence indicates that Tyr103 is the major site of radical formation.[31] EPR has also shown that there are radicals formed on other unidentified residues during the $MbFe^{III}/H_2O_2$ reaction.

Since EPR has failed to unambiguously identify major, let alone minor radical sites in Mb and other proteins, a new technology was developed using spin trapping and peptide mass mapping techniques. Spin traps are molecules designed to react with and stabilize radical centers. In EPR this allows for the accumulation of a radical spin adduct so as to detect and analyze its paramagnetic signal.[71] The spin trap, 2-methyl-2-nitroso-propane (MNP), was used to form spin adducts (Figure 1.4) with the protein-based radicals formed in the $MbFe^{III}/H_2O_2$ reaction. Reduction of the adducts was performed

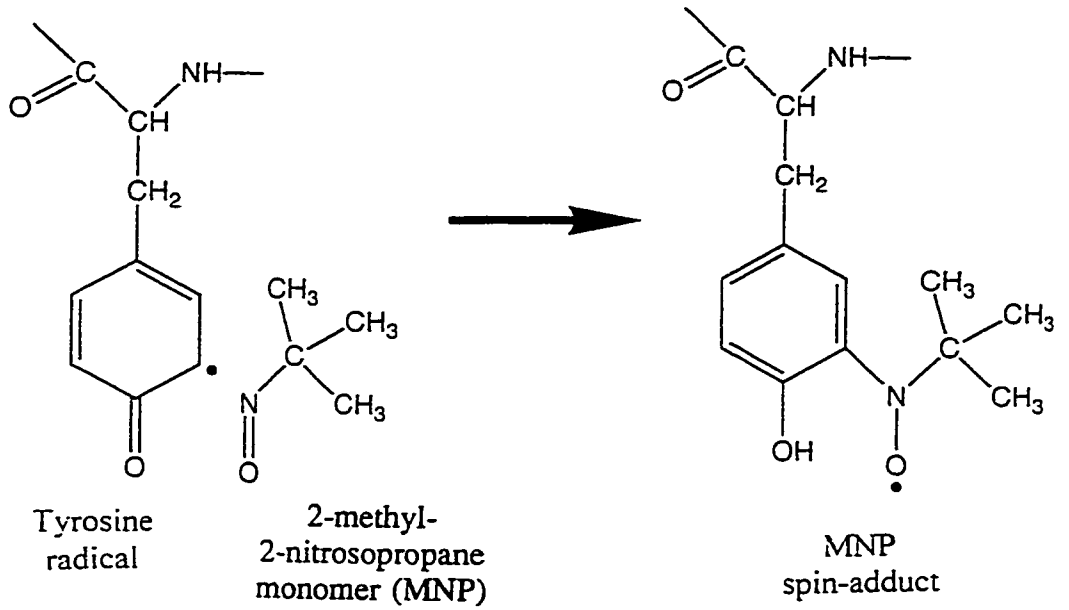

Figure 1.4 MNP spin adduct formation on a tyrosine-based radical.

with ascorbate, since the stability of the MNP adduct was increased and preservation of the spin adduct's paramagnetic nature was not necessary. Peptide mass mapping and sequencing were then used to identify the covalently-modified residue that formed the MNP adduct. The results of this study are presented in Chapter 5.

The identification of the amino acid residues that act as electron donors in the $MbFe^{III}/H_2O_2$ reaction may give insight into the mechanism of radical formation in Mb and into the possibility of these radicals carrying out lipid oxidation *in vivo*. Since Mb has been designed for a cell environment that includes activated oxygen species such as peroxide,[72] localization of the sites of radical formation should indicate how well Mb was designed to deal with radical formation in its globin moiety.

1.5 Scope and Outline of Thesis

A detailed study of the $MbFe^{III}/H_2O_2$ reaction was performed to establish conditions for complete Fe^{IV}=O formation without side reactions that damage the globin or heme. The secondary structure of $MbFe^{IV}$=O and $MbFe^{III}$ under a range of pH conditions was investigated to probe for protein structural changes that might alter the intramolecular electron transfer pathway through the globin from His48 to the Fe^{IV}=O heme. The autoreduction of $MbFe^{IV}$=O was monitored under various conditions to ensure that the pulse radiolysis experiments were performed while the heme was primarily in the Fe^{IV}=O state (Chapter 2).

HHMb was first derivatized at surface histidines with a_5Ru and the His48 derivative was purified and characterized. Intramolecular electron transfer was initiated

by pulse radiolysis and the $Ru^{II} \rightarrow Fe^{IV}=O$ electron transfer rates were monitored at pH 7.0. The temperature and a_5RuMb concentration dependence of the rates were also investigated (Chapter 3).

The driving force dependence of the $Ru^{II} \rightarrow Fe^{IV}=O$ electron transfer rates was probed by preparing a_4PyrRuHis48 and a_4IsnRuHis48 derivatives of Mb. The effect of pH and pD was additionally investigated since $Fe^{IV}=O$ reduction to Fe^{III}-OH_2 requires the transfer of one electron and two protons (Chapter 4).

Locating the protein-based radicals formed during the $MbFe^{III}/H_2O_2$ reaction was performed by forming stable spin adducts at the sites of radical formation. Peptide mass mapping and collisionally induced dissociation (CID) sequencing identified the radical forming residues. The $MbFe^{III}/H_2O_2$ reaction was also carried out at lower pH and in the presence of a chaotropic agent to monitor the effect of these conditions on the Mb spin adducts formed (Chapter 5).

Conclusions and suggestions for further study are found in Chapter 6. Chapters 3 and 5 are extended versions of published communications,[73,74] while Chapter 4 is a published paper[75] (all in the Journal of the American Chemical Society). The data in Chapter 2 is currently being prepared for publication. Chapters 3 to 5 have several figures added that were not included in the publications, and all figures and table numbering systems were changed to the format of this thesis.

References

1. Poulos, T.; Finzel, B. In *Peptide and Protein reviews Vol 4*, Hearn, M.T.W. Ed.;Marcel Dekker: New York, **1984**; pp 115-171.
2. Tajima, G.-I.; Shikama, K. *Int. J. Biochem.* **1993**, *25*, 101-105.
3. George, P.; Irvine, D.H. *Biochem. J.* **1952**, *52*, 511-517.
4. Babcock, G. T.; Wilkström, M. *Nature* **1992**, *356*, 301.
5. Malmström, B. G. *Acc. Chem. Res.* **1993**, *26*, 332.
6. Mueller, E.J.; Loida, P. J.; Sligar, S. G.; In *Cytochrome P450 Structure, Mechanism and Biochemistry 2nd Edn.* Ortiz de Montellano, P. R., Ed.; Plenum Press: New York, 1995; pp 83-124;
7. Poulos, T. L.; Cupp-Vickery, J.; Li, H. In *Cytochrome P450 Structure, Mechanism and Biochemistry 2nd Edn.* Ortiz de Montellano, P. R., Ed.; Plenum Press: New York, 1995; pp 125-150;
8. Raag, R.; Poulos, T.L. *Biochemistry* **1991**, *30*, 2674.
9. English, A.M.; Tsaprailis, G.; *Advances Inorg. Chem.* **1995**, *43*, 79.
10. Poulos, T.L.; Kraut, J. *J.Biol.Chem.* **1980**, *255*, 8199.
11. Poulos,T.L.; Finzel, B.C. In *Peptide and Protein Reviews Vol 4*, Hearn, M.T.W. Ed.; Marcel Dekker, Inc. **1984**, New York, pp 136-140.
12. Miller, M.A.; Shaw, A.; Kraut, J. *Nature Struc. Biol.* **1994**, *1*, 524.
13. Chance, M.; Powers, L.; Kumar, C.; Chance, B. *Biochemistry* **1986**, *26*, 1259.
14. Welinder, K.G. *Curr. Opin. Struct. Biol.* **1992**, *2*, 388.
15. Erman, J.E.; Vitello, L.B.; Miller, M.A.; Shaw, A.; Brown, K.A.; Kraut, J. *Biochemistry* **1993**, *32*, 9798.

16. Vitello, L.B.; Erman, J.E.; Miller, M.A.; Wang, J.; Kraut, J. *Biochemistry* **1993**, *32*, 9807.

17. Erman, J.E.; Vitello, L.B.; Miller, M.A.; Kraut, J. *J. Am. Chem. Soc.* **1992**, *114*, 6592.

18. Finzel, B.C.; Poulos, T.L.; Kraut, J. *J. Biol. Chem.* **1984**, *259*, 13027.

19. Rodriguez-Lopez, J.N.; Smith, A.T.; Thorneley, R.N.F. *J. Biol. Chem.***1996**, *271*, 4023-4030.

20. Rodriguez-Lopez, J.N.; Smith, A.T.; Thorneley, R.N.F. *J. Biol. Inorg. Chem.* **1996**, *1*, 136-142.

21. Nagano, S.; Tanaka, M.; Ishimori, K.; Watanabe, Y.; Morishima, I. *Biochemistry* **1996**, *35*, 14251.

22. Scholes, C.P.; Liu, Y.; Fishel, L.A.; Farnum, M.F.; Mauro, J.M.; Kraut, J. *Isr. J. Chem.* **1989**, *29*, 85.

23. Sivaraja, M.; Goodin, D.B.; Smith, M.; Hoffman, B.M. *Science* **1989**, *245*, 738.

24. Isied, S.S. In "*Metal Ions in Biological Systems: Electron Transfer Reactions in Metalloproteins*", Sigel, H.; Sigel, A., Eds; Marcel Dekker: New York, **1991**; Vol. 27, pp 1-56.

25. Miller, V.P.; Goodin, D.B.; Friedman, A.E.; Hartmann, C.; Ortiz de Montellano, P.R. *J. Biol. Chem.* **1995**, *270*, 18413.

26. Davey, C.A.; Fenna, R.E. *Biochemistry* **1996**, *35*, 10967-10973

27. Sinclair, R.; Hallam, S.; Chen, M.; Chance, B.; Powers, L. *Biochemistry* **1996**, *35*, 1512.

28. Yonetani, T,; Schleyer, H. *J. Biol. Chem.* **1967**, *242*, 1974.

29. Evans, S.V.; Brayer, G.D. *J. Mol. Biol.* **1990**, *213*, 885.

30. Erman, J.E.; Yonetani, T. *Biochim. Biophys. Acta* **1975**, *393*, 350.

31. Davies, M.J. *Biochim. Biophys. Acta* **1991**, *1077*, 86-90.

32. Kelman, D.J.; DeGray, J.A.; Mason, R.P. *J. Biol. Chem.* **1994**, *269*, 7458-7463.

33. Miller, M.A.; Han, G.W.; Kraut, J. *Proc. Natl. Acad. Sci. USA* **1994**, *91*, 11118.

34. Romero, F.J.; Ordonez, I.; Arduini, A.; Cadenas, E.; *J. Biol. Chem.* **1992**, *267*, 1680-1688.

35. Allentoff, A.J.; Bolton, J.L.; Wilks, A.; Thompson, J.A.; Ortiz de Montellano, P.R. *J.Am.Chem.Soc.* **1992**, *114*, 9744.

36. Sawyer, D.T.;*Encyclopedia of Inorganic Chemistry, Oxygen*: Inorganic Chemistry, pp 2947-2985.

37. Klapper, M.H.; Faraggi, M. *Quart. Rev. Biophys.* **1979**, *12*, 465.

38. Gunther, M.R.; Kelman, D.J.; Corbett, J.T.; Mason, R.P. *J. Biol. Chem.* **1995**, *270*, 16075.

39. Wilks, A.; Ortiz de Montellano, P.R. *J. Biol. Chem.* **1992**, *267*, 8827.

40. Brown, M.S.; Goldstein, J.L. *Annu. Rev. Biochem.* **1983**, *52*, 223-261.

41. Rice-Evans, C.; Green, E.; Paganga, G.; Cooper, C.; Wrigglesworth, J. *FEBS* **1993**, *326*, 177-182.

42. Hanan, T.; Shaklai, N. *FEBS* **1995**, *233*, 930-936.

43. Choe, Y.S.; Rao, S.I.; Ortiz de Montellano, P.R. *Arch. Biochem. Biophys.* **1994**, *314*, 126-131.

44. Giulivi, C.; Cadenas, E. *FEBS* **1993**, *332*, 287-290.

45. Giulivi, C.; Cadenas, E. *Arch. Biochem. Biophys.* **1993**, *303*, 152-158.

46. Iwatsuki, M.; Niki, E.; Stone, D.; Darley-Usmar, V.M. *FEBS* **1995**, *360*, 271-276.

47. Evans, P.J.; Akanmu, D.; Halliwel, B. *Biochem. Pharmacol.* **1994**, *48*, 2173-2179.

48. Trost, L.C.; Wallace, K.B. *Biochem. Biophys. Res. Comm.***1994**, *204*, 30-37.

49. Palinski, W.; Rosenfield, M.E.; Yla-Hertuala, S.; Gurtner, G.C.; Socher, S.S.; Butler, S.W.; Parthasarathy, S.; Carew, T.E.; Steinberg, D.; Witztum, J.L. *Proc. Natl. Acad. Sci.* **1989**, *86*, 1372-1376.

50. Galaris, D.; Edy, L.; Arduini, A.; Cadenas, E.; Hochstein, P. *Biochem. Biophys. Res. Comm.* **1989**, *160*, 1162-1168.

51. Turner, J.J.O.; Rice-Evans, C.A.; Davies, M.J.; Newman, E.S.R. *Biochem. J.* **1991**, *277*, 833-837.

52. Doroshow, J.H.; Locker, G.Y.; Myers, C.E. *J. Clin. Invest.* **1980**, *65*, 128-135.

53. Dunford, H.B. In *Peroxidases in Chemistry and Biology*, Everse, J.; Everse, K.E.; Grisham, M.B. Eds.; CRC Press: Boca Raton, Fl 1991; Vol II, pp 1-24.

54. Miller, M.A.; Vitello, L.; Erman, J.E. *Biochemistry* **1995**, *34*, 12048.

55. Huang, J.; Dunford, H.B. *Can. J. Chem.* **1990**, *68*, 1990.

56. Coulson, A.F.W.; Erman, J.E.; Yonetani, T. *J. Biol. Chem.* **1971**, *246*, 917.

57. Ator, M.A.; Ortiz de Montellano, P.R. *J. Biol. Chem.* **1987**, *262*, 1542.

58. Purcell, W.L.; Erman, J.E. *J. Am. Chem. Soc.* **1976**, *98*, 7033.

59. Crutchley, R. J.; Ellis, W. R. Jr.; Gray, H. B. *J. Am. Chem. Soc.* **1985**, *107*, 5002.

60. Lieber, C. M.; Karas, J. L.; Gray, H. B. *J. Am. Chem. Soc.* **1987**, *109*, 3778.

61. Isied, S. S. In *Electron Transfer in Inorganic, Organic and Biological Systems*, Bolton, J. R.; Mataga, N.; McLendon, G., Eds.; Advances in Chemistry Series No. 228; American Chemical Society: Washington, DC, 1991; pp 229-245.

62. Yocom, K.M.; Shelton, J.B.; Shelton, J.R.; Schroeder, W.A.; Worosila, G.; Ised, S.S.; Bordignon, E.; Gray, H.B. *Proc. Natl. Acad. Sci.* **1982**, *79*, 7052.

63. McLendon, G. *J. Phys. Chem.* **1989**, *93*, 7130.

64. Winkler, J. R.; Gray, H. B. *Chem. Rev.* **1992**, *92*, 369.

65. Jackman, M.P.; McGinnis, J.; Powls, R.; Salmon, A.G.; Sykes, A.G. *J. Am. Chem. Soc.* **1988**, *110*, 5880.

66. Fox, T.; Hazzard, J.T.; Edwards, S.L.; English, A.M.; Poulos, T.L.; Tollin, G. *J. Am. Chem. Soc.* **1990**, *112*, 7426.

67. Gray, H.B.; Winkler, J.R. *Annu. Rev. Biochem.* **1996**, *65*, 537.

68. English, A.M.; Fox, T.; Tsaprailis, G.; Fenwick, C.W.; Wishart, J.F.; Hazzard, J.T.; Tollin, G.; ACS Advances in Chemistry Series, in press

69. Kang, C.H.; Ferguson-Miller, S.; Margoliash, E. *J. Biol. Chem.* **1977**, *252*, 919.

70. Newman, E.S.R.; Rice-Evans, C.A.; Davies, M.J. *Biochem. Biophys. Res. Com.* **1991**, *179*, 1414.

71. Perkins, M.J.; *Advances Phys. Org. Chem.*; Gold, V. and Bethell, D. Eds.**1980**, *17*, 1-64.

72. Bunn, H.F.; Forget, B.G.; In *Hemoglobin: Molecular, Genetic, and Physiological Aspects*; W.B. Saunders Co., Philadelphia, **1986**, pp 634-662.

73. Fenwick, C.; Marmor, S.; Govindaraju, K.; English, A.M.; Wishart, J.F.; Sun, J. *J. Am. Chem. Soc. Com.* **1994**, *116*, 3169.

74. Fenwick, C.W.; English, A.M. *J. Am. Chem. Soc. Com.* **1996**, *118*, 12236.

75. Fenwick, C.W.; English, A.M.; Wishart, J.F. *J. Am. Chem. Soc.* **1997**, *119*, 4758.

2.0 Oxidation of $MbFe^{III}$ by H_2O_2

2.1 Introduction

The formation of the Fe^{IV}=O heme in Mb is believed to follow a mechanism similar to that proposed for heme peroxidases in Chapter 1.[1] However, $MbFe^{III}$ oxidation to $MbFe^{IV}$=O has been reported to require >1 molar equivalent of H_2O_2[2,3] in contrast to peroxidases[4,5] which require 1 molar equivalent for Fe^{IV}=O formation. There is no clear explanation of why $MbFe^{IV}$=O formation requires >1 equivalent of H_2O_2, but experimentation at different pHs has revealed that up to 2 molar equivalents of H_2O_2 are needed under alkaline conditions (pH 8)[6] and 3 molar equivalents under acidic conditions (pH 4.5).[7] The reaction of $MbFe^{III}$ with H_2O_2 is irreversible,[8] and the excess H_2O_2 required for Fe^{IV}=O formation is believed to be consumed in side reactions at the porphyrin or other locations on the globin.[6]

$MbFe^{III}$ has α and β bands at 630 and 502 nm in its visible absorption spectrum, while $MbFe^{IV}$=O exhibits intense charge transfer bands at 546 and 586 nm.[9] Spectroscopic investigation of $MbFe^{III}$ oxidation by H_2O_2 shows that a reaction intermediate with an absorption maximum at 525 nm[10] also exists, and it is proposed to be an unspecified $MbFe^{III}$-(H_2O_2) complex.

The $MbFe^{III}/H_2O_2$ reaction not only forms Fe^{IV}=O, but at pHs under 8.5[2] a green chromophore is formed that absorbs maximally at 586 nm.[10] This chromophore is formed in higher yield under acidic conditions (pH < 6) and the third equivalent of H_2O_2 that reacts with $MbFe^{III}$ has been implicated in the formation of this 586-nm absorbing species which has been linked to oxidative damage to the heme[11,12] and/or protein.[13] The green

chromophore is redox insensitive, being unaffected by the addition of ferrocyanide, and strongly-binding ferrous heme ligands such as CO or NO have no spectral effect.[14] Choleglobin is a pigment identified as one of the $MbFe^{III}/H_2O_2$ reaction byproducts[15] resulting from the oxidative cleavage of the porphyrin ring by peroxides, but it is not the 586-nm absorbing species. Different investigators have also noted that acetone or 2-butanone heme extraction at low pH (<2) fails to remove part of a green chromophore from the globin fraction.[7,11] Analysis of the heme-linked protein was performed by peptide mapping of a Mb sample that had been reacted with H_2O_2 at pH 4.5 to maximize formation of the 586-nm product. HPLC separation of protease-digested Mb revealed several potential heme-linked peptides. Mass analysis of the peptides tentatively identified Tyr103 as a site of heme to polypeptide crosslinking.[11]

Our objective of studying Fe^{IV}=O heme reactivity in Mb by intramolecular electron transfer requires that Fe^{IV}=O formation be complete, and that Fe^{IV}=O be the unique heme product of the $MbFe^{III}/H_2O_2$ reaction under the conditions used. Given the excess consumption of H_2O_2, the reports of protein-based radical formation[16] as well as heme-globin cross-linking, the $MbFe^{III}/H_2O_2$ reaction was studied to establish conditions under which formation of unwanted oxidation byproducts was minimized or eliminated. The methods used to investigate the products of the $MbFe^{III}/H_2O_2$ reaction were HPLC analysis, electrospray mass spectrometry (ESI-MS), and tryptic digestion followed by spectroscopic analysis and mass mapping of the peptides.

Reversed-phase HPLC separates compounds based on hydrophobicity and size.[17] Thus, HPLC analysis of the $MbFe^{III}/H_2O_2$ reaction products was carried out since

chemically altered species should be retained differently on a C18 column from unmodified $MbFe^{III}$. The effects of reduction and acid treatment of $MbFe^{IV}$=O were also investigated since chemical modification and crosslinking were previously observed following $MbFe^{IV}$=O acidification or cyanide treatment.[11] Considering that the globin denatures and the $MbFe^{IV}$=O autoreduction process is faster under acidic conditions (< pH 4.3) as discussed below, the reported heme/globin modifications may have resulted partly from Fe^{IV}=O autoreduction.

ESI-mass spectrometric analysis of the $MbFe^{III}/H_2O_2$ reaction products was used here to probe chemical modification of the globin. ESI-MS is a soft ionization technique which multiply charges an analyte[18] and allows the analysis of samples with molecular weights up to ~150 kDa.[19] A quadrupole mass analyzer was used to determine the mass changes in the $MbFe^{III}/H_2O_2$ products with a resolution of ± 0.01%.[20]

Peptide mapping has become an essential and routine procedure in the analysis of protein samples.[21] Covalently modified peptides can be readily identified by peptide mass mapping which was used here to further probe for internal crosslinking or chemical modification in the $MbFe^{III}/H_2O_2$ reaction products. Trypsin, which cleaves after basic residues (Lys and Arg except when followed by Pro), is the most commonly used protease due to its high specificity,[22] and was used to digest H_2O_2- oxidized and unreacted $MbFe^{III}$. The digested protein samples were separated on a HPLC column and the eluting peptides where analyzed for their absorbance, fluorescence, and/or mass properties. Peptide maps of the $MbFe^{III}/H_2O_2$ reaction products were compared to those of untreated $MbFe^{III}$ to identify peptides with altered spectroscopic properties or changes in mass.

Peptide absorption at 210 and 280 nm corresponds to that of the peptide backbone and aromatic amino acids (Trp and Tyr), respectively,[22] while heme absorbs at 400 nm. Fluorescence detection was used to differentiate between Tyr- and Trp-containing peptides, since both residues have excitation maxima close to 280 nm (λ_{max} values for Tyr and Trp are 274.6 and 279.8 nm, respectively),[22] but have emission maxima at 303 and 348 nm, respectively. The fluorescence of Tyr and Trp residues is also sensitive to modifications that alter their aromatic nature.[22] Mass analysis of the tryptic peptides was carried out, and the observed masses compared to the predicted masses from the globin sequence and the trypsin cleavage sites.

Apart from chemical modification of the heme and globin in the $MbFe^{III}/H_2O_2$ reaction products, protein conformational changes could also affect rates of electron transfer. The secondary structure of Mb as a function of oxidation state and pD was monitored in D_2O by FTIR examination of the amide I' and II regions.[23] The amide I' bands arise from stretching of the peptide backbone C=O groups and appear between 1600 and 1700 cm^{-1}. The υ(C=O) frequency is affected by secondary structure so that features such as α-helix and β-sheet are assigned to characteristic frequencies within the amide I' region.[24,25] Hence, alteration of protein secondary structure can be detected by changes in the amide I' bands. The amide II bands arise from a bending mode involving the peptide N-H groups. Addition of a protein to D_2O allows one to determine if regions of its polypeptide are more flexible under certain experimental conditions, since solvent accessible regions quickly undergo peptide NH⇌ND exchange in D_2O. This results in loss of amide II intensity (N-H bending) between 1525 and 1600 cm^{-1} and an increase in

amide II' intensity (N-D bending) between 1400 and 1490 cm^{-1} in the IR spectrum.[26]

Local conformational changes in the heme pocket of Mb have also been investigated using FTIR. The stretching vibration of the CO ligand bound to the Fe^{II} ion in $MbFe^{II}$-CO gives rise to two major bands at 1965 and 1945 cm^{-1}. These bands have been assigned to linear and bent FeCO conformers, respectively,[27] and steric hinderance and the electrostatic potential[28] created by the distal His64 are mainly responsible for the bent CO conformer being predominant at neutral pH. However, upon protonation of His64 at lower pH, the 1965-cm^{-1} band increases in intensity at the expense of the 1945-cm^{-1} band since the protonated His64 swings out towards the solvent and opens up the heme pocket. Hence, the FTIR CO bands of $MbFe^{II}$-CO were measured in this work at different pH and pD values to investigate solvent accessibility to the heme,[29] since the latter is important in the Fe^{IV}=O reduction process (Chapter 4).

In addition to peroxidase-like activity, Mb has been found to have low levels of catalase,[6] oxidase,[30] and lipoxygenase[31] activities. Some researchers have suggested that the low catalase activity (k_{cat} = 2.5 x 10^{-5} s^{-1}),[6] is responsible for the requirement of >1 molar equivalent of H_2O_2 in the formation of $MbFe^{IV}$=O since Fe^{III} heme is regenerated in the catalase cycle:

$$MbFe^{III} + H_2O_2 \rightarrow Mb^{\bullet}Fe^{IV}=O + H_2O \qquad 2.1a$$

$$Mb^{\bullet}Fe^{IV}=O + H_2O_2 \rightarrow MbFe^{III} + O_2 + H_2O \qquad 2.1b$$

where $Mb^{\bullet}$ is an unidentified radical. The catalase cycle of Mb is not strictly catalytic

since O_2 production is reported to cease as chemically modified Mb accumulates.[6] Reinvestigation of O_2 produced during the $MbFe^{III}/H_2O_2$ reaction was performed with a Clark oxygen electrode to probe Mb catalase activity. Specifically, the amount of O_2 liberated vs $MbFe^{III}/H_2O_2$ stoichiometry was monitored to determine how much H_2O_2 was decomposed via a catalase-like pathway. In addition to measuring O_2 production, the rate of H_2O_2 decomposition during the $MbFe^{III}/H_2O_2$ reaction was measured using the 2,2'-azino-di-(3-ethyl-benzthiazoline-6-sulfonic acid) (ABTS)-peroxidase system.[32,33] ABTS is very slowly oxidized by H_2O_2, but in the presence of a peroxidase, such as horseradish peroxidase (HRP), it is rapidly oxidized to a dark green chromophore [ABTS(ox)]:

$$\underset{\text{pale green}}{2\ \text{ABTS}} + H_2O_2 + 2\ H^+ \xrightarrow{\text{HRP}} \underset{\text{dark green}}{2\ \text{ABTS(ox)}} + 2\ H_2O \qquad 2.2$$

A final concern in investigations of $MbFe^{IV}=O$ redox reactivity is its stability under different experimental conditions. Autoreduction of the $Fe^{IV}=O$ heme in Mb by endogenous donors within the globin has been found to be first order.[6] The autoreduction rates are pH dependant below pH 9.0,[2] and between pH 5 and 7 there is a linear increase in the rate constant with decreasing $[H^+]$.[2] To ensure that intramolecular electron transfer studies were performed before significant $Fe^{IV}=O$ decay had occurred, the loss of $MbFe^{IV}=O$ and the formation of $MbFe^{III}$ due to autoreduction were followed spectrophotometrically to obtain the half-life of $MbFe^{IV}=O$ at a given pH.

2.2 Materials

Horse heart myoglobin and bovine catalase were purchased from Sigma and modified sequencing grade trypsin from Boehringer Mannhein. Buffer salts, acids, sodium ascorbate, and 30% H_2O_2 were obtained from Fisher as were the acetonitrile and trifluoroacetic acid used in the HPLC separations. D_2O (99.9%) was purchased from Aldrich and CO gas (99.3%) was purchased from Union Carbide. Chromatographic separations were performed using C18 columns (1 x 250 mm and 4.6 x 250 mm; Vydac) fitted to a HP 1090 HPLC with a UV/vis diode-array detector or fluorescence detector. Electrospray mass spectrometry was performed on either a Finnigan SSQ 7000 or a Sciex API III. Anaerobic studies were carried out in a MBraun MB 120 glove box fitted with an analog oxygen analyzer. The Clark O_2 electrode and potentiometer were made by the Concordia Science Technical Center. Lyophilizations were performed in a Savant Speedvac. FTIR measurements were taken on a Nicolet 205 FTIR spectrometer equipped with a deuterated triglycerine sulfate (DTGS) detector and purged with dry air. A dismountable IR cell (Model 116) with 13- x 2-mm CaF_2 windows and a 50-μm Teflon spacer were obtained from Wilmad, New Jersey.

2.3 Methods

2.3.1 *Reaction of H_2O_2 with $MbFe^{III}$:* Stock solutions of 100 μM $MbFe^{III}$ (concentrations were determined spectrophotometrically, ε_{409} = 188 $mM^{-1}cm^{-1}$, ε_{502} = 11.6 $mM^{-1}cm^{-1}$)[9] and 100 mM H_2O_2 (from 30% w/v H_2O_2 solution) were prepared in 100 mM phosphate (Pi) buffer at pH 7.0. Spectra of 5 μM $MbFe^{III}$ and $MbFe^{IV}$=O were recorded

in the Pi buffer, using a $MbFe^{IV}=O$ sample that was prepared by reacting 1 mL of $MbFe^{III}$ stock with 5 µL of H_2O_2 stock (1:5 molar ratio) in an Eppendorf tube for 5 min and diluted to 5 µM in a quartz semi-micro cuvette. Absorbances were measured from 250 to 700 nm in a Beckman DU 650 scanning UV/vis spectrophotometer at a scan speed of 600 nm/min.

The reaction of $MbFe^{III}$ with H_2O_2 was studied spectrophotometrically as a function of H_2O_2 concentration. $MbFe^{III}$ stock solution (1 mL) was added to a semi-micro quartz cuvette and 0.5 to 10 µL of H_2O_2 stock (0.5 - 10 molar equivalents) was pipetted onto the inner lip of the cuvette and remained as a drop above Mb solution. The $MbFe^{III}/H_2O_2$ reaction was initiated by covering the cuvette with parafilm and inverting 3 times to thoroughly mix the reactants. The decay of $MbFe^{III}$ (ε_{502} =11.6 $mM^{-1}cm^{-1}$) and the formation of $MbFe^{IV}=O$ (ε_{546} =12.5 $mM^{-1}cm^{-1}$) were followed at 502 and 546 nm, respectively, and the rate constant was calculated for the $MbFe^{III}/H_2O_2$ reactions with 10 molar equivalents of H_2O_2 with the aid of MINSQ Software (Micromath), using pseudo-first-order and two concurrent first-order kinetic analysis.

2.3.2 *pH Dependence of the $MbFe^{III}/H_2O_2$ Reaction:* Stock solutions of 25 µM $MbFe^{III}$ were prepared in 100 mM Pi buffers at pH 7.0, 6.7 and 6.4, and in 0.1 M sodium acetate buffers at pH 6.0, 5.7 and 5.4. A stock solution of 25 mM H_2O_2 was prepared in distilled water. The $MbFe^{III}/H_2O_2$ reaction was initiated on addition of 10-fold molar excess H_2O_2 (10 µL H_2O_2 stock into 1 mL Mb stock) and monitored spectrophotometrically as in Section 2.3.1. The change in absorption vs time was used to calculate the pseudo-first order rate constants for the formation of $MbFe^{IV}=O$ and the

decay of $MbFe^{III}$.

2.3.3 *HPLC Analysis of the $MbFe^{III}/H_2O_2$ Reaction Products:* Stock solutions of 100 μM $MbFe^{III}$ and 100 mM H_2O_2 were prepared in 100 mM Pi buffer at pH 7.0, and 500 μL of the Mb stock was mixed with 20 μL of the H_2O_2 stock (5-fold molar excess H_2O_2) in an Eppendorf tube. The sample was left to stand at room temperature for 4-5 min, and 100-μL aliquots were added to 3 separate Eppendorf tubes and treated as follows: sample 1 was reacted with a catalytic amount of catalase for 5 min, followed by reduction with excess sodium ascorbate for 5 min and acidification with 5 μL of glacial acetic acid (final pH ~3.5); sample 2 was let stand at room temperature for 12 h, followed by acidification with 5 μL of glacial acetic acid; sample 3 was reacted with a catalytic amount of catalase (1 μL of < 0.1 μM catalase) for 5 min, followed by acidification with 5 μL of glacial acetic acid. Procedures 1-3 were carried out to differentiate between chemical modification of Mb caused by formation and decay of the protein-based radicals (sample 1), Fe^{IV}=O autoreduction (sample 2) and acid-catalyzed autoreduction of Fe^{IV}=O (sample 3).

Sample 1-3 and an untreated $MbFe^{III}$ control were analyzed by HPLC. A 20-μL aliquot of each Mb sample was loaded onto a Vydac C18 column (4.6 x 250 mm) at 1 mL/min and eluted using a linear (25-65%) CH_3CN gradient in 0.05% TFA over 30 min. Polypeptide- and heme-containing peaks in the eluate were identified spectrophotometrically by monitoring absorption at 210, 280, and 400 nm.

2.3.4 *ESI-MS Analysis of the $MbFe^{III}/H_2O_2$ Reaction Products:* Analysis of oxidized Mb was performed by either off-line or on-line HPLC mass spectrometry (LC-

MS). The latter allowed desalting, separation and mass analysis of a sample in one step, whereas the former involved HPLC separation of the reaction products as described in Section 2.3.3 and the polypeptide peaks were collected and lyophilized in a Speedvac. The dried samples were re-suspended in a 1:1 methanol/water solution containing 0.5% acetic acid to give ~5-10 μM protein and infused directly into the electrospray source at 1-2 μL/min. For on-line LC-MS analysis, the protein samples (30-100 picomol) were loaded onto a homemade C18 column (1- x 10-mm packed stainless steel tubing) at 80 μL/min and washed with 15% CH_3CN containing 0.05% TFA for 3 min. The protein remained bound to the C18 column until the solvent system was changed to 65% CH_3CN + 0.05% TFA, at which point the column eluate was directly fed into the electrospray source. All the MS data were collected in profile mode, averaged over a minimum of 10 scans and the spectra deconvoluted to reveal the mass of the analyzed protein. Resolution of the quadrupole mass analyzer is ~2000,[19] which is defined by the ability of the MS to distinguish between ions of different mass-to-charge ratios [resolution = $Mass_1$ / ($Mass_1$ - $Mass_2$)]. Samples were also mass analyzed on a Sciex API III ESI-MS using the direct infusion method.

2.3.5 *Analysis of Mb Tryptic Digests:* Digestion was performed on an untreated $MbFe^{III}$ control and on samples 1 to 3 from Section 2.3.3. Before digestion, HPLC separation of the globin from the heme was performed under the conditions given in Section 2.3.3, and protein fractions were lyophilized in a Speedvac and re-suspended in 100 mM $NaHCO_3$, pH 8.0. Digestion was carried out on 10 μM Mb with sequencing grade trypsin (50:1, w/w) at 37°C for 4 h. The reaction was stopped by lowering the pH

to 2 with acetic acid, and a 20-μL aliquot containing ~4 μg of digested Mb was loaded onto a Vydac C18 microbore column (1 x 250 mm) and separated using a linear CH_3CN gradient (0 to 55%) in 0.05% TFA over 90 min. The Mb tryptic peptides separated by HPLC were analyzed by absorbance, fluorescence, and ESI-MS. The absorbance of the HPLC effluent was monitored at 210, 280 and 400 nm on a HP diode-array detector, while the fluorescence was monitored at 303 and 350 nm following excitation at 280 nm on a fluorescence detector (HP 1046a). Mass analysis of the tryptic peptides was performed on a Finnigan SSQ 7000 by feeding the effluent from the HPLC directly into the electrospray source.

2.3.6 *Oxygen Electrode Study of the Catalase Activity of Mb:* Stock solutions of 40 μM $MbFe^{III}$ and 25 mM H_2O_2 were prepared in 100 mM Pi, pH 7.0. A Pt cathode where O_2 was reduced to H_2O_2 was maintained at -0.6 V[34] vs a Ag/AgCl reference electrode. The cathode surface was covered with a drop of O_2 electrolyte solution (Kodak) and a gas permeable teflon membrane (Yellow Springs Instrument Inc.) was secured over the end of the electrode with an o-ring. The electrochemical measurements were carried out in a 2-mL sealed cell with two inlets, one for the electrode assembly, and the other was sealed with a small teflon tube, through which H_2O_2 was introduced with a syringe. A Hoffman clamp was used to crimp the teflon tube closed after each injection of H_2O_2.

Calibration of the electrode was performed with a catalase solution and known concentrations of H_2O_2. The electrochemical cell was filled with 2 mL of a 0.5-μM catalase solution in 100 mM Pi buffer (pH 7.0) and a stir bar was added. The cell was sealed and special care was taken to remove air bubbles from the reservoir. The catalase

solution was stirred at ~120 r.p.m. and a 25-μL gas-tight Hamilton syringe was used to inject 8, 12, 16, and 20 μL of H_2O_2 stock solution successively through the teflon tubing. After each injection, the O_2 produced from the catalase reaction equilibrated between the cell solution and the electrode solution in < 1min. The change in voltage following O_2 production was recorded on a chart recorder and used to prepare a standard curve from which the concentration of O_2 produced during the $MbFe^{III}/H_2O_2$ reaction was determined. A standard curve was prepared each day, and the reaction reservoir was thoroughly washed after standardization to ensure that all the catalase was removed. Before the Mb solutions were analyzed, buffer only was loaded into the cell which was sealed and 20 μL of H_2O_2 added. The cell was deemed free of catalase if no increase in O_2 was detected at the electrode.

Oxygen production during the $MbFe^{III}/H_2O_2$ reaction was monitored following addition of $MbFe^{III}$ stock (2 mL) to the cell. The gas-tight syringe was used to introduce 8, 12, 16, or 20 μL of stock H_2O_2 solution into the stirred $MbFe^{III}$ solution, and the change in cell voltage was recorded. When the reaction had reached completion, as determined by a stable cell voltage, the solution was left stirring for 10 min, and an additional aliquot of H_2O_2 was injected into the cell and the cell voltage recorded again. The additional injection of H_2O_2 monitored O_2 production starting from $MbFe^{IV}=O$ rather than $MbFe^{III}$ since $MbFe^{IV}=O$ had not autoreduced. A fresh $MbFe^{III}$ solution was used for each H_2O_2 concentration and the analyses were carried out in triplicate. The quantity of O_2 produced after each addition of H_2O_2 was determined using the standard curve.

The $MbFe^{III}/H_2O_2$ reaction was also monitored under anaerobic conditions to probe

the effects, if any, of O_2 on Mb catalatic activity. $MbFe^{III}$ and H_2O_2 stock solutions were degassed under Ar for ~ 3 h and experiments were performed under N_2 in a glove box as described above. An oxygen analyzer attached to the glove box monitored < 2 p.p.m. of O_2 in the box during the course of the experiments.

2.3.7 *Rate of H_2O_2 Consumption During the $MbFe^{III}/H_2O_2$ Reaction:* The following stock solutions where prepared in 100 mM Pi buffer (pH 7.0): 200 μM $MbFe^{III}$ (prepared as in Section 2.3.1); 0.1 μM HRP + 200 μM ABTS (ε_{403} = 102.2 $mM^{-1}cm^{-1}$ and ε_{340} = 360 $mM^{-1}cm^{-1}$, respectively);[35,32] 200 μM ABTS; and 1 mM H_2O_2 (from 30% H_2O_2 solution). The $MbFe^{III}/H_2O_2$ reaction was initiated by pipetting 0.5 mL of H_2O_2 stock solution into 0.5 mL $MbFe^{III}$ in an Eppendorf tube and gently vortexing. Aliquots (50 μL) of the reaction mixture were removed at 10-s intervals, diluted to 1 mL in a quartz semi-micro cuvette containing HRP + ABTS or ABTS only. The formation of ABTS(ox) was monitored spectrophotometrically (ε_{730nm} = 12,950 $M^{-1}cm^{-1}$).[32] The absorbance difference at 730 nm in the presence and absence of HRP allowed the concentration of H_2O_2 remaining in the Eppendorf tube to be determined vs time.

2.3.8.1 *FTIR analysis of $MbFe^{III}$ and $MbFe^{IV}$=O Secondary Structure* : A solution of 3 mM Mb was prepared (ε_{409} = 188 $mM^{-1}cm^{-1}$) in 100 mM Pi buffer in D_2O and the pD adjusted to 7.4 assuming pD = pH (measured) + 0.4.[36] $MbFe^{IV}$=O was prepared by reacting 20 μL of Mb stock with 1 μL of 60 mM H_2O_2 stock in D_2O. Unreacted H_2O_2 was removed after 3 min with the addition of a catalytic amount of catalase (1 μL of ~1 μM catalase in D_2O buffer) and the final Mb concentration was adjusted to 2.5 mM . For secondary structure comparison the $MbFe^{III}$ stock was also adjusted to 2.5 mM and ~5 μL

of $MbFe^{III}$ or $MbFe^{IV}$=O solution was loaded into the IR cell between two CaF_2 windows separated by a 50-μm Teflon spacer. The FTIR spectra presented are averages of 500 scans recorded at a resolution of 2 cm^{-1} and a scan rate of ~ 1/s. Analysis of $MbFe^{III}$ secondary structure as a function of pD was also performed as described above. $MbFe^{III}$ solutions (3 mM) were prepared in 100 mM Pi at pD 7.0 and 6.5, and in 100 mM sodium acetate at 6.0, 5.7 and 5.3. All samples prepared in D_2O were left to equilibrate at room temperature overnight.

2.3.8.2 *FTIR Analysis of $MbFe^{II}$-CO as a Function of pH and pD*: $MbFe^{II}$-CO was prepared by passing CO gas over 25 μL of $MbFe^{III}$ in a sealed Eppendorf tube for 5-10 min, followed by the addition of < 1 μL of saturated dithionite solution (prepared anaerobically and buffered to match the pH/D of the $MbFe^{III}$ solution). FTIR measurements were taken within 30 min of formation of $MbFe^{II}$-CO using the procedure given in Section 2.3.8.1.

2.3.9 *Rate of $MbFe^{IV}$=O Autoreduction as a Function of pH*: Stock solutions of 200 μM $MbFe^{III}$ and 0.1 M H_2O_2 were prepared in 50 mM Pi buffer at pH 7.0. $MbFe^{IV}$=O autoreduction was investigated in 100 mM Pi at pH 7.0, 6.5 and 6.2, and in 100 mM acetate at pH 5.9 and 5.6. $MbFe^{IV}$=O was formed by reacting 1 mL of Mb stock with 10 μL of H_2O_2 stock (5 molar equivalents of H_2O_2) for 5-6 min and unreacted peroxide was removed with a catalytic amount of catalase (Section 2.3.3). The $MbFe^{IV}$=O sample was diluted to 5 μM in the appropriate buffer and absorbance changes due to the formation of $MbFe^{III}$ and decay of $MbFe^{IV}$=O at 409 and 421 nm, respectively, were used to monitor the autoreduction process. First-order rate constants were calculated from the

absorption data with MINSQ Software (Micromath). Autoreduction of the Fe^{IV}=O center formed in the reaction of $MbFe^{III}$ with 0.5 molar equivalents of H_2O_2 was also monitored (Section 2.3.1) since $MbFe^{IV}$=O was observed to decay more quickly in the presence of $MbFe^{III}$.

2.4 Results

2.4.1-*Reaction of H_2O_2 with $MbFe^{III}$:* The Soret maxima of $MbFe^{III}$ and $MbFe^{IV}$=O are at 409 nm and 421 nm, respectively (Figure 2.1). The visible absorption region shows the α, β bands of $MbFe^{III}$ at 502 and 630 nm and charge transfer bands of $MbFe^{IV}$=O at 546 and 586 nm (Figure 2.2).

The reaction of $MbFe^{III}$ with H_2O_2 resulted in $MbFe^{III}$ decay and $MbFe^{IV}$=O formation. The % formation of $MbFe^{IV}$=O vs H_2O_2/$MbFe^{III}$ ratio is shown in Figure 2.3 and listed in Table 2.1 together with the % decay of $MbFe^{III}$. At 0.5 and 1 molar ratios of H_2O_2/$MbFe^{III}$ the % decay of $MbFe^{III}$ was consistently smaller that the % formation of $MbFe^{IV}$=O. This discrepancy may be caused by the formation of a reaction intermediate[10] that spectrophotometrically resembles $MbFe^{III}$ and results from its reaction with 1 molar equivalent of H_2O_2, rather than the 2 molar equivalents necessary for $MbFe^{IV}$=O formation. Complete formation of $MbFe^{IV}$=O (~99%) was observed with ≥ 5-fold molar excess H_2O_2 in the $MbFe^{III}$/H_2O_2 reaction. The data for the reaction at 10-fold molar excess of H_2O_2 with 100 μM $MbFe^{III}$ appear to be well fit by pseudo-first-order kinetics for both Fe^{IV}=O formation and Fe^{III} decay. However, the second-order rate constants calculated for $MbFe^{III}$ decay are consistently smaller (k_2 = 147 ± 6 $M^{-1}s^{-1}$) than those for

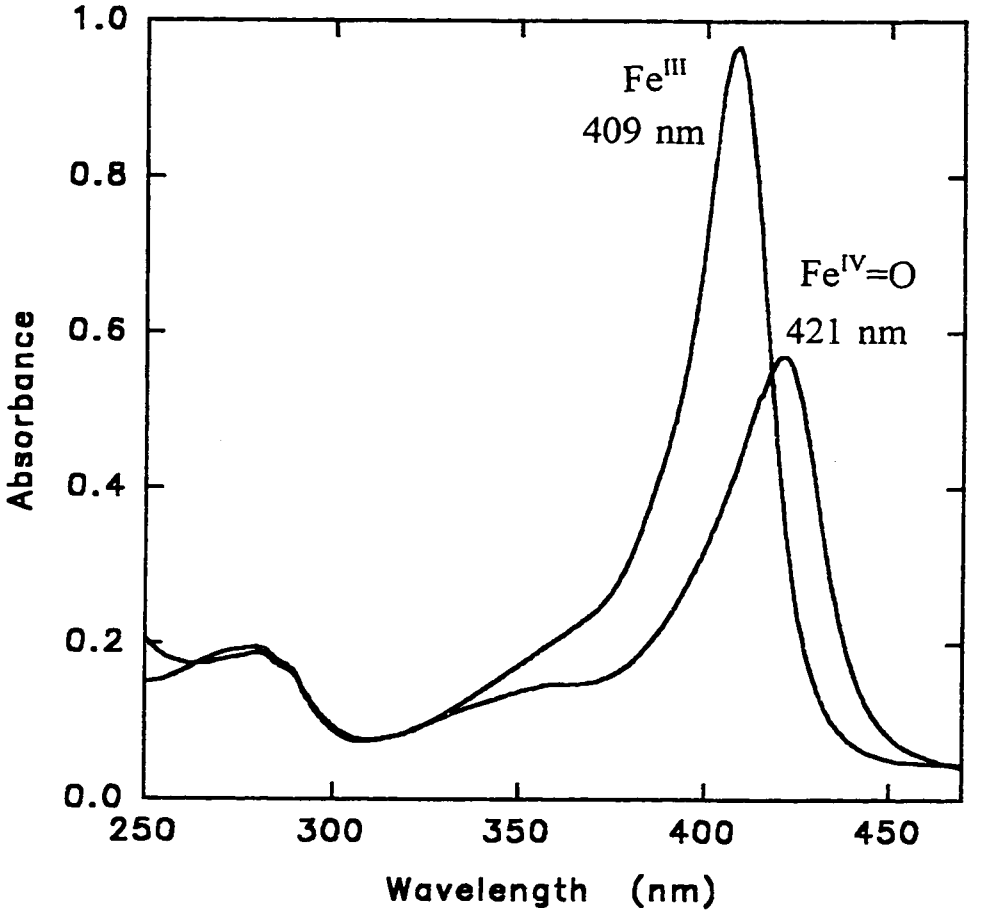

Figure 2.1 Soret absorption spectra of 5 μM $MbFe^{III}$ and $MbFe^{IV}$=O in 100 mM phosphate buffer, pH 7.0.

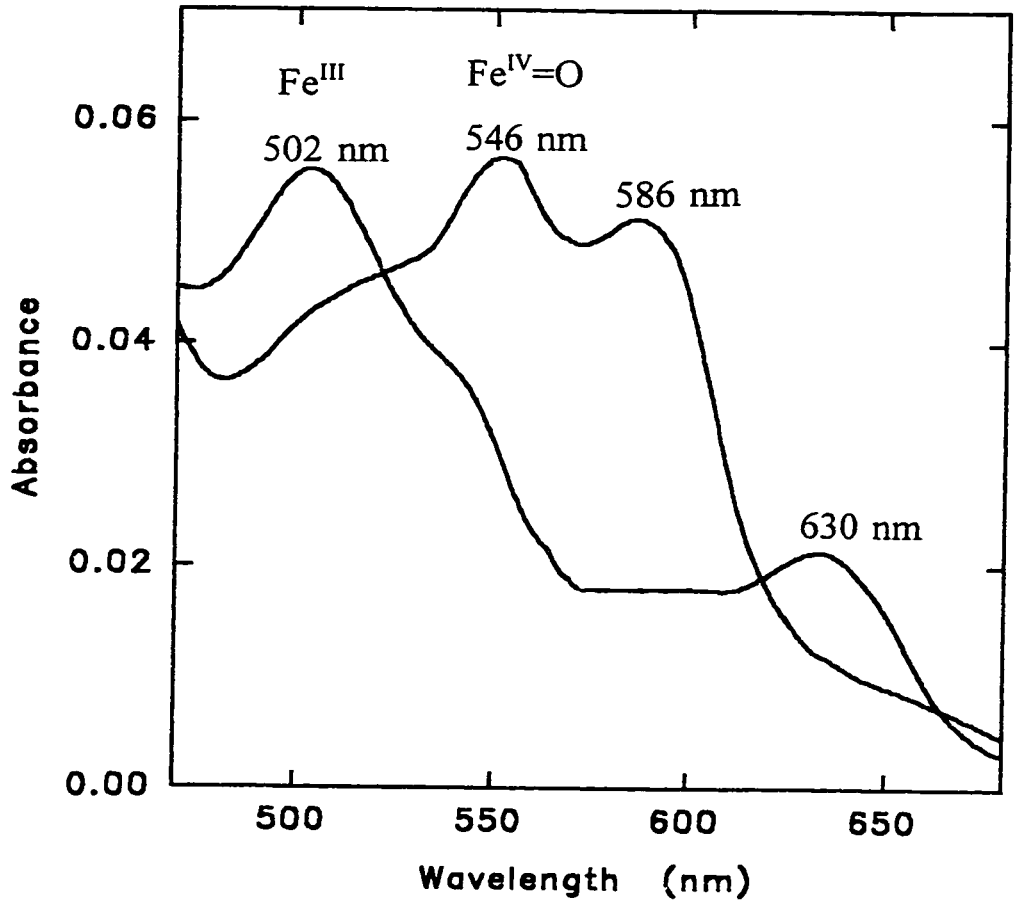

Figure 2.2 Visible absorbance spectra of 5 μM $MbFe^{III}$ and $MbFe^{IV}$=O in 100 mM phosphate buffer, pH 7.0.

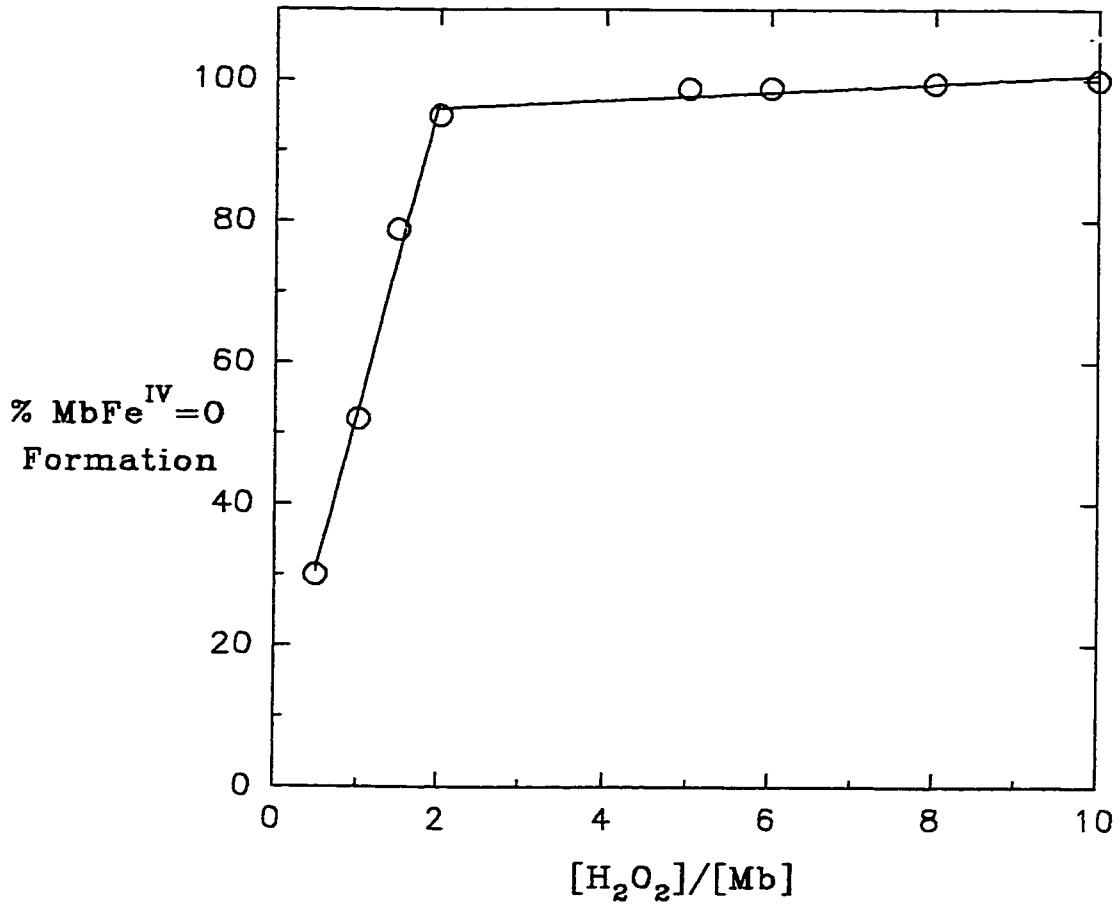

Figure 2.3 The % MbFe^{IV}=O formed on reaction with different molar ratios of H_2O_2. 100 µM MbFe^{III} was reacted with 0.5 to 10 molar equivalents of H_2O_2 and the % MbFe^{IV}=O formation was determined from the absorbance change at 546 nm (Figure 2.2).

Figure 2.4 Analysis (solid lines) of the $MbFe^{III}/H_2O_2$ reaction by pseudo first-order kinetics (a) and by two concurrent first-order processes (b). $MbFe^{III}$ (100 μM) was reacted with 10 molar equivalents of H_2O_2 and the reaction was followed by measuring $MbFe^{IV}$=O formation at 546 nm and $MbFe^{III}$ decay at 502 nm (dots).

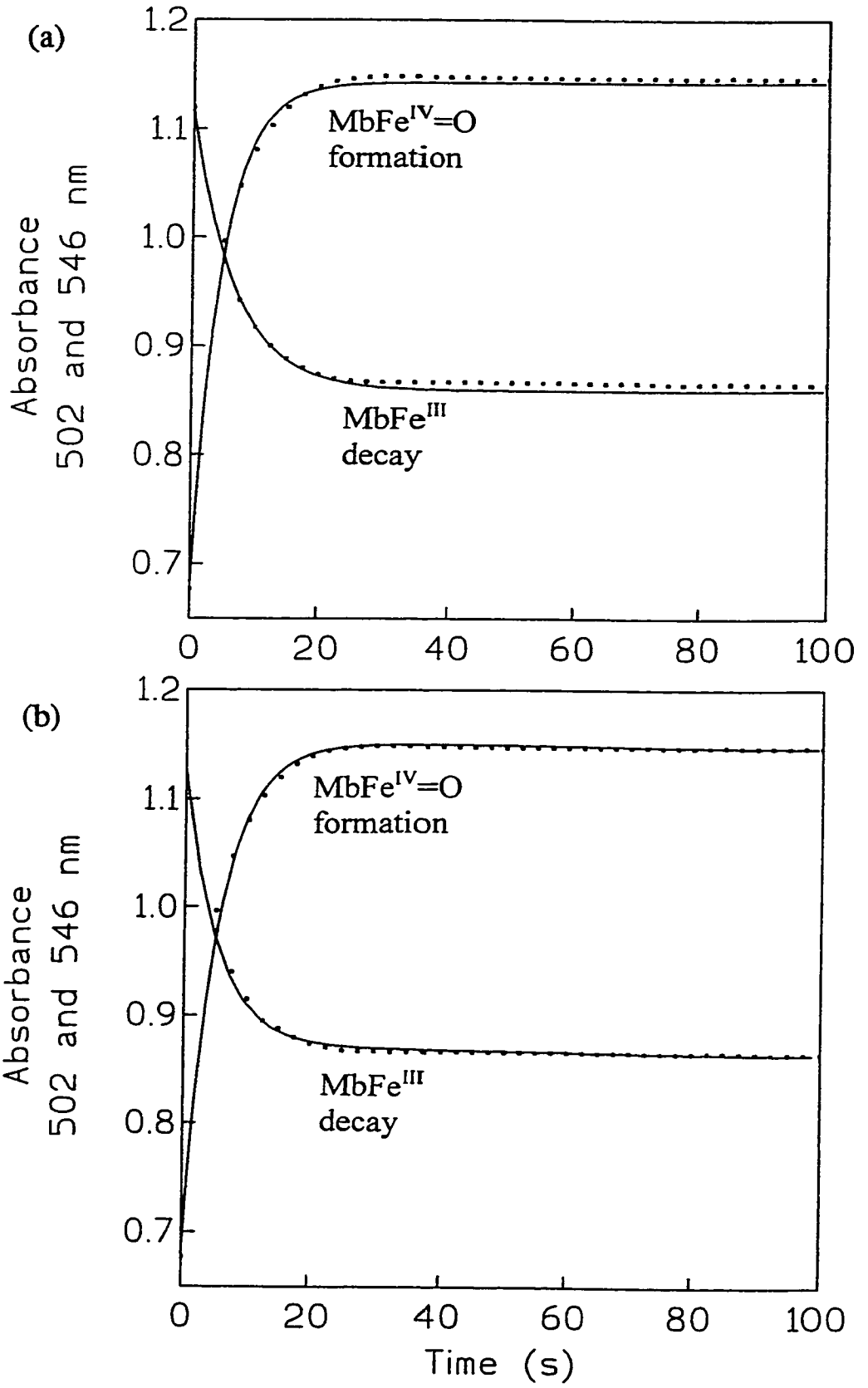
(a)
1.2
1.1
1.0
0.9
0.8
0.7
Absorbance
502 and 546 nm
MbFe^{IV}=O
formation
MbFe^{III}
decay
0
20
40
60
80
100
(b)
1.2
1.1
1.0
0.9
0.8
0.7
Absorbance
502 and 546 nm
MbFe^{IV}=O
formation
MbFe^{III}
decay
0
20
40
60
80
100
Time (s)

$MbFe^{IV}=O$ formation (k_2 = 215 ± 7 $M^{-1}s^{-1}$). Reanalysis of the data assuming that two concurrent first-order processes are occurring gives a better fit to the experimental data than fitting by a single first-order process (Figures 2.4a vs 2.4b). The faster component yields similar bimolecular rate constants for $MbFe^{IV}=O$ formation (k_2 = 200 $M^{-1}s^{-1}$) and $MbFe^{III}$ (k_2 = 195 $M^{-1}s^{-1}$) decay. The slower first-order process (k_1 = 0.004 s^{-1}), which has 10% of the amplitude (determined by comparing the total absorbance change at 502 and 546 nm for each process) of the faster component, is ascribed to a H_2O_2-linked process that results in decay of heme absorption as discussed in Section 2.5. The literature second-order rate constant for $MbFe^{IV}=O$ formation is 210 $M^{-1}s^{-1}$, which was calculated from rate data obtained in the presence of 10 - 20 molar excess of H_2O_2.[7] As expected only the rate data from the formation of $Fe^{IV}=O$ in the presence of 10-fold molar excess H_2O_2 yields a k_2 close to the literature value.

2.4.2 *pH Dependence of $MbFe^{III}/H_2O_2$ Reaction*: The curves for the decay of $MbFe^{III}$ and the formation of $MbFe^{IV}=O$ in the presence of 10-fold molar excess H_2O_2 at pH 7 and 5.4 are shown Figure 2.5. The kinetics were analyzed in terms of two concurrent first-order processes (Section 2.4.1) and the bimolecular rate constants derived from the major, faster phase between pH 7.0 and pH 5.4 are listed in Table 2.2 for $Fe^{IV}=O$ formation and Fe^{III} decay. The data reveal that there is no change in either the rate of the bimolecular reaction between $MbFe^{III}$ and H_2O_2 (Table 2.2), or in the slower first-order process (k_1 ≈ 0.001 s^{-1}) in the pH range from 7.0 to 5.4.

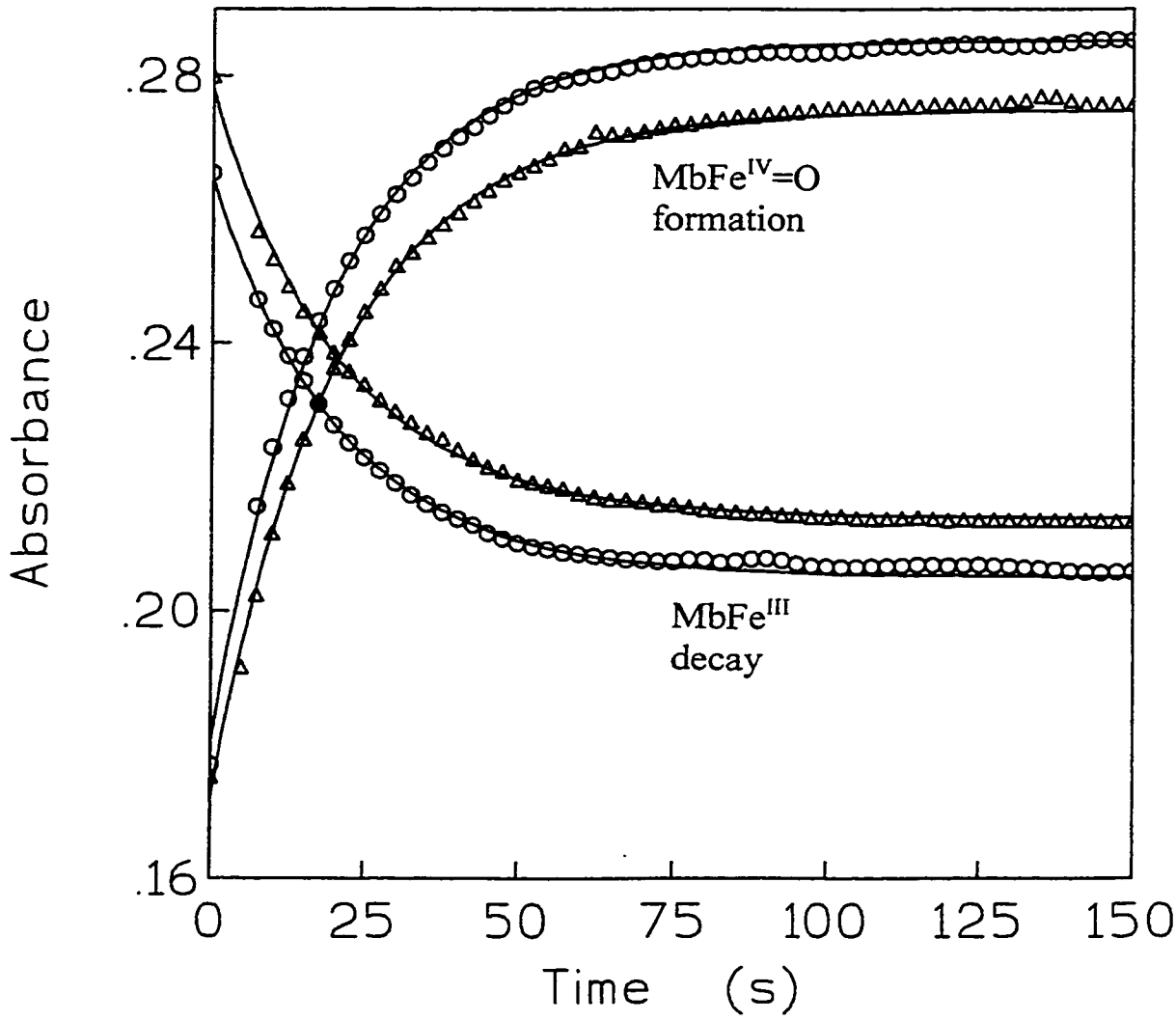

Figure 2.5 Observed absorbance change at 546 nm (Fe^{IV}=O formation) and 502 nm (Fe^{III} decay) vs time following addition of 10 molar equivalents of H_2O_2 to 25 μM $MbFe^{III}$ at pH 7.0 (O) and 5.4 (Δ). The curves are offset from one another for clarity. The solid lines show the fit of the experimental points by two concurrent first-order kinetic processes.

Table 2.1 % formation of $MbFe^{IV}=O$ with different molar ratios of H_2O_2 in the $MbFe^{III}/H_2O_2$ reaction[a]

H_2O_2/Mb Molar Ratio	% $MbFe^{III}$ decay (502 nm)	% $MbFe^{IV}=O$ Formation (546 nm)
0.5	25.6 %	33.0 %
1	48.5 %	56.7 %
1.5	78.7 %	78.8 %
2	95.4 %	94.5 %
5	98.8 %	98.5 %
6	98.9 %	98.7 %
8	99.5 %	99.5 %
10	100 %	100 %

[a] 100 μM $MbFe^{III}$ was reacted with different molar ratios of H_2O_2 in 0.1 M phosphate buffer, pH 7, at 25 °C. The decay of $MbFe^{III}$ and formation of $MbFe^{IV}=O$ were followed spectrophotometrically at 502 and 546 nm, respectively (Figure 2.2).

Table 2.2 Second-order rate constants for the reaction of $MbFe^{III}$ with 10 molar equivalents of H_2O_2 at different pH values[a]

pH	k_2 $(M^{-1}s^{-1})$[b] $MbFe^{III}$ Decay	k_2 $(M^{-1}s^{-1})$[b] $MbFe^{IV}$=O Formation
7.0	192	196
6.7	186	196
6.4	194	192
6.0	180	193
5.7	185	192
5.4	186	186

[a] 25 μM $MbFe^{III}$ in 100 mM Pi at pH 7.0, 6.7 and 6.4 and in 100 mM sodium acetate at pH 6.0, 5.7, 5.4 was reacted with 10 molar equivalents of H_2O_2. The decay of $MbFe^{III}$ and the formation of $MbFe^{IV}$=O were followed spectrophotometrically at 502 and 546 nm, respectively. The kinetic data were fitted by two concurrent first-order processes, and the faster process was assigned to the initial reaction of $MbFe^{III}$ with H_2O_2 which generates the Fe^{IV}=O heme.

[b] The average k_2 is 190 ± 4 $M^{-1}s^{-1}$ at all pHs for both $MbFe^{III}$ decay and $MbFe^{IV}$=O formation.

2.4.3 *HPLC Analysis of the $MbFe^{III}/H_2O_2$ Reaction Products:* $MbFe^{III}$ samples were reacted with 5-fold molar excess H_2O_2 as outlined in Section 2.3.3. The HPLC chromatograms for untreated $MbFe^{III}$ and the $MbFe^{III}/H_2O_2$ reaction products (samples 1 to 3; Section 2.3.3) are shown in Figures 2.6 to 2.9. A 280-nm peak at 16.4 min is observed in the chromatogram of untreated $MbFe^{III}$ corresponding to the globin, and a separate 400-nm peak for the heme appears at 20.5 min (Figure 2.6). Sample 1 has an identical elution profile to untreated $MbFe^{III}$ with the globin and heme fractions eluting at 16.4 and 20.5 min, respectively (Figure 2.7). Samples 2 and 3 also have major peaks at 16.4 and 20.5 min; however, there are at least five new minor heme-containing peaks that absorb at 400 nm, and these are eluted at 13.8, 15.5, 16.4, 17.2, and 17.6 min (Figures 2.8 and 2.9). Monitoring absorbance at 280 nm shows that samples 2 and 3 have at least three separate globin peaks at 16.4, 16.8, and 17.6 min, while the low 280-nm absorbance at 20.5 min is attributed to heme only. However, heme is co-eluted with globin at 16.4 and 17.6 min and these peaks correspond, respectively, to ~1% and 8 % of the total heme in sample 2, and 2% and 15% of the heme in sample 3.

2.4.4 *ESI-MS Analysis of the $MbFe^{III}/H_2O_2$ Reaction Products:* The results of MS analysis of untreated $MbFe^{III}$ and samples 1-3 are summarized in Table 2.3. The deconvoluted mass spectra[37] of sample 1 and untreated $MbFe^{III}$ (Figure 2.10) contain only one peak at mass 16950, which corresponds to the mass of native globin. The deconvoluted mass spectra of samples 2 and 3 also exhibit a peak at mass 16950, which corresponds to ~80-95% of the sample as calculated from the peak intensities. However, accurate quantitation cannot be performed by ESI-MS since peak intensities depend upon

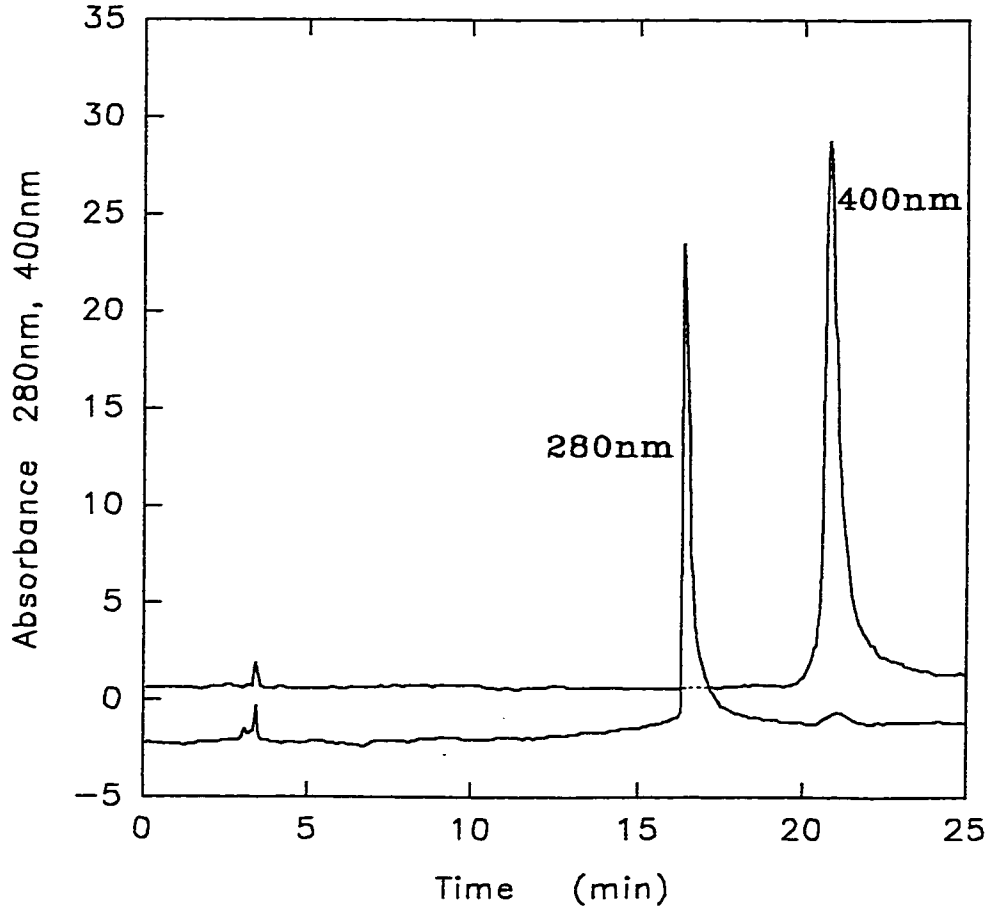

Figure 2.6 Separation of $MbFe^{III}$ by reversed phase C18 HPLC. The Mb components were separated using a linear CH_3CN gradient (25-65 % CH_3CN + 0.05% TFA) over 30 min with the elution monitored at 280 and 400 nm.

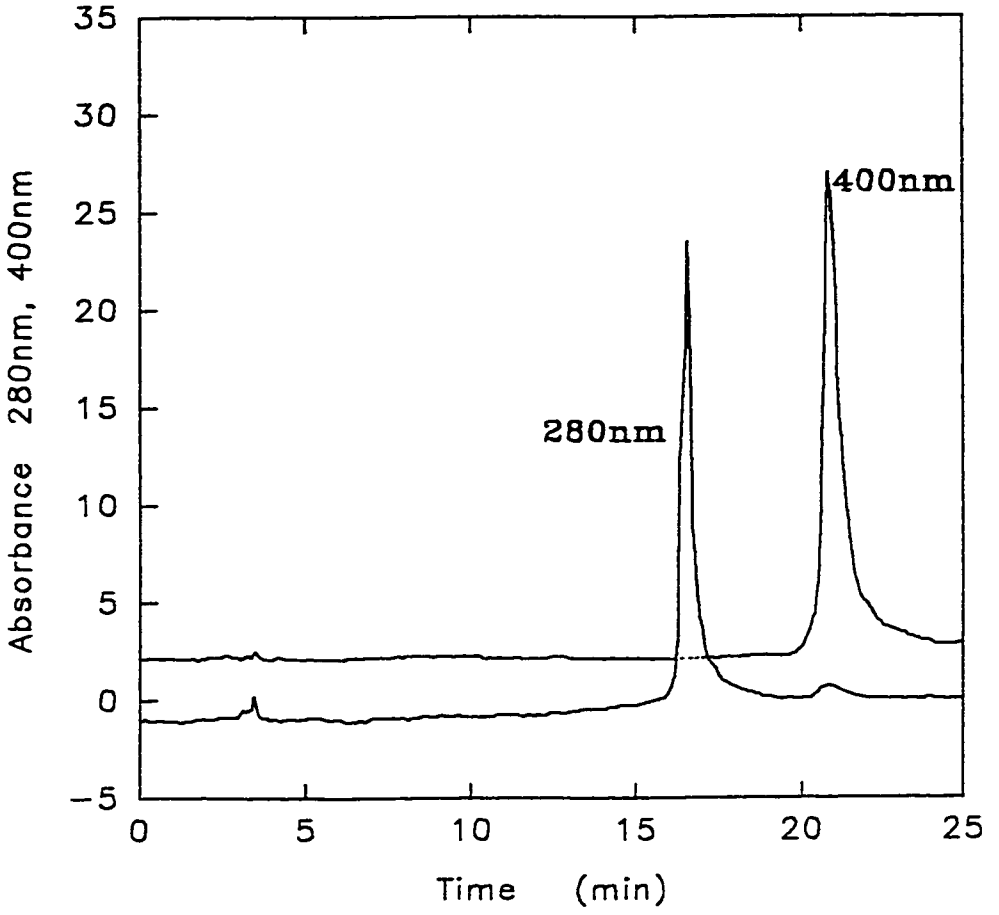

Figure 2.7 Separation of sample 1 by reversed phase C18 HPLC. Sample 1 was formed by reacting $MbFe^{III}$ with 5-fold molar excess of H_2O_2 for ~5 min, followed by catalase addition, reduction with ascorbate, and acidification to pH 3.5. HPLC separation was performed as in Figure 2.6.

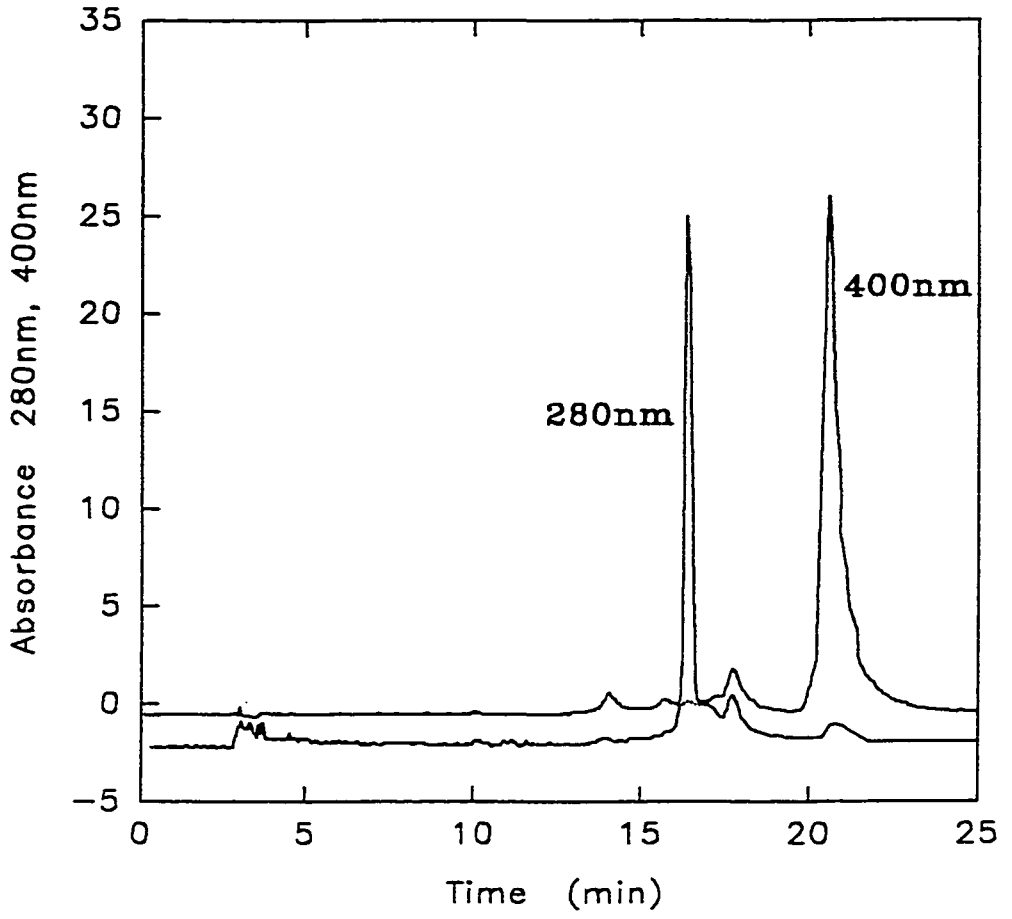

Figure 2.8 Separation of sample 2 by reversed phase C18 HPLC. Sample 2 was formed by reacting $MbFe^{III}$ with 5-fold molar excess of H_2O_2 for ~5 min, followed by the addition of catalase, and autoreduction of the Fe^{IV}=O center overnight at room temperature. HPLC separation was performed as in Figure 2.6.

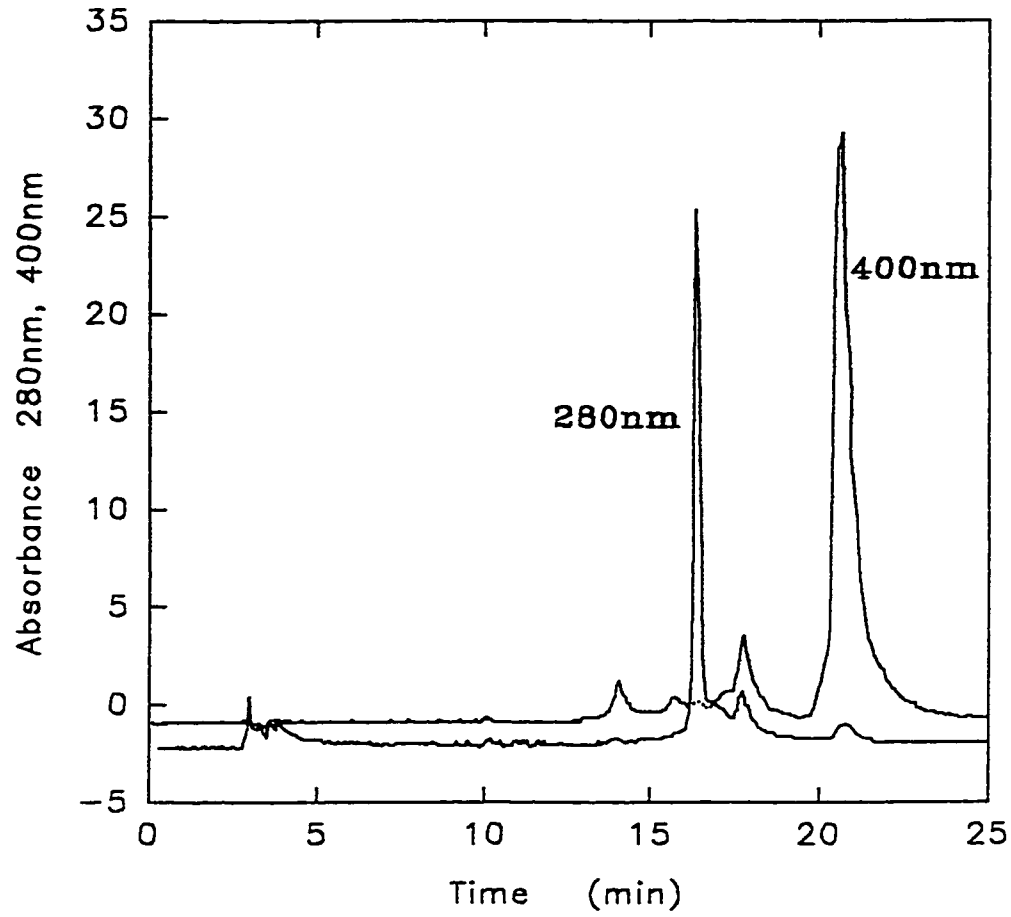

Figure 2.9 Separation of sample 3 by reversed phase C18 HPLC. Sample 3 was formed by reacting $MbFe^{III}$ with 5-fold molar excess of H_2O_2 for ~5 min, followed by catalase addition, and acidification to pH 3.5 with acetic acid. HPLC separation was performed as in Figure 2.6.

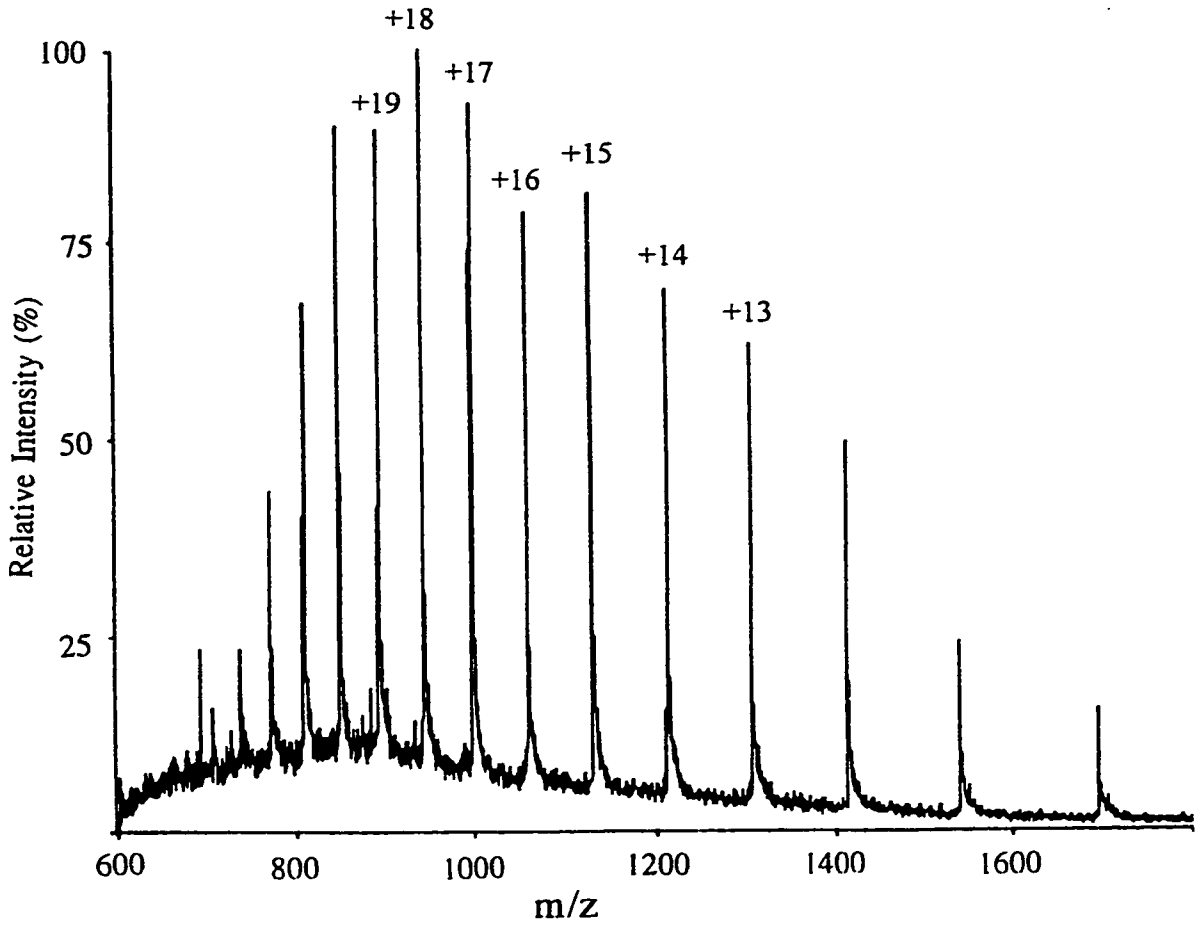

Figure 2.10 ESI mass spectrum of untreated $MbFe^{III}$. MS was performed by direct infusion in methanol/H_2O + 5% acetic acid. The charge state of the individual peaks are labeled and the deconvoluted mass of the globin was calculated to be 16950 Da.

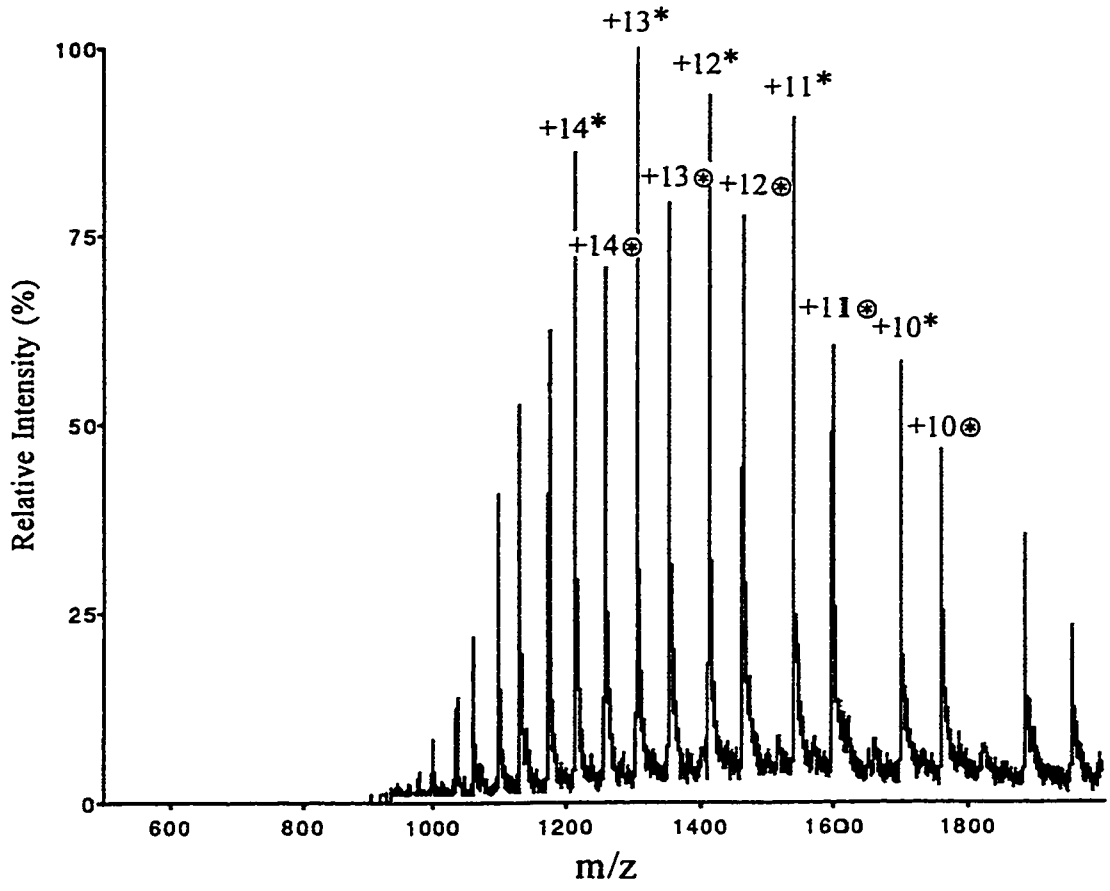

Figure 2.11 ESI mass spectrum of a 50:50 mixture of 16.4- (mainly unmodified globin) and 17.6-min (globin + heme species) sample 3 HPLC peaks from Figure 2.9. MS was performed by direct infusion of the sample in a CH_3CN/H_2O + 5% acetic acid solution. The charge state of the individual peaks are labeled with * and ● identifying the globin (16950 Da) and heme/globin crosslinked species (17583 Da), respectively.

Table 2.3 ESI-MS analysis of untreated $MbFe^{III}$ and the $MbFe^{III}/H_2O_2$ reaction products (samples 1-3)[a]

Protein	Mass (Da)	Assignment
Untreated $MbFe^{III}$	16950	globin
Sample 1	16950	globin
Sample 2	16950 16966 17583	globin globin + oxygen globin + oxygen + heme
Sample 3	16950 16966 17583	globin globin + oxygen globin + oxygen + heme

[a] MS analysis was performed by direct infusion of ~30-100 pmol of desalted protein or by on-line LC-MS (Section 2.3.4). The $MbFe^{III}/H_2O_2$ reaction products (samples 1-3) were treated as outlined in Section 2.3.3

the relative charging capacity of different analytes.[38] Minor peaks were also observed in the spectra of samples 2 and 3 at mass 16966 and 17583 Da, and were assigned to Mb + oxygen and Mb + heme + oxygen, respectively (Table 2.3). The mass spectrum of a 50:50 mixture of the 16.4- and 17.6-min HPLC peaks from sample 3 (Section 2.4.3; Figure 2.9) reveals two major species with masses of 16950 and 17583 Da (Figure 2.11).

2.4.5 *Analysis of Tryptic Digests of Untreated $MbFe^{III}$ and $MbFe^{III}/H_2O_2$ Reaction Products (Samples 1-3):* The tryptic digests of untreated $MbFe^{III}$ and those of samples 1 to 3 gave identical HPLC elution profiles as monitored at 210 and 280 nm (Figures 2.12 to 2.15). However, heme co-eluted with the *undigested* Mb peak at 110 min in samples 2 and 3 (400-nm absorption not shown in Figures 2.14 and 2.15), but not in sample 1 nor in untreated $MbFe^{III}$. The elution profiles as monitored by emission at 303 nm and 350 nm, corresponding to Tyr and Trp fluorescence, respectively, were identical in all four samples. LC-MS mass analysis of the tryptic digests confirmed that none of the $MbFe^{III}/H_2O_2$ reaction products possessed peptides with altered mass. However, a 17582-Da peak co-eluted with undigested globin (16950 Da) in samples 2 and 3 and is assigned to a globin-heme crosslinked species with an additional oxygen (Table 2.3).

2.4.6 *Oxygen Electrode Study of the Catalase Activity of Mb:* The increase in oxygen concentration ($\Delta[O_2]$) during the turnover of H_2O_2 by 40 μM $MbFe^{III}$ and by previously-oxidized $MbFe^{III}$ ($MbFe^{IV}$=O, Section 2.3.5) is listed in Table 2.4. The results are the average of experiments performed under aerobic and anaerobic conditions, since the $\Delta[O_2]$ values were found to be identical. In catalase decomposition of H_2O_2, 1 mol of O_2 is produced per 2 mol of H_2O_2 consumed (reaction 2.1 a and b). Figure 2.16 shows the relation between the moles of H_2O_2 converted into O_2 for the $MbFe^{III}/H_2O_2$ and $MbFe^{IV}$=O/H_2O_2 reactions. As can be seen from this figure, there is a linear relationship between the moles of H_2O_2 reacted with $MbFe^{III}$ or $MbFe^{IV}$=O, and the moles of H_2O_2 converted to O_2. The x-intercepts in Figure 2.16 show that 81 and 2 μM H_2O_2 are not

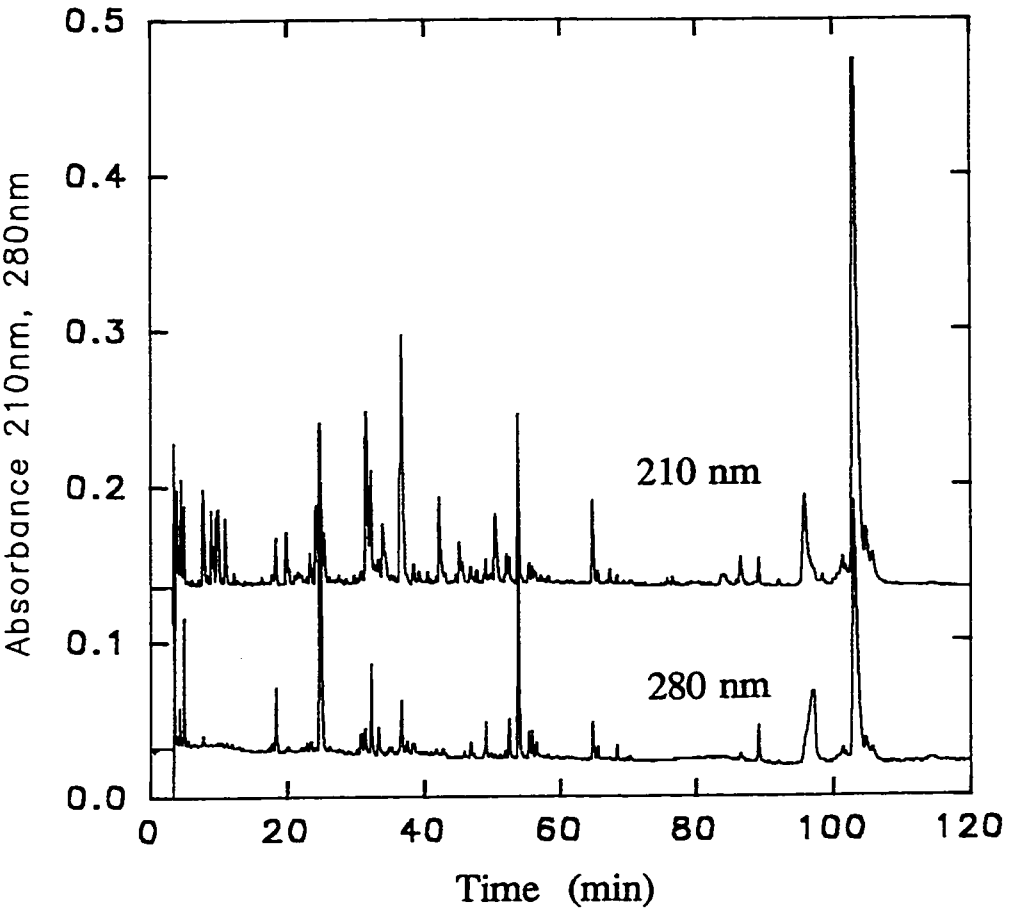

Figure 2.12 Separation of tryptic digested $MbFe^{III}$ by reversed phase C18 HPLC. Digestion was performed with a 1:50 (w/w) trypsin to Mb solution in 100 mM $NaHCO_3$ (pH 8.0) at 37 °C for 4 h. The Mb peptides were separated using a linear CH_3CN gradient (0 to 55% CH_3CN + 0.05% TFA) over 90 min, and the eluate was monitored at 210, 280 and 400 nm (latter not shown for clarity).

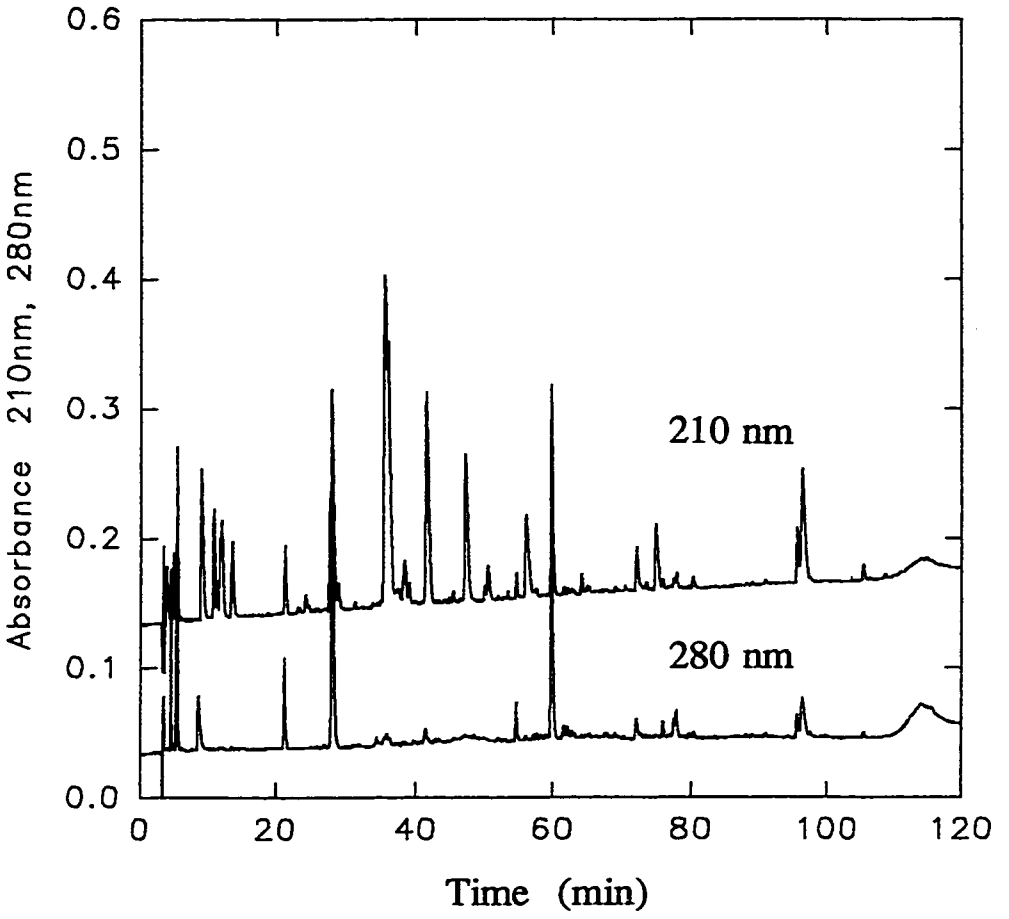

Figure 2.13 Separation of tryptic digested $MbFe^{IV}=O$ sample 1 by reversed phase C18 HPLC. Mb sample was digested and separated as indicated in Figure 2.12.

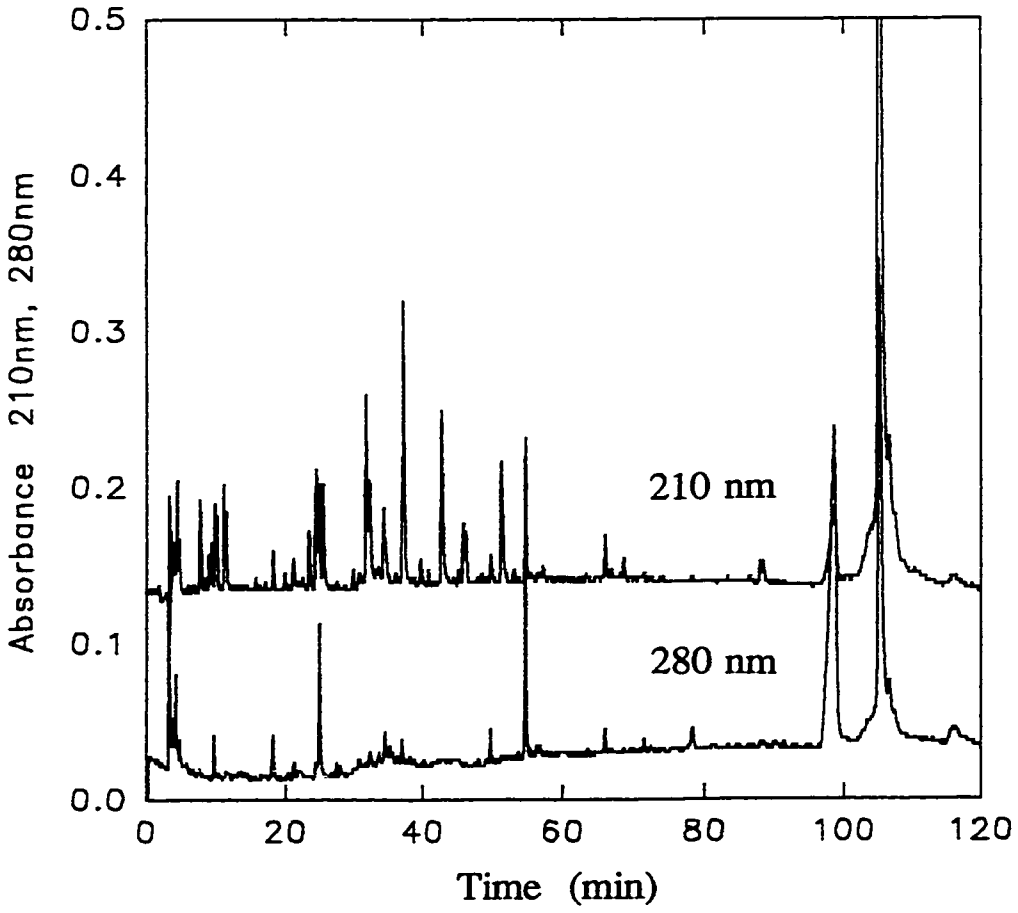

Figure 2.14 Separation of tryptic digested MbFe^{IV}=O sample 2 by reversed phase C18 HPLC. Mb sample was digested and separated as indicated in Figure 2.12.

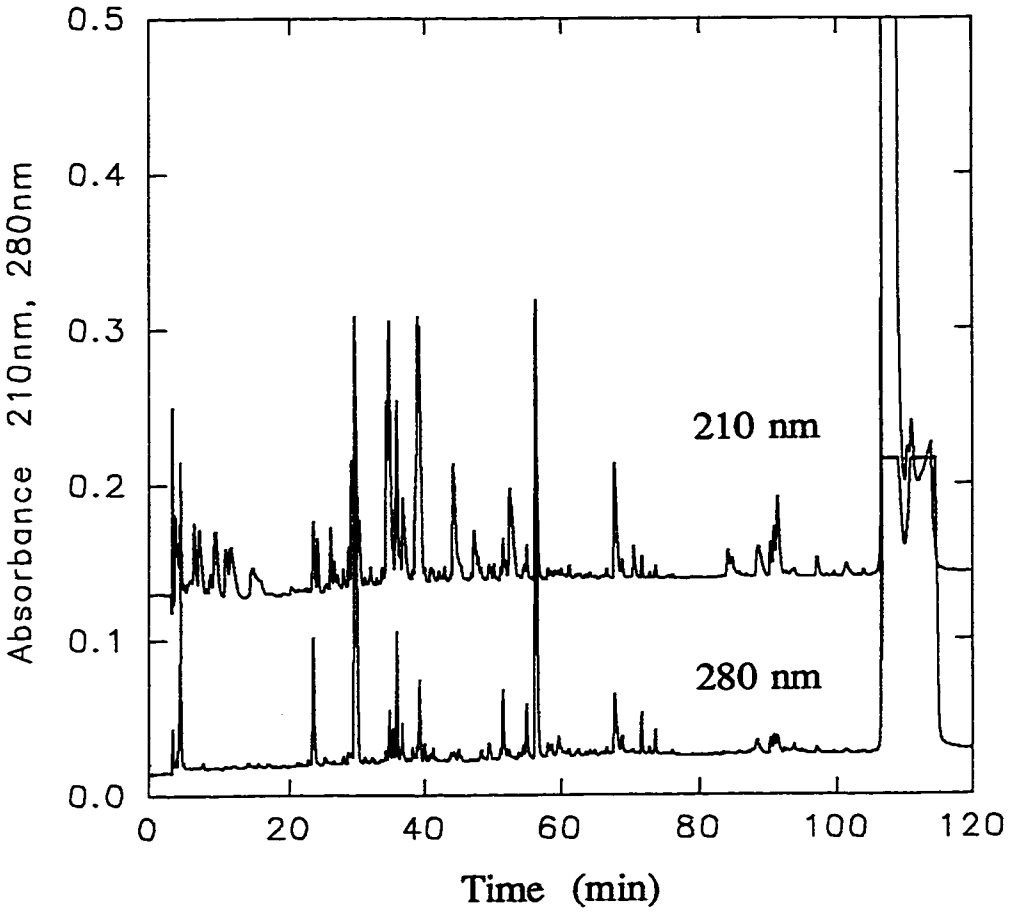

Figure 2.15 Separation of tryptic digested $MbFe^{IV}=O$ sample 3 by reversed phase C18 HPLC. Mb sample was digested and separated as indicated in Figure 2.12.

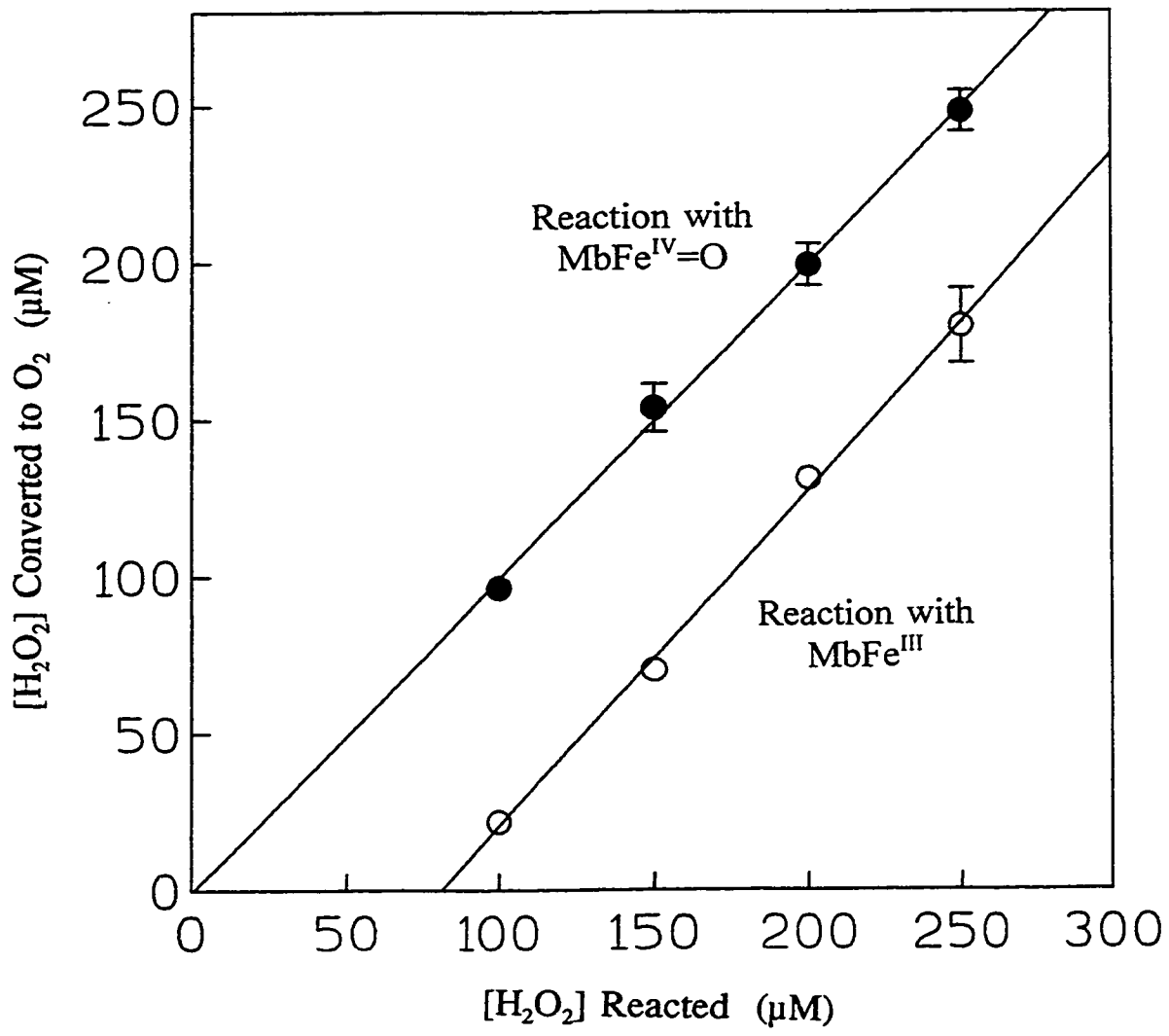

Figure 2.16 Oxygen electrode monitoring of the catalase-like activity in Mb. Plots show the amount of H_2O_2 converted to O_2 in the presence of 40 μM $MbFe^{III}$ (O) and $MbFe^{IV}$=O (●) vs the concentration of H_2O_2 added to the reaction.

converted to O_2 by $MbFe^{III}$ and $MbFe^{IV}$=O, respectively. Since 40 μM Mb was present in solution, this reveals that 2 mol of H_2O_2 are required to "prime" the catalase activity of $MbFe^{III}$, but $MbFe^{IV}$=O is already primed and decomposes H_2O_2 via catalase activity only.

Table 2.4 Oxygen production from the catalase activity of $MbFe^{III}$ and $MbFe^{IV}$=O[a]

$[H_2O_2]$ added (μM)	$\Delta[O_2]$ (μM) produced in H_2O_2 turnover by $MbFe^{III}$	$\Delta[O_2]$ (μM) produced in H_2O_2 turnover by $MbFe^{IV}$=O
100	11.9 ± 1.6	48.2 ± 1.9
150	35.1 ± 0.6	76.9 ± 3.9
200	65.7 ± 1.3	99.7 ± 3.3
250	89.9 ± 2.9	124.1 ± 3.3

[a] Turnover of H_2O_2 by 40 μM Mb in 100 mM Pi (pH 7.0) at 25 °C. A Clark electrode was used to measure the production of O_2 as described in Section 2.3.6.

2.4.7 *Rate of H_2O_2 Consumption During the $MbFe^{III}/H_2O_2$ Reaction:* The H_2O_2 concentration remaining in solution vs time after mixing 100 μM $MbFe^{III}$ with 500 μM H_2O_2 is shown in Figure 2.17. It is possible to differentiate HRP-catalyzed oxidation of ABTS by H_2O_2 from Mb-catalyzed oxidation since the latter is ~200-fold slower at the

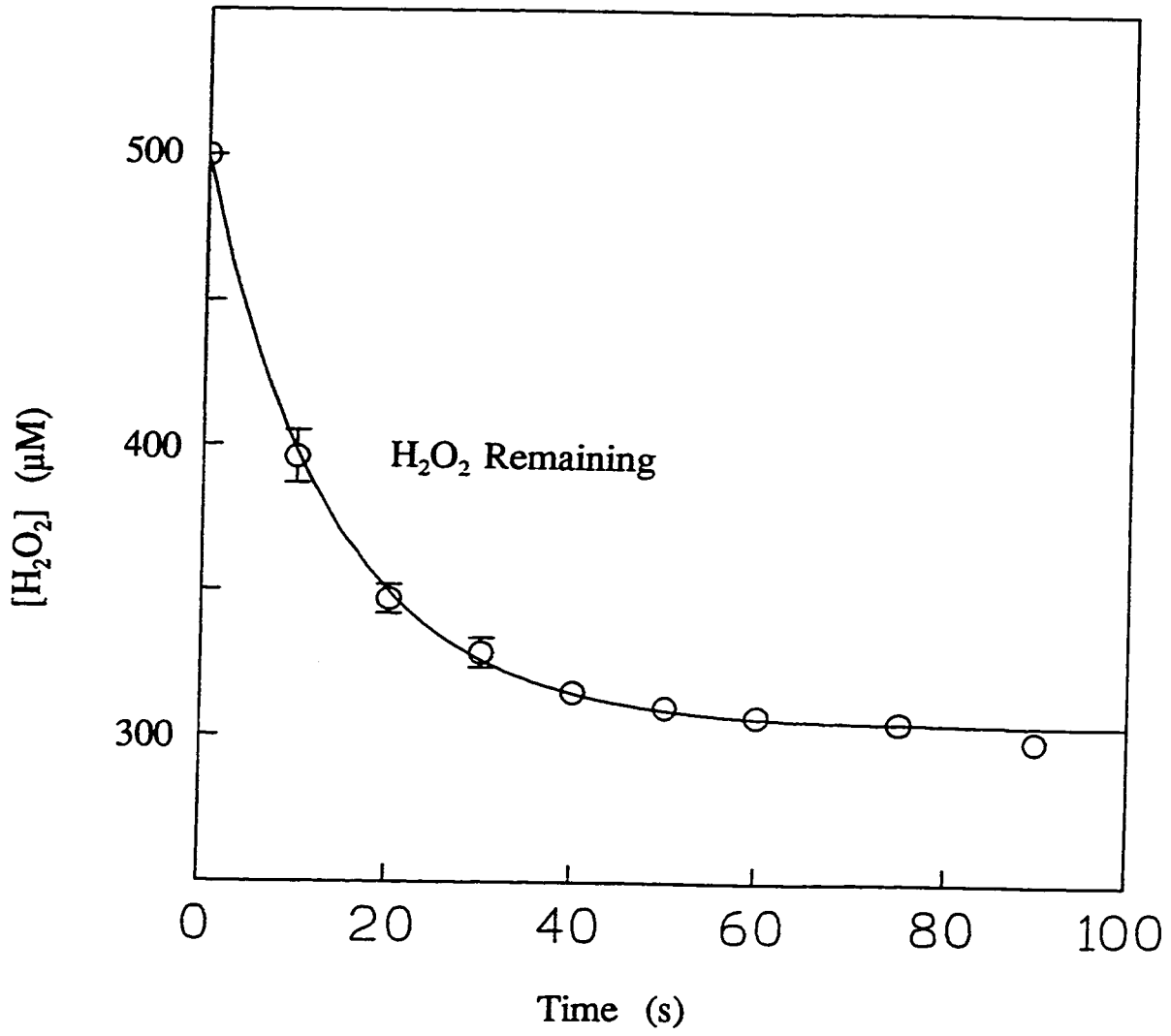

Figure 2.17 Consumption of H_2O_2 during the $MbFe^{III}/H_2O_2$ reaction. The concentration of H_2O_2 that remains vs time after mixing 100 μM $MbFe^{III}$ with 500 μM H_2O_2 as determined by the ABTS-peroxidase system. The solid line shows the fit of the experimental points to first-order kinetics.

enzyme concentrations used in the reaction. H_2O_2 disappearance within the first 100 s followed first-order kinetics with a rate constant of 0.060 s^{-1}, which is the same as that for $MbFe^{IV}$=O formation under identical conditions (Section 2.4.1). The change in H_2O_2 concentration from the start to the end of the first-order process was 200 μM after which H_2O_2 consumption was much slower since "primed" Mb consumed H_2O_2 via its slow catalase-like activity (Section 2.4.6).

2.4.8.1 *FTIR Analysis of $MbFe^{III}$ and $MbFe^{IV}$=O Secondary Structure:* The amide I' (1700-1620 cm^{-1}) and II (1550-1510 cm^{-1}) FTIR bands of $MbFe^{III}$ and $MbFe^{IV}$=O at pD 7.4 are shown in Figure 2.18. The major component in the amide I' region is a peak at 1649 cm^{-1} assigned to α-helical absorption. Changing the oxidation state of the heme iron from Fe^{III} to Fe^{IV}=O results in slight broadening of the 1649-cm^{-1} α-helix band but there is no loss in intensity of the amide II band at 1545 cm^{-1}. The amide I' and II bands of $MbFe^{III}$ are shown in Figure 2.19 between pD 7 and 5.3. There is no discernable change in the shape of the amide I' nor II band envelopes, indicating that the secondary structure of $MbFe^{III}$ is essentially unaffected by changes in pD over this range.

2.4.8.2 *FTIR Analysis of $MbFe^{II}$-CO as a Function of pH and pD*: The stretching vibration of the iron-bound CO in $MbFe^{II}$-CO gives rise to two major bands at 1965 and 1945 cm^{-1}.[27] The υ(CO) bands as a function of pH/D and are shown in Figures 2.20 and 2.21. The 1965-cm^{-1} band increases in intensity relative to the ~1945-cm^{-1} band at low pH/D, and the effect is more dramatic in D_2O. The relative intensity of the higher

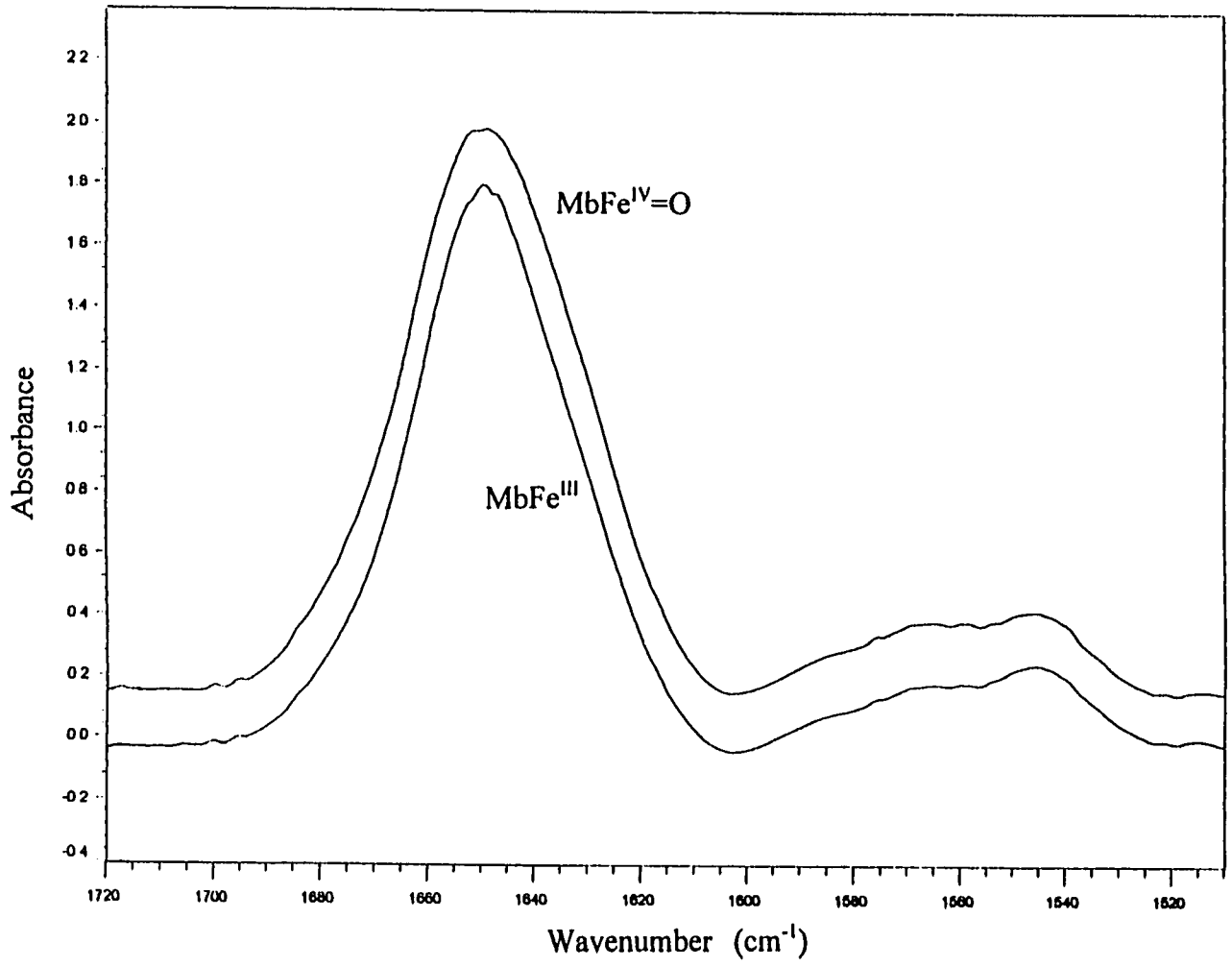

Figure 2.18 FTIR spectra in the amide I' and II regions of 2.5 mM $MbFe^{III}$ and $MbFe^{IV}$=O. Mb samples were prepared in 0.1 M Pi buffer in D_2O at pD 7.4.

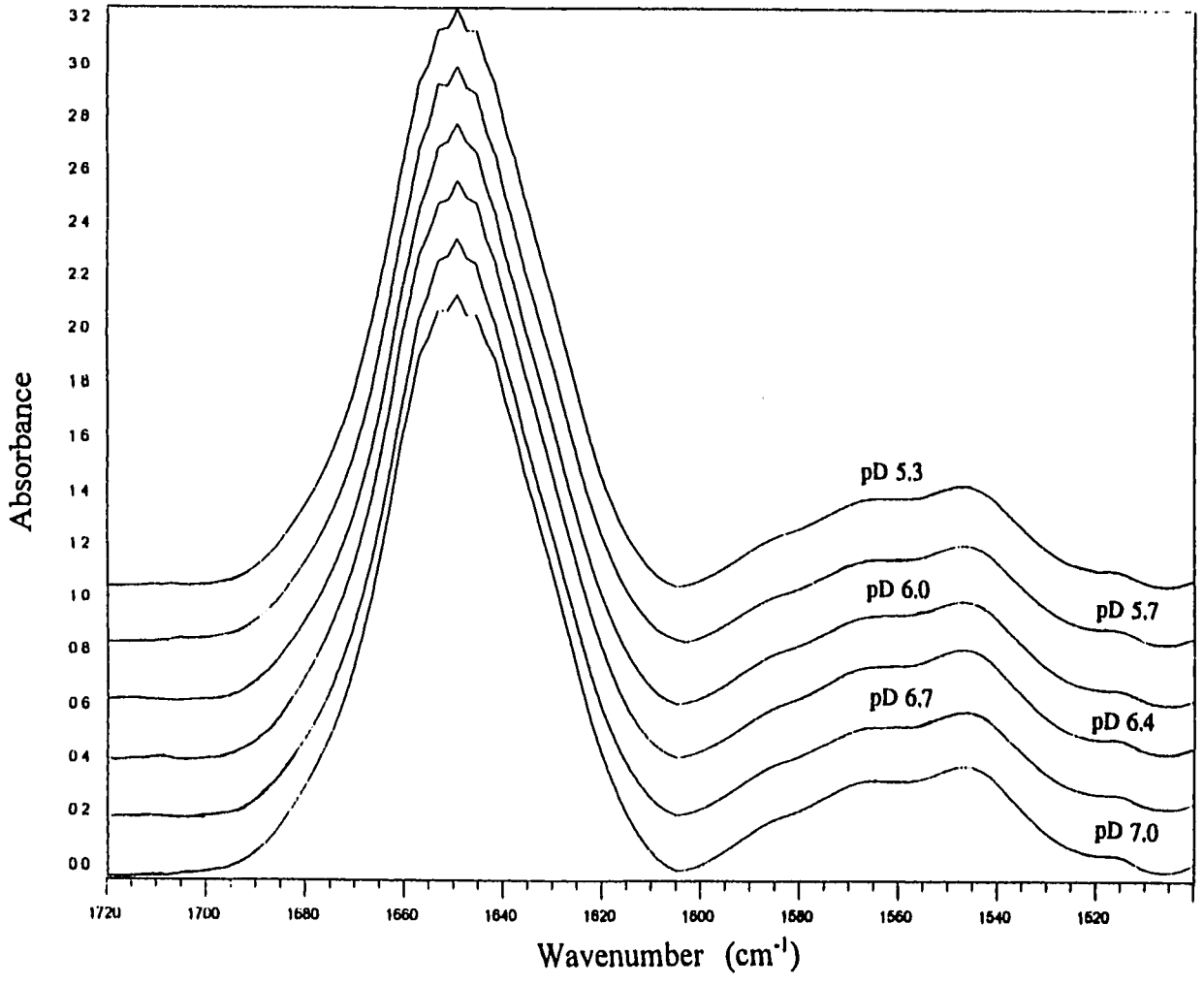

Figure 2.19 FTIR spectra in the amide I' and II region of 2.5 mM $MbFe^{III}$ over the pD range from 7.0 to 5.3. Mb samples were prepared in the D_2O buffers given in Section 2.3.8.1, and the pD values are indicated on the spectra.

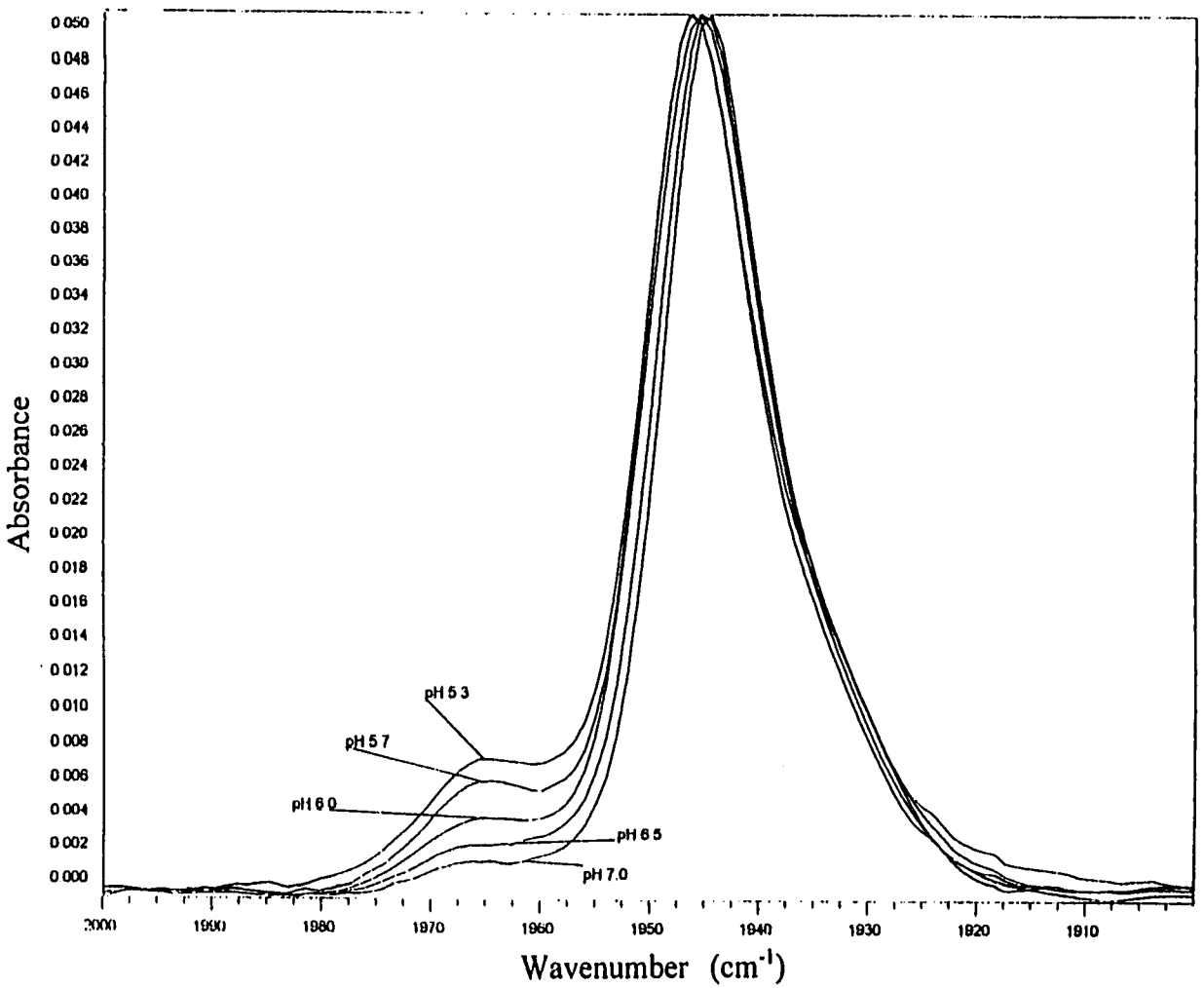

Figure 2.20 FTIR spectra of the υ(CO) bands of 2.5 mM $MbFe^{II}$-CO as a function of pH. The Mb samples were prepared in the buffers listed in Section 2.3.8.2.

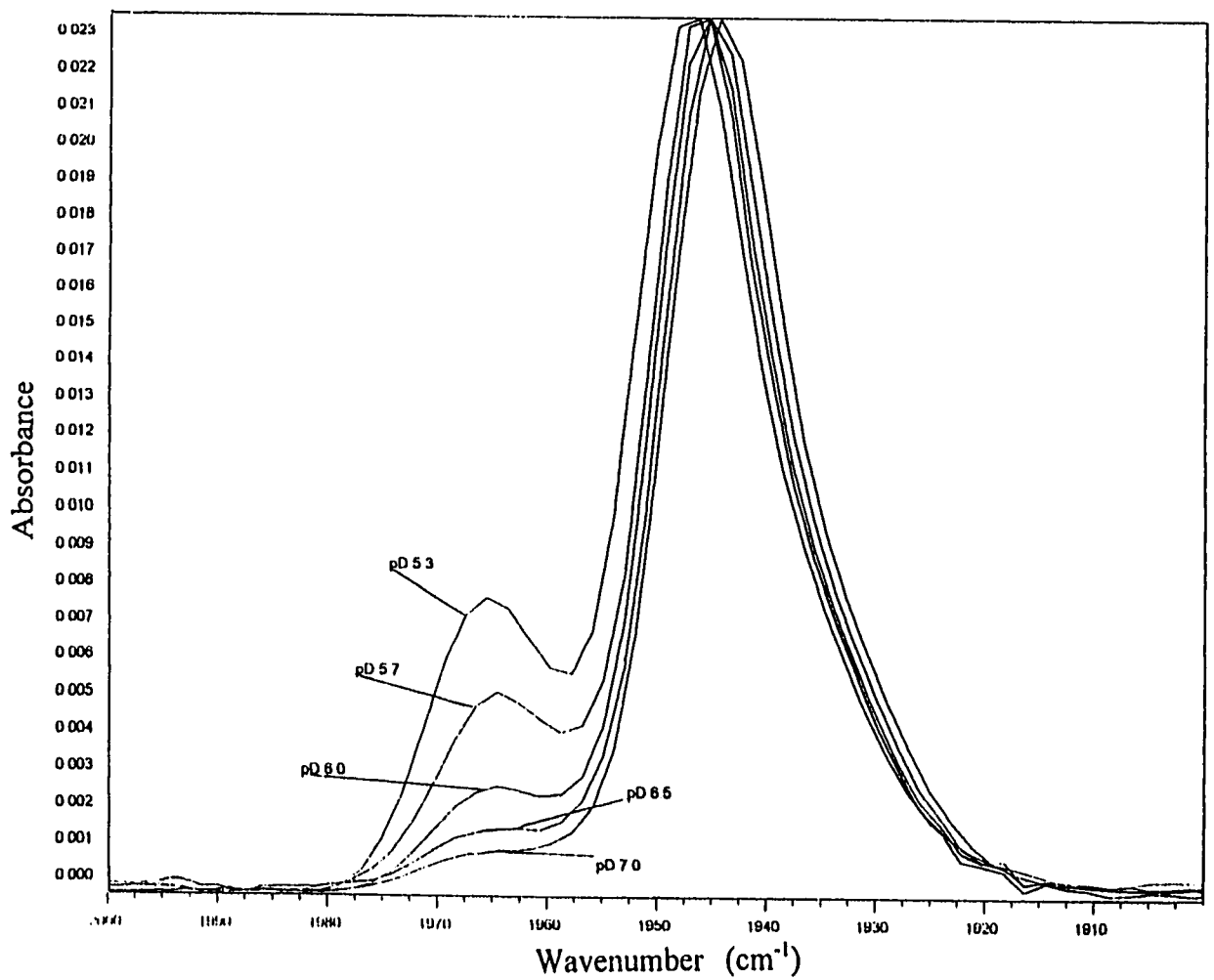

Figure 2.21 FTIR spectra of the ν(CO) bands of 2.5 mM $MbFe^{II}$-CO as a function of pD. Mb samples were prepared in the D_2O buffers given in Section 2.3.8.2.

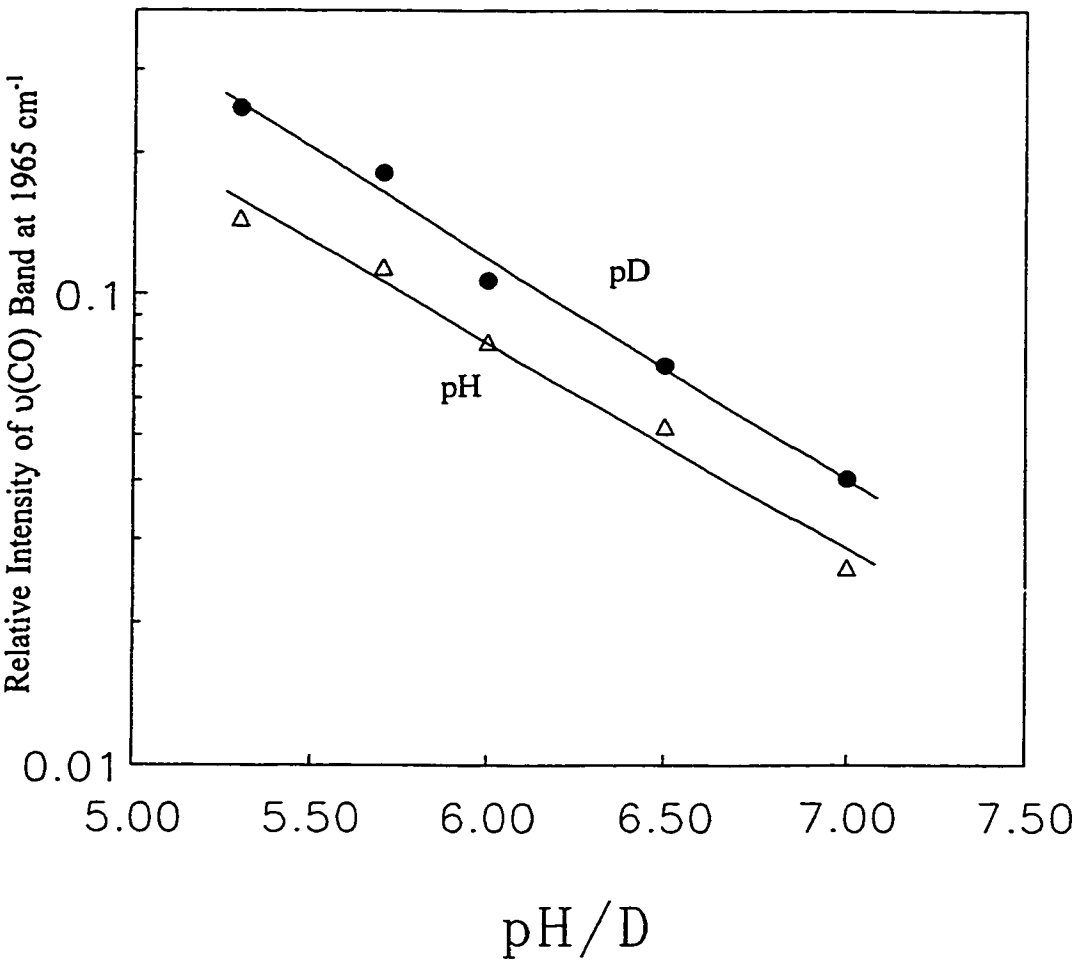

Figure 2.22 Relative intensity of the υ(CO) band at 1965 cm^{-1} of 2.5 mM $MbFe^{II}$-CO vs pH and pD. Plot of log intensity vs pH/D in H_2O (Δ) and D_2O (●).

frequency υ(CO) band vs pH/D is listed in Table 2.5 and plots of log intensity vs pH/D in Figure 2.22 are separated by ~ +0.4 pH units in H_2O and D_2O. In addition, the 1945-cm^{-1} band was found to blue shift by 2 cm^{-1} in H_2O and 3.7 cm^{-1} in D_2O on decreasing the pH/D from 7.0 to 5.3.

Table 2.5 Relative intensity of υ(CO) band at 1965 cm^{-1} vs pH/D[a]

pH/D	Relative intensity of υ(CO) at 1965 cm^{-1} in D_2O	Relative intensity of υ(CO) at 1965 cm^{-1} in H_2O
7.0	0.0404	0.0262
6.5	0.0705	0.0523
6.0	0.107	0.0791
5.7	0.181	0.114
5.3	0.249	0.143

[a] Intensities were calculated by dividing the 1965-cm^{-1} peak height by the sum of peak heights of the 1965- and 1945-cm^{-1} bands. Experimental details are given in the captions to Figures 2.20 and 2.21.

2.4.9 *Autoreduction of* $MbFe^{IV}=O$*:* Autoreduction of $MbFe^{IV}=O$, monitored spectrophotometrically, is a first-order process, as shown in Figures 2.23a and b.

Figures 2.23 a and b Autoreduction process of $MbFe^{IV}=O$ at pH 6.2 (a) and 5.6 (b). Absorbance change at 546 nm ($Fe^{IV}=O$ decay) and 502 nm (Fe^{III} formation) vs time were followed to monitor $MbFe^{IV}=O$ autoreduction. The solid lines show the fit of the experimental points by first-order kinetics.

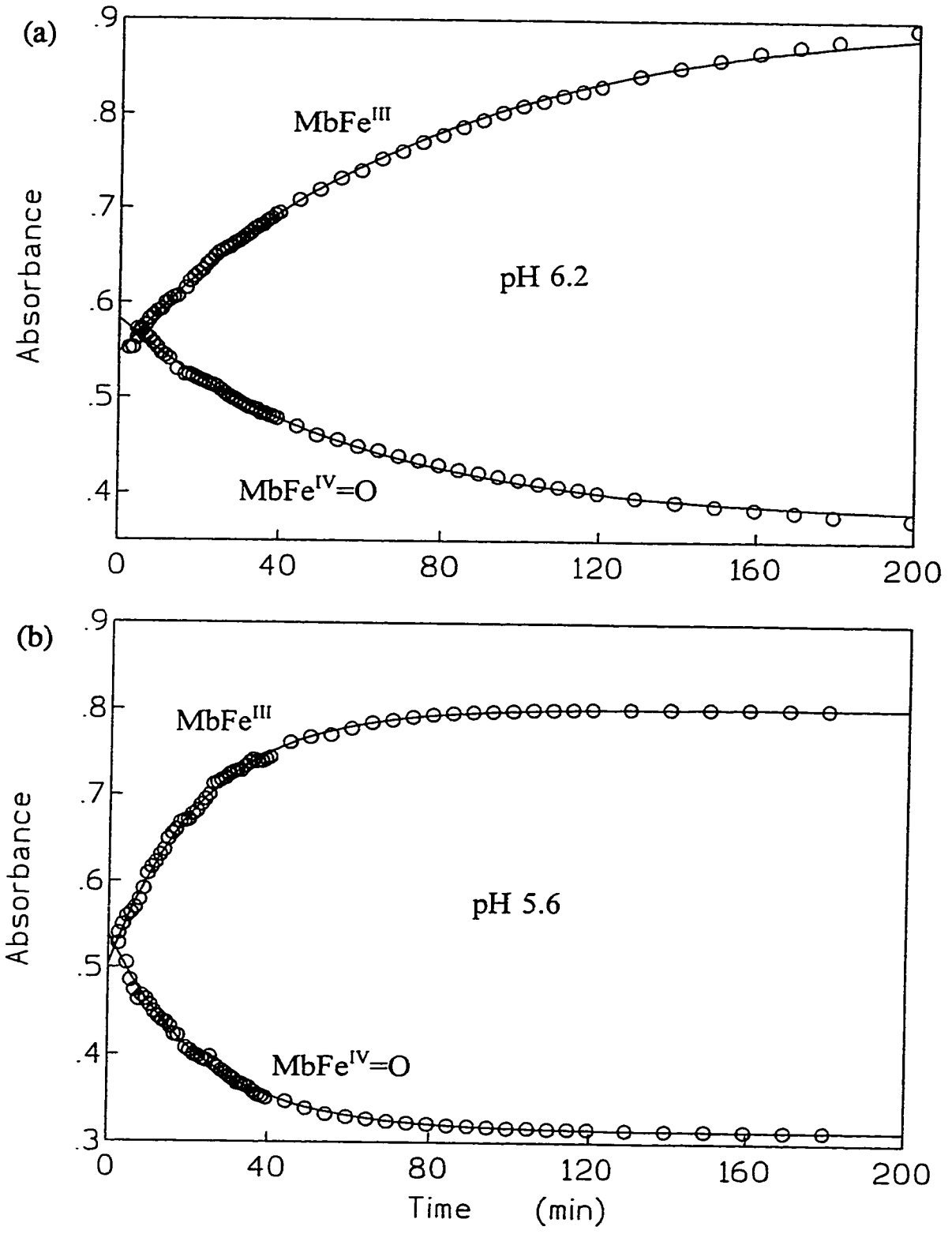
(a)
.9
.8
.7
.6
.5
.4
Absorbance
MbFe^III
pH 6.2
MbFe^IV=O
0
40
80
120
160
200
(b)
.9
.8
.7
.6
.5
.4
.3
Absorbance
MbFe^III
pH 5.6
MbFe^IV=O
0
40
80
120
160
200
Time (min)

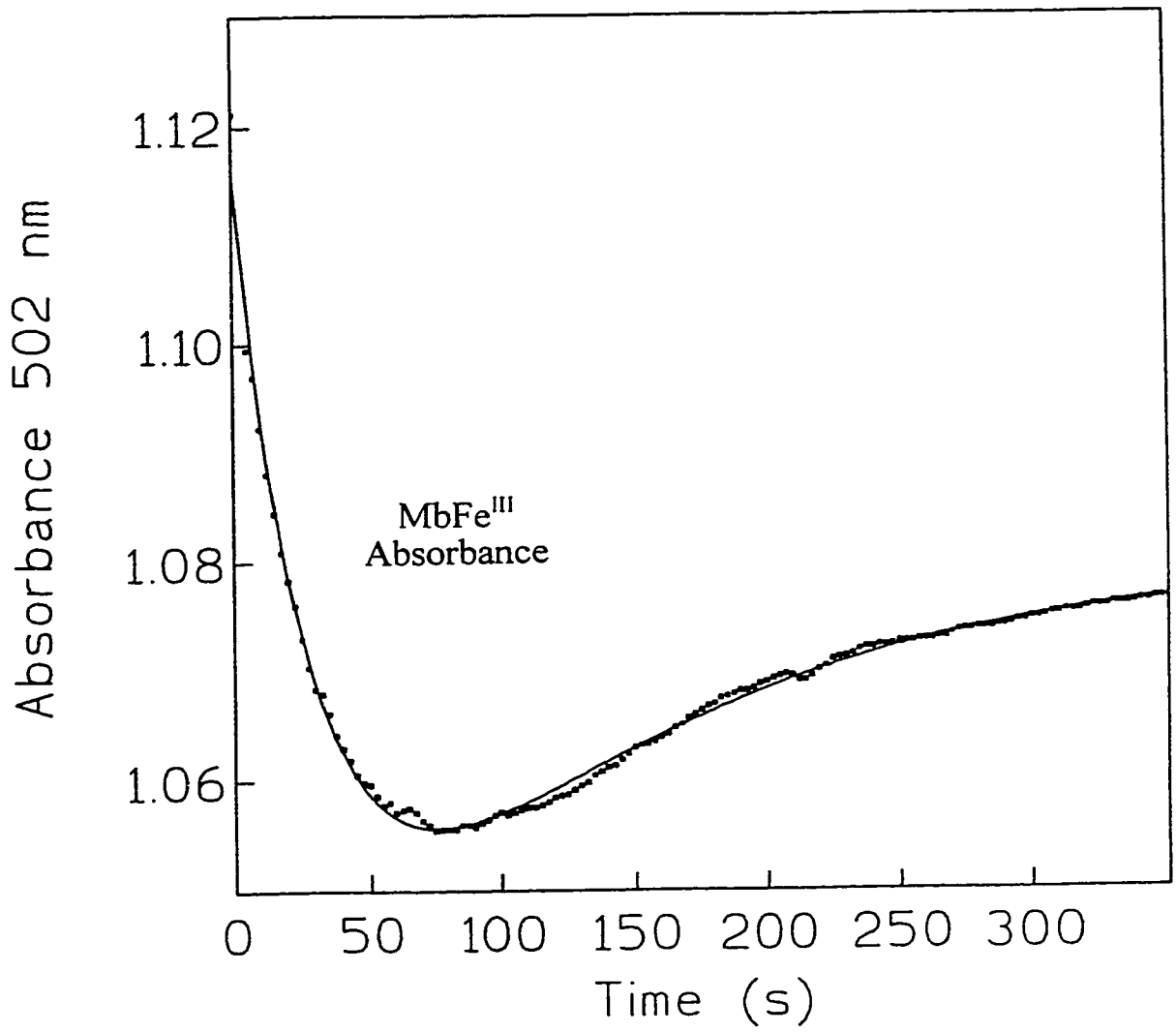

Figure 2.24 $MbFe^{IV}=O$ autoreduction in incompletely formed $MbFe^{IV}=O$. Absorbance change at 502 nm vs time following the reaction of $MbFe^{III}$ with 0.5 molar equivalent of H_2O_2 at pH 7.0.

When formation of $MbFe^{IV}=O$ is incomplete, as occurs when 0.5 molar equivalent of H_2O_2 are reacted with 1 molar equivalent of $MbFe^{III}$, the autoreduction process is biphasic with a portion of the $MbFe^{IV}=O$ decaying with a half-life of ~ 100 s and the remaining $MbFe^{IV}=O$ decaying with a half-life of 124 min at pH 7.0 (Figure 2.24).

Table 2.6 Half-life of $MbFe^{IV}=O$ autoreduction vs pH[a]

pH	Half-Life (min)
7.0	124
6.5	66
6.2	44
5.9	26
5.6	16

[a] The rate of $MbFe^{IV}=O$ (200 μM) autoreduction was followed spectrophotometrically by monitoring the formation of $MbFe^{III}$ and the decay of $MbFe^{IV}=O$ at 502 and 546 nm, respectively.

2.5 Discussion

The stoichiometry of the reaction of $MbFe^{III}$ with H_2O_2 confirms earlier reports that ~2 molar equivalents of H_2O_2 are needed for complete formation of $MbFe^{IV}=O$ at pH

7.0.[6] However, the second-order rate constant for $MbFe^{III}$ decay on reaction with H_2O_2 is consistently smaller than that for Fe^{IV}=O formation. Analysis of the $MbFe^{III}/H_2O_2$ reaction (1:10 molar equivalents) by two concurrent first-order processes gives a bimolecular rate constant of 195 $M^{-1}s^{-1}$ for the faster phase when Fe^{III} decay and Fe^{IV}=O formation are monitored at 409 and 421 nm, respectively. The slower reaction results in bleaching of the Soret absorption between 400 and 430 nm, and causes the discrepancy in the rate constants for Fe^{III} decay and Fe^{IV}=O formation when these are analyzed as simple first-order processes. The slow bleaching of the Soret absorption is attributed to H_2O_2-linked oxidation of the heme and/or heme dissociation from the globin. Both ring-oxidized and free heme would exhibit much less intense absorption between 400 and 430 nm compared to globin-associated Fe^{III} or Fe^{IV}=O heme.[39] The loss of Soret absorbance is ~40-fold slower than the $MbFe^{IV}$=O forming phase and is H_2O_2 dependent, being arrested upon addition of catalase.

The rate constants for the $MbFe^{IV}$=O formation and $MbFe^{III}$ decay, corrected for the concurrent slow process, were found to be unchanged between pH 7.0 and 5.4 (Table 2.2). As mentioned previously (Section 2.1), protonation of distal His64 becomes more facile below pH 7.0 and the protonated His64 swings out of the heme pocket towards the solvent. However, the pH independence of the $MbFe^{III}/H_2O_2$ reaction indicates that the accessibility of H_2O_2 to the heme iron is not rate-limiting in Fe^{IV}=O formation. In H_2O_2 cleavage by heme peroxidases, the conserved distal His acts as a proton acceptor from H_2O_2 and HOO^- binds to the Fe^{III} ion. Heterolytic cleavage of the O-O bond is promoted by back proton transfer from the distal His to the β oxygen of the peroxy anion.[40] Site

directed mutants of heme peroxidases reveal that the distal His is a key active-site residue in Fe^{IV}=O formation and is responsible for the high reactivity with H_2O_2.[41,42] At lower pH, the distal His64 of Mb is partially protonated (pK_a ~6)[43] and the protonated form is unable to accept a proton. Hence, the absence of a pH effect on the rate constants in Table 2.2 suggests that H_2O_2 deprotonation is not rate-limiting in $MbFe^{IV}$=O formation between pH 7.0 and 5.4. The fact that the distal His52 to Leu mutant of CCP has a bimolecular rate constant for its reaction with H_2O_2 similar to that of $MbFe^{III}$ (236 - 731 $M^{-1}s^{-1}$, depending upon buffer system used)[42] indicates that His64 is not an effective acid/base catalyst in Fe^{IV}=O formation in Mb.

Oxidative damage in Mb on exposure to H_2O_2 has been reported under various conditions of pH and H_2O_2 concentration.[30,8] For the purpose of studying Fe^{IV}=O heme redox reactivity in Mb by intramolecular electron transfer, it was necessary to determine if the globin portion of Mb was altered upon Fe^{IV}=O formation, during the decay of protein-based radicals, during Fe^{IV}=O autoreduction, or during acid-catalyzed autoreduction of Fe^{IV}=O. HPLC analysis of samples 1-3, prepared as outlined in Section 2.3.3, shows that the $MbFe^{III}/H_2O_2$ reaction products reduced with ascorbate (sample 1) had minimal damage to the globin or heme since the HPLC elution profile of sample 1 was essentially identical to that of untreated $MbFe^{III}$ (Figure 2.6 and 2.7). Since Fe^{IV}=O formation was complete in sample 1 and the protein radicals had decayed before addition of ascorbate ($t_{1/2}$ ≈ 7-30 s for decay of the protein-based radicals formed in $MbFe^{III}/H_2O_2$ reaction as monitored by EPR),[15,44] irreversible damage to the globin is <u>not</u> caused during Fe^{IV}=O formation and protein-based radical decay. HPLC profiles of $MbFe^{IV}$=O samples

that were left to autoreduce over 12 h at pH 7 (sample 2) or at low pH (sample 3) also exhibited major peaks corresponding to unmodified globin and heme. However, significant amounts of chemically modified heme and globin were present in samples 2 and 3, as demonstrated by the appearance of 5 minor additional heme-absorbing peaks and 2 globin peaks in the HPLC profiles in Figures 2.8 and 2.9. The damage to the globin or heme could not be reversed with reductants,[7] revealing that autoreduction of Fe^{IV}=O is the main cause of chemical modification in the $MbFe^{III}/H_2O_2$ reaction products. Autoreduction at low pH increased the relative amounts of the HPLC peaks assigned to modified Mb (Figure 2.8 vs 2.9), but did not increase the number of products over autoreduction at neutral pH. These observations are consistent with a previous report that chemical modification of Mb in the $MbFe^{III}/H_2O_2$ reaction products is greater under acidic conditions.[2] The slow H_2O_2-linked oxidation reported in Section 2.4.1 is not expected to contribute significantly to the chemical modification of Mb since catalase was added to remove excess H_2O_2 before the slow reaction was 2% complete.

HPLC analysis of samples 2 and 3 also revealed a peak at 17.6 min (Figures 2.8 and 2.9) where heme and globin co-elute. ESI-MS analysis of this peak revealed a species with a mass of 17583 Da, which corresponds to globin (16950 Da) + heme (616 Da) + oxygen (16 Da). Since the MS analysis was performed under acidic conditions where the heme dissociates from the polypeptide,[45,46] it is reasonable to assume that the heme is crosslinked to the globin in the 17583-Da species (Figure 2.11).[11] In addition to the 17.6-min peak, MS analysis of the globin fractions of samples 2 and 3 at 16.4 min (Figures 2.8 and 2.9) revealed species with masses of 16950 Da and 16966 Da,

corresponding to unmodified globin and globin + oxygen, respectively (Table 2.3). ESI-MS analysis of both untreated $MbFe^{III}$ and ascorbate-reduced $MbFe^{IV}$=O (sample 1) yielded only the 16950-Da peak of unmodified globin (Figure 2.10, Table 2.3), confirming that the polypeptide undergoes no modifications that alter its mass in ascorbate-reduced $MbFe^{IV}$=O.

The tryptic digests of untreated $MbFe^{III}$ and $MbFe^{III}/H_2O_2$ samples 1-3 (Section 2.4.5) gave virtually identical HPLC peptide maps as monitored by absorbance at 210 and 280 nm, fluorescence at 303 and 350 nm, and mass. ESI-MS analysis revealed that the small discrepancies in peptide elution seen in Figures 2.12 to 2.15 are due to incomplete tryptic digestion and not to chemical modification. Detection of some modified peptides was expected in $MbFe^{IV}$=O that had undergone autoreduction (samples 2 and 3), since the HPLC and MS analyses of the undigested samples (Figures 2.8 and 2.9; Table 2.3) revealed the presence of chemically-modified Mb. However, heme absorption at 400 nm in the undigested Mb peak (data not shown) indicates that the heme crosslinked fraction is resistant to digestion. This observation is not surprising since the $MbFe^{III}$ holoprotein is much more difficult to digest with trypsin than the apoprotein.[11] The 16966-Da peak observed in the mass spectra of undigested samples 2 and 3 was not observed in the peptide mass maps. Thus, although the globin species with a mass of 16966 Da was digested by trypsin, no mass-modified peptides were found in the maps. Possible explanations for this are: (1) a modified peptide was not detected because the 16966-Da globin species represents only a small fraction (< 5%) of the total globin; (2) globin modification in samples 2 and 3 was not at one specific site but the 16966-Da peak

contained a heterogeneous mixture of modified globin species; and (3) the modification(s) was (were) not stable enough to survive digestion and LC-MS analysis. Previous investigators of chemical modification in the $MbFe^{III}/H_2O_2$ reaction products report that heme is crosslinked to the globin in 4-10% and 18-25% of the products when the reaction was carried out at pH 7.4 and 4.5, respectively. The heme-globin crosslink was reported to be through Tyr103, and although less forcing conditions were used here (1:20 $MbFe^{III}/H_2O_2$ for 30 min in the published study vs 1:5 $MbFe^{III}/H_2O_2$ for 5 min in this study), the heme-globin species with a mass of 17583 Da (Table 2.3) may be also crosslinked through Tyr103. Modification at Tyr103 would be reasonable considering its involvement in the formation of a protein-based radical (Chapter 5).

Analysis of O_2 evolution from the $MbFe^{III}/H_2O_2$ reaction reveals that two molar equivalents of H_2O_2 must react with $MbFe^{III}$ before catalase-like activity is observed. In contrast, addition of H_2O_2 to preformed $MbFe^{IV}$=O resulted in complete disproportionation of H_2O_2 into O_2 and H_2O. Since the protein-based radicals were allowed to decay in the $MbFe^{IV}$=O sample before further treatment with H_2O_2, the catalase cycle in Mb must not involve the primary radical sites. The switching on of catalase-like activity explains how Mb is able to decompose 5-10 molar equivalents of H_2O_2 without causing excessive damage to the globin. The catalase-like activity of Mb was reported 30 years ago,[6] but the priming required for the initiation of the catalase-like cycle, which enhances our understanding of the O_2 evolving mechanism, has not been previously reported.

H_2O_2 consumption (Figure 2.14) on mixing 100 μM $MbFe^{III}$ and 500 μM H_2O_2 reveals that the initial 200-μM drop in H_2O_2 concentration occurred with a rate constant

of 0.060 s^{-1}. The H_2O_2 consumed corresponds to the two molar equivalents needed to prime $MbFe^{III}$ for catalase activity and the initial rate of H_2O_2 consumption is the same as that of $MbFe^{IV}$=O formation (Table 2.1). Hence, the O_2 production and H_2O_2 consumption data confirm that four oxidizing equivalents from H_2O_2 are consumed in the formation of $MbFe^{IV}$=O from $MbFe^{III}$ at neutral pH *without* the release of O_2. Despite this, reduction with ferrocyanide reveals that $MbFe^{IV}$=O retains only one oxidizing equivalent, this being the Fe^{IV}=O heme.[3] The $MbFe^{IV}$=O species primed for catalase activity does not require the presence of protein-based radicals. Hence, the mechanism of Fe^{IV}=O formation in the $MbFe^{III}/H_2O_2$ reaction may involve rapid formation and decay of protein-based radicals. Since Fe^{IV}=O formation in the reaction of Fe^{III} heme peroxidases with H_2O_2 consumes only two oxidizing equivalents, side reactions on the globin may account for the consumption of four oxidizing equivalents by Mb. However, a detailed mechanism which takes into account all the experimental observations has yet to be elucidated.

Secondary structure analysis of $MbFe^{IV}$=O and $MbFe^{III}$ by FTIR reveals only slight broadening in the amide I' bands of $MbFe^{IV}$=O compared to $MbFe^{III}$ (Figure 2.10). In addition, between pH 7 and 5.4, $MbFe^{III}$ shows no changes in its amide I' bands nor amide II bands, suggesting that intramolecular electron transfer rates in Mb will not be altered due to pH-dependant changes in protein secondary structure. Steady-state fluorescence investigations also detected no structural changes in Mb (Fe^{III}, Fe^{III}-CN, Fe^{III}-azide, Fe^{II}, Fe^{II}-O_2, and Fe^{II}-CO)[47] over the same pH range.

FTIR analysis of $MbFe^{II}$-CO shows that the relative intensities of the υ(CO) bands

are pH dependent between pH 7 and 5.3, with the higher frequency band increasing in intensity with decreasing pH. Plots of the log of the relative intensities in H_2O and D_2O of the higher frequency υ(CO) band (1965 cm^{-1}) vs pH/D are separated by +0.4 pH units (Figure 2.19). This is the magnitude of the equilibrium isotope effect (ΔpK_a) predicted for acids,[48] and is attributed to the protonated distal His64, which swings out of the heme cavity. The slope of the lines in Figure 2.19 is -0.45, whereas a slope of -1 is expected for uptake of a single proton. However, the opening of the heme pocket in Mb depends on the pK_a of His64, which changes from 6.0 to 3.8 on shifting conformation from open to closed-pocket forms.[43] This shift in pK_a of the His64 or alternatively a second protonation step in the heme pocket opening,[49,50] would be consistent with the observed slopes of 0.5 in Figure 2.22. In contrast, the rate constant for CO binding to $MbFe^{II}$ (k_{CO}) is pH dependent with a pK_a of ~6 and the plot of log k_{CO} vs pH has a slope of 1.[43]

The small blue shift in the frequency of 1945-cm^{-1} υ(CO) band from pH/D 7.0 to 5.3 indicates that even in the closed pocket conformation of $MbFe^{II}$-CO there are slight differences in the CO environment. This could be due to a global pH-induced change in Mb or to protonation of a heme propionic group. Protonation or deuteration of the heme could cause small localized conformational changes in the pocket that alter the electron withdrawing properties of the heme so as to affect the υ(CO) frequency.

The combined FTIR investigations of the amide I' and II bands reveal that the pH-dependent movement of His64, as evidenced by the change in υ(CO) of $MbFe^{II}$-CO, is a localized structural change that does not affect protein secondary structure. The crystal structure of Mb with a bulky ligand[51] revealed that formation of the open-pocket

conformation is confined to a local conformational change involving His64, consistent with the FTIR findings.

The autoreduction process of fully formed $MbFe^{IV}=O$ (Section 2.4.9) was found to be pH dependent as previously described.[2] The faster rate of $MbFe^{IV}=O$ autoreduction in samples containing $MbFe^{III}$ (products of the reaction of 0.5 molar equivalent of H_2O_2 with $MbFe^{III}$) may be due to a bimolecular reduction process involving $MbFe^{III}$ or formation of an unstable $MbFe^{III}/H_2O_2$ intermediate.[10] However, for the purpose of the proposed electron transfer studies, the half-life of $MbFe^{IV}=O$ (Table 2.6) is sufficiently long when $MbFe^{III}$ is fully converted into $MbFe^{IV}=O$.

2.6 Conclusions

Based on the investigations in this chapter, the proposed intramolecular electron transfer studies to be carried out on Mb should not be affected by: (1) chemical modification to Mb on the formation of $MbFe^{IV}=O$, (2) conformational changes in the protein secondary structure caused by the changes in heme oxidation state or by pH changes between 7.0 and 5.4, (3) nor by the competing process of $MbFe^{IV}=O$ autoreduction which is sufficiently slow ($t_{1/2} \geq 16$ min; Table 2.6).

References

1. Poulos, T.; Finzel, B. In *Peptide and Protein reviews Vol 4*, Hearn, M.T.W. Ed.;Marcel Dekker: New York, **1984**; pp 115-171.
2. Tajima, G.-I.; Shikama, K. *Int. J. Biochem.* **1993**, *25*, 101-105.

3. George, P.; Irvine, D.H. *Biochem. J.* **1952**, *52*, 511-517.

4. English, A.M. In *Encyclopedia of Inorganic Chemistry Vol 4*, King, R.B., Ed.: John Wiley & Sons: Chichester, **1994**: pp 1682-1697.

5. Poulos, T.L.; Fenna, R.E. In *Metal Ions in Biological Systems Vol 30: Metalloenzymes Involving Amino Acid Residues and Related Radicals*, Siegel, H.; Siegel A., Eds; Marcel Dekker: New York, **1994**; pp 25-75.

6. Yonetani, T.; Schleyer, H. *J. Biol. Chem.* **1967**, *242*, 1974-1979.

7. Fox, J.B.Jr.; Nicholas, R.A.; Ackerman, S.A.; Swift, C.E. *Biochemistry* **1974**, *13*, 5178-5186.

8. King, N.K.; Winfield, M.E. *J. Biol. Chem.* **1963**, *238*, 1520-1528.

9. Tamura, M.; Asakura, T.; Yonetani, T. *Biochimi. Biophys. Acta* **1973**, *295*, 467.

10. King, N.K.; Winfield, M.E. *Aust. J. Biol. Sci.* **1966**, *19*, 211-217.

11. Catalano, C.E.; Choe, Y.S.; Ortiz de Montellano, P.R. *J. Biol. Chem.* **1989**, *264*, 10534-10541.

12. Whitburn, K.D. *Arch. Biochem. Biophys.* **1987**, *253*, 419-430.

13. Kelso, N.; King, T.; Winfield, M. *J. Biol. Chem.* **1963**, *238*, 1520-1528.

14. Fox, J.B.Jr.; Nicholas, R.A.; Ackerman, S.A.; Swift, C.E. *Biochemistry* **1974**, *13*, 5178-5186.

15. Lemberg, R.; Legge, J.W.; Lockwood, W.H. *Biochem. J.* **1941**, *35*, 328.

16. Davies, M.J. *Biochimi. Biophys. Acta* **1991**, *1077*, 86-90.

17. Waterfield, M.D. In *Practical Protein Chemistry, A. Handbook*, Ed. A. Darbre; John Wiley & Sons; Chichester, **1986**, pp 198-200.

18. Ashton, D.S.; Beddell, C.R.; Cooper, D.J.; Green, B.N.; Oliver, R.W.A *Org. Mass. Spectrom.***1993**, *28*, 721-728.

19. Huang, L.Q.; Paiva, A. Bhat, R.; Wong, M.; *J. Am. Soc. Mass Spec.* **1996**, *7*, 1219-1226.

20. Siuzdak, G. In *Mass Spectrometry For Biotechnology;* Academic Press: San Diego, **1996**, p 43.

21. Gullick, W.J. In *Practical Protein Chemistry, A. Handbook*, Ed. A. Darbre; John Wiley & Sons: Chichester, **1986**, pp 220-223.

22. Wilkinson, J.M. In *Practical Protein Chemistry, A. Handbook*, Ed. A. Darbre; John Wiley & Sons: Chichester, **1986**, pp 170-174.

23. Zhao, X.-J.; Sampath, V.; Caughey, W.S. *Biochem. Biophys. Res. Comm.* **1994**, *204*, 537-543.

24. Susi, H.; Byler, D.M. *Methods of Enzymology*, **1986**, *130*, 290.

25. Krimm, S.; Bandekar, J. *Adv. Prot. Chem.* **1986**, *38*, 181.

26. Creighton, T.F. In *Proteins: Structures and Molecular Properties 2nd Ed.*; W.H. Freeman and Company: New York, **1993**, pp 282-286.

27. Balasbramanian, S.; Lambright, D.G.; Boxer, S.G. *Proc. Natl. Acad. Sci. USA* **1993**, *90*, 4718-4722.

28. Li, T.; Quillin, M.L.; Phillips, G.N. Jr.; Olson, J.S. *Biochemistry* **1994**, *33*, 1433.

29. Fersht, A. In *Enzyme Structure and Mechanism 2nd ed*; W.H. Freeman and Company: New York **1985**, pp 170-174.

30. Osawa, Y.; Korzekwa, K. *Proc. Natl. Acad. Sci. USA* **1991**, *88*, 7081-7085.

31. Rao, S.I.; Wilks, A.; Hamberg, M.; Ortiz de Montellano, P.R. *J. Biol. Chem.* **1994**, *269*, 7210-7216.

32. Childs, R.E.; Bradsley, W.G. *Biochem. J.* **1975**, *145*, 93-103.

33. Groome, N.P. *J. Clin. Chem. Clin. Biochem.* **1980**, *18*, 345-349.

34. Harris, D.C. In *Quantitative Chemical Analysis, 2nd Ed.*; W.H. Freeman and Company: New York, **1982**; p 484.

35. Schonbaum, G.R. *J. Biol. Chem.* **1973**, *248*, 502.

36. Schowen, K.J.B. In *Transition States of Biochemical Processes*, Gandour, R.D.; Schowen, R.L. Eds. Plenum Press: **1987**; p. 243.

37. Deconvolution of an ESI-MS spectrum gives the mass of the sample analyzed.

38. Siuzdak, G. In *Mass Spectrometry For Biotechnology;* Academic Press: San Diego, **1996**; p 71.

39. Falk, J.E. In *Porphyrins and Metalloporphyrins Vol. 2*; Elsevier Publishing Company: Amsterdam, **1964**; p18-19 and p 72-85.

40. English, A.M.; Tsaprailis, G. *Advances Inorg. Chem.* **1995**, *43*, 79-125.

41. Erman, J.E.; Vitello, L.B. *J. Am. Chem. Soc.* **1992**, *114*, 6592.

42. Erman, J.E.; Vitello, L.B.; Miller, M.A.; Shaw, A.;Brown, K.A.; Kraut, J. *Biochemistry* **1993**, *32*, 9798.

43. Morikis, D.; Champion, M.P.; Springer, B.A.; Sligar, S.G. *Biochemistry* **1989**, *28*, 4791.

44. Kelman, D.J.; DeGray, J.A.; Mason, R.P. *J. Biol. Chem.* **1994**, *269*, 7458-7463.

45. Kata, V.; Chait, B.T. *J. Am. Chem. Soc.* **1991**, *113*, 8534-8535.

46. Feng, R.; Konishi, Y. *J. Am. Soc. Mass. Spec.***1993**, *4*, 638.

47. Postnikova, G.B.; Komarov, Y.E.; Yumakova, E.M. *Eur. J. Biochem.* **1991**, *198*, 233-239.

48. Schowen, K.B.J. In *Transition States of Biochemical Processes*; Gandour, R.D.; Schowen, R.L., Eds; Plenum Press: New York, **1978**; pp 225-283.

49. Chance, M.R.; Campbell, B.; Hoover, R.; Friedman, J.M. *J. Biol. Chem.* **1987**, *262*, 6959.

50. Campbell, B.F.; Chance, M.R.; Friedman, J.M. *J. Biol. Chem.* **1987**, *262*, 14885.

51. Johnson, K.A.; Olson, J.S.; Phillips, G.N. Jr. *J. Mol. Biol.* **1989**, *207*, 459.

3.0 Intramolecular Reduction of the Fe^{IV}=O Center in Myoglobin at Neutral pH

3.1 Introduction

Like heme peroxidases and other heme enzymes, myoglobin (Mb) forms an oxyferryl (Fe^{IV}=O) heme on reacting with peroxides.[1,2,3,4,5] The study of Fe^{IV}=O centers is of interest since it is thought that all heme enzymes form Fe^{IV}=O at one stage in their catalytic cycles. Direct investigation of Fe^{IV}=O in most heme enzymes is limited since it exists as a short lived reaction intermediate. However, study of the stable Fe^{IV}=O centers in peroxidases and Mb is expected to reveal some of the factors that control Fe^{IV}=O reactivity in all heme enzymes.

An important advance in our ability to study redox centers in proteins came with the development of techniques to study intramolecular electron transfer (ET) reactions. The best established technology involves the derivatization of a protein's surface histidines with ruthenium complexes.[6,7,8] The protein matrix holds the two redox centers at a fixed distance, and pulse radiolysis or flash photolysis techniques are used to selectively oxidize or reduce one of the metal (redox) centers, and the kinetic intermediate relaxes to the thermodynamic product by intramolecular ET. The rate of the observed ET step varies with the driving force between the donor and acceptor, the reorganizational energy (λ) of the donor-acceptor complex, and the tunneling matrix element (H_{AB}) for the ET pathway as described by the Marcus equation (eq 1.6).[9,10]

Intramolecular ET has been extensively studied in sperm whale (SW) and recombinant human (RH) Mb. Most studies have involved attachment of a ruthenium

complex to His48, which is 12.7 Å from the heme edge. $Ru^{II} \rightarrow Fe^{III}$-$OH_2$ ET was studied as a function of driving force (0.02 to 0.35 eV)[11,12] by attaching ruthenium complexes with different reduction potentials to His48. From the observed ET rates, λ was estimated to be 1.48 eV and H_{AB} for the ET pathway 0.01 cm^{-1}.[9]

ET was also studied in metalloderivatives of Mb. Derivatization of Zn-, Pd-, Cd-, and Mg-Mbs at His48 with ruthenium complexes allowed alteration of the reduction potential at the metalloporphyrin as well as at the ruthenium centers. The higher driving forces in the metalloderivatives (0.61 to 1.17 eV) compared to Fe-Mb resulted in faster ET rates through the protein and the λ was calculated to be 1.26 eV.[13,14] The lower λ for the non-iron metalloporphyrin systems compared to that for the $MbFe^{III/II}$ systems is attributed to dissociation of the H_2O axial ligand on reducing six-coordinate $MbFe^{III}$-OH_2 to $MbFe^{II}$, which is five-coordinate.[15] The non-iron metalloporphyrin systems studied remain five-coordinate throughout the ET process.[9]

Our lab has recently investigated intramolecular ET to the Fe^{IV}=O heme of cytochrome c peroxidase (CCP) from a_5Ru^{II} (a = NH_3) bound at His60.[16] The ET rate was found to be slow (3.2 s^{-1}) considering the driving force (~1 eV) and separation (21.8 Å) of the redox centers. By comparison, Zn-SWMb with a_5Ru attached to His116 exhibited an ET constant of 89 s^{-1} at a driving force of 0.82 eV and an edge-to-edge Ru complex to porphyrin distance of 20.1 Å.[9] The slower ET rate in CCP was interpreted as arising from a large λ for the Fe^{IV}=O heme. Recently it has become apparent that the ET rate constants reported for Zn-Mb at 19-22 Å are considered upper limits because of unresolved bimolecular contributions; hence, comparison of ET rates in a_5Ru^{II}(His60)-

CCP(Fe^{IV}=O) with the Zn-Mb values may not be meaningful. An obvious test of the large postulated λ is to directly compare intramolecular ET rates between Fe^{IV}=O and a_5Ru centers (attached to His48) in Mb with the corresponding rates in Zn-SWMb and Zn-RHMb. Since the Fe^{IV}=O heme of horse heart myoglobin (HHMb) is significantly more stable than that of SWMb,[17] the former protein was chosen for this study. A a_5Ru group was attached to the surface His48 of HHMb, and rates of ET between the a_5Ru center and the Fe^{III} and Fe^{IV}=O hemes were measured by pulse radiolysis at Brookhaven National Laboratory. The most direct through-bond electron-transfer pathway from His48 to the heme is shown in Figure 3.1.

3.2 Materials and Methods

HHMb (Sigma) derivatized with pentaammineruthenium (a_5Ru^{III} from $[a_5Ru^{III}Cl]Cl_2$; Johnson Matthey) was prepared as previously described,[13] except that $a_5Ru^{II}(H_2O)$ and HHMb were left to react for 1 h rather than 30 min. Fast protein liquid chromatography (FPLC; Pharmacia) on a Mono S cation exchange column was used to separate the ruthenated products into single derivatives with a_5Ru covalently attached to each of the three surface histidines shown in Figure 3.2 (His 48, 81 and 116). The identity of the derivatives was confirmed by peptide mass mapping as outlined in detail in Chapter 4.

The reduction potential for $a_5Ru^{III/II}$ covalently bound to His48 of HHMb was determined by differential pulse voltammetry as described in Chapter 4. Peak potentials were measured for 100 μM a_5Ru(His48)Mb in N_2-saturated 50 mM Pi buffer (pH 7.0)

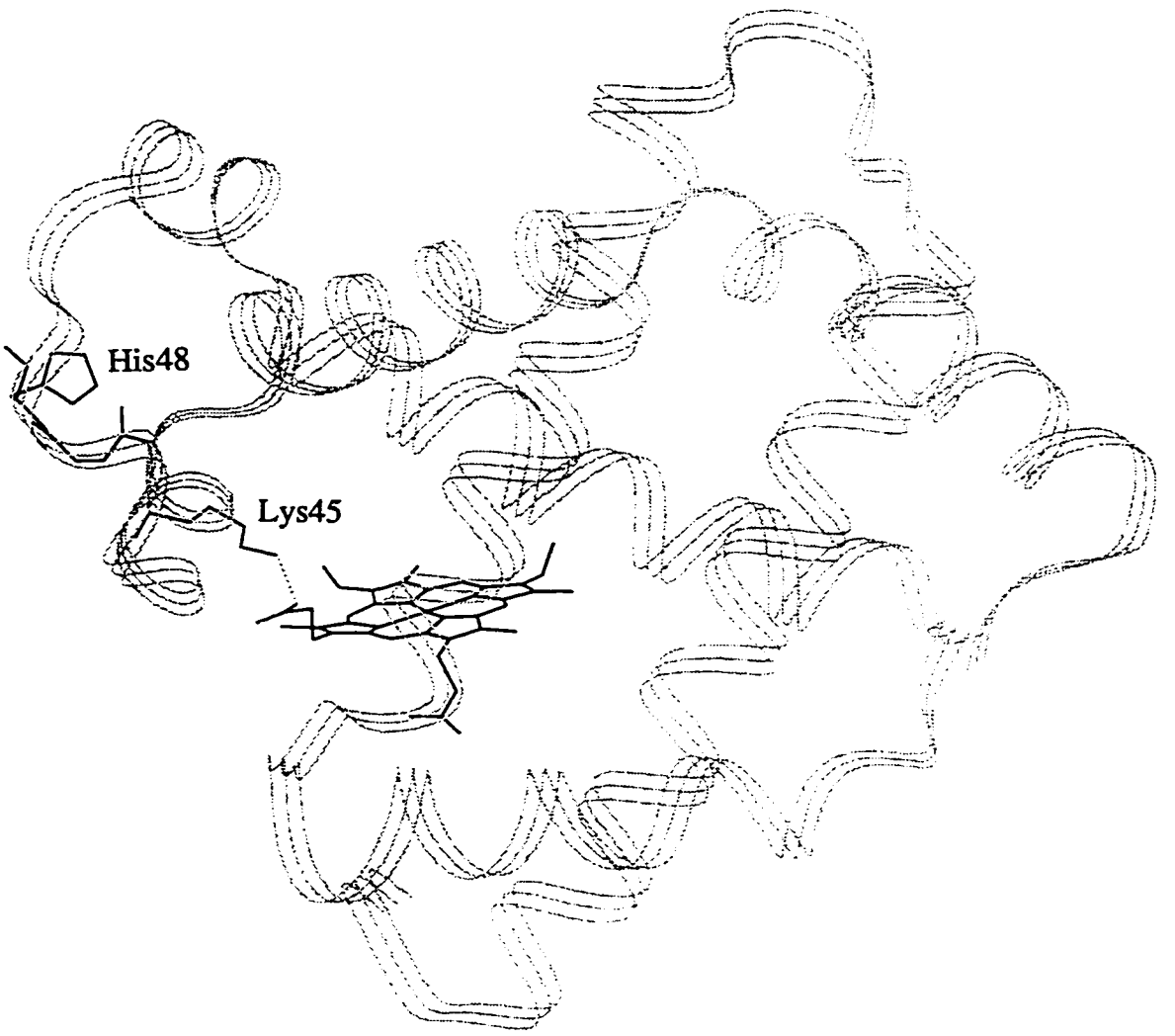

Figure 3.1 The shortest through-bond electron-transfer pathway between His48 and the heme in HHMb. The dashed line represents H-bonding between Lys45 and the heme propionate and the diagram was drawn using the X-ray coordinates for the 1.9-Å structure of HHMb.[22]

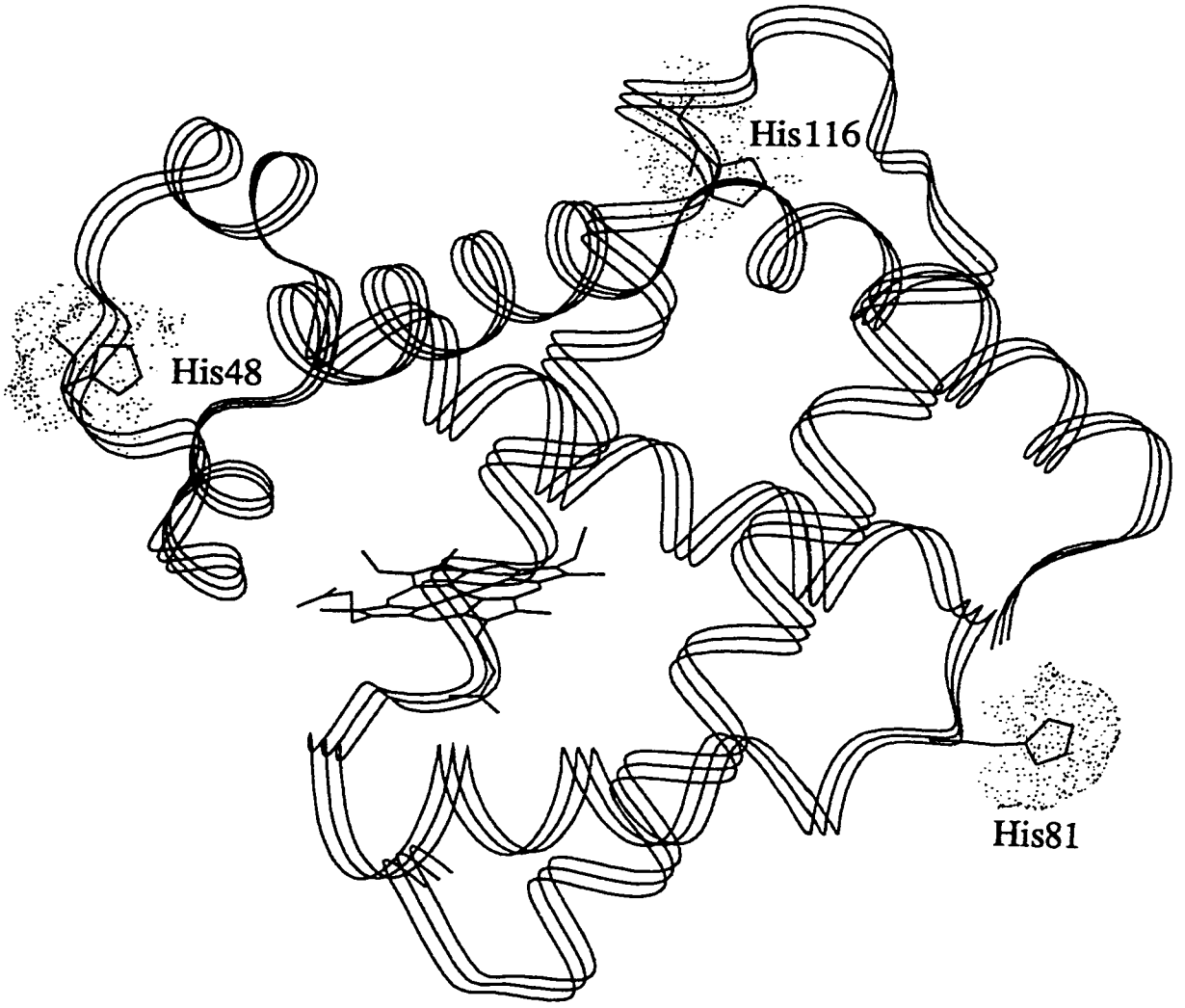

Figure 3.2 Cα backbone of HHMb with its heme and three surface histidines. Shaded areas represent the solvent-exposed surfaces of the histidine residues.

containing 10 mM 4.4'-bipyridine at pulse amplitudes of 10-50 mV. E°' was obtained from the intercept of the observed potential vs amplitude plot.[19]

HHMb (0.5-10 μM) solutions were prepared in N_2O-saturated 40 mM sodium phosphate reaction buffer at pH 7.0 containing 12 mM HCOONa to generate $CO_2\bullet^-$ radicals via reaction with OH•. Unless otherwise specified, pulse radiolysis experiments were performed at 25 °C using 2.0- or 6.0-cm path lengths. The dose in each pulse was chosen to generate sufficient $CO_2\bullet^-$ to reduce ≤10% of the protein. The ET reaction was followed spectrophotometrically by following the formation or decay of $HHMbFe^{III}\text{-}OH_2$, $HHMbFe^{II}$, and $HHMbFe^{IV}=O$ which exhibit Soret maxima at 409 (ε = 188 $mM^{-1}cm^{-1}$), 434 (ε = 135 $mM^{-1}cm^{-1}$), and 421 nm (ε = 123 $mM^{-1}cm^{-1}$), respectively.[20] The ratio of $CO_2\bullet^-$ reacting with Ru^{III} and Fe^{III} centers was determined by monitoring at 434 nm the amount of $MbFe^{II}$ formed on the millisecond and second time scales due to direct reduction by $CO_2\bullet^-$ and to intramolecular ET from Ru^{II}, respectively. $MbFe^{IV}=O$ was prepared by reacting 200-400 μM $HHMbFe^{III}$ with a 5-fold molar excess of H_2O_2 in argon degassed reaction buffer at pH 7.0. When the sample was fully converted to the $Fe^{IV}=O$ state (λ_{max} = 421 nm), excess peroxide was removed with a catalytic amount of bovine catalase (Sigma).

Pulse radiolysis was performed using the 60-ns electron pulses from a 2-MeV Van de Graaff accelerator. Transient absorption data were obtained using a conventional halogen lamp-filter-sample-monochromator-PMT detection system and fit by first-order kinetics. Dosimetry of the electron pulse was performed by measuring the initial absorbance of the di(thiocyanate) radical anion (ε_{472}= 7950 $M^{-1}cm^{-1}$) generated by

radiolysis of N_2O-saturated 0.01 M KSCN solution (G = 6.13 radicals / 100 eV absorbed).

To determine if the ET pathway was modified during $MbFe^{III}$ oxidation by H_2O_2, a_5Ru^{III}(His48)$MbFe^{IV}$=O, prepared as previously mentioned, was back titrated within 1 h to $MbFe^{III}$-OH_2 with 2,2'-azinobis[3-ethylbenzothiazoline-6-sulfonic acid] (ABTS; Boehringer Mannheim). The oxidation products were removed by ultrafiltration (Amicon) and Ru^{II}→Fe^{III} ET rates in a_5Ru^{III}(His48)$MbFe^{III}$-OH_2 were remeasured.

3.3 Results and Discussion

The bimolecular rate constant for the reduction of native $HHMbFe^{III}$-OH_2 by $CO_2\bullet^-$ was determined to be 2 x 10^8 M^{-1} s^{-1} by monitoring the appearance of $HHMbFe^{II}$ at 434 nm. Bimolecular reduction of the a_5Ru^{III}(His48) center in modified HHMb by $CO_2\bullet^-$ was found to have a rate constant ~6-fold higher than that for heme reduction; thus, 85% of the reduction occurred at the Ru^{III} center. The reduction potential for $a_5Ru^{III/II}$(His48) in HHMb was found to be 76 ± 1 mV vs NHE. Since the reduction potential for $HHMbFe^{III/II}$ is 57 mV,[21] the Ru and heme potentials are closely matched and the observed rate constant for intramolecular ET from Ru^{II} to the heme follows reversible first-order kinetics:

$$a_5Ru^{III}(His48)—Fe^{III}—OH_2 \xrightarrow[CO_2\bullet^-]{\text{fast}} a_5Ru^{II}(His48)—Fe^{III}—OH_2 \qquad (3.1)$$

$$a_5Ru^{II}(His48)—Fe^{III}—OH_2 \underset{k_{-1}}{\overset{k_1}{\rightleftharpoons}} a_5Ru^{III}(His48)—Fe^{II} + H_2O \qquad (3.2)$$

The observed rate constant ($k_{obs} = k_1 + k_{-1}$) is 0.059 ±0.003 s^{-1}, which is essentially identical to that observed previously for the a_5Ru(His48) derivative of SWMb.[12,22,23] Also, as with SWMb,[12] addition of CO trapped the Fe^{II} heme and transformed the equilibrium in eq 3.2 into an irreversible reaction. These results establish that the kinetics and thermodynamics[24,12] of ET in the a_5Ru(His48) derivatives of SWMb and HHMb are very similar, which is not surprising since the structures of the two proteins are also very similar.[18]

The rate of intramolecular ET to the Fe^{IV}=O heme of HHMb was measured after reaction with excess H_2O_2. Following the 60-ns pulse, rapid reduction of Ru^{III} by $CO_2^{\bullet -}$ occurred, and slow reduction of the Fe^{IV}=O to Fe^{III}-OH_2 heme was observed at 409 nm and 421 nm:

$$a_5Ru^{II}(His48)—Fe^{IV}=O \xrightarrow{k_{obs}} a_5Ru^{III}(His48)—Fe^{III}—OH_2 \qquad (3.3)$$

The change in heme absorbance at 409 nm and the fit by first-order kinetics are shown in Figure 3.3. The dependence of the k_{obs} on the initial concentration of a_5Ru^{III}(His48)—Fe^{IV}=O is shown in Figure 3.4. The rates are essentially independent of protein concentration, establishing that bimolecular ET processes are insignificant, and the average value of k_{obs} is 0.19 ± 0.02 s^{-1} for eq 3.3. This rate constant is 5-6 orders of magnitude smaller than those measured for Ru/Zn SWMb and RHMb,

$$a_5Ru^{III}(His48)—{}^3ZnP^* \xrightarrow{k_f} a_5Ru^{II}(His48)—ZnP^+ \xrightarrow{k_b} a_5Ru^{III}(His48)—ZnP \qquad (3.4)$$

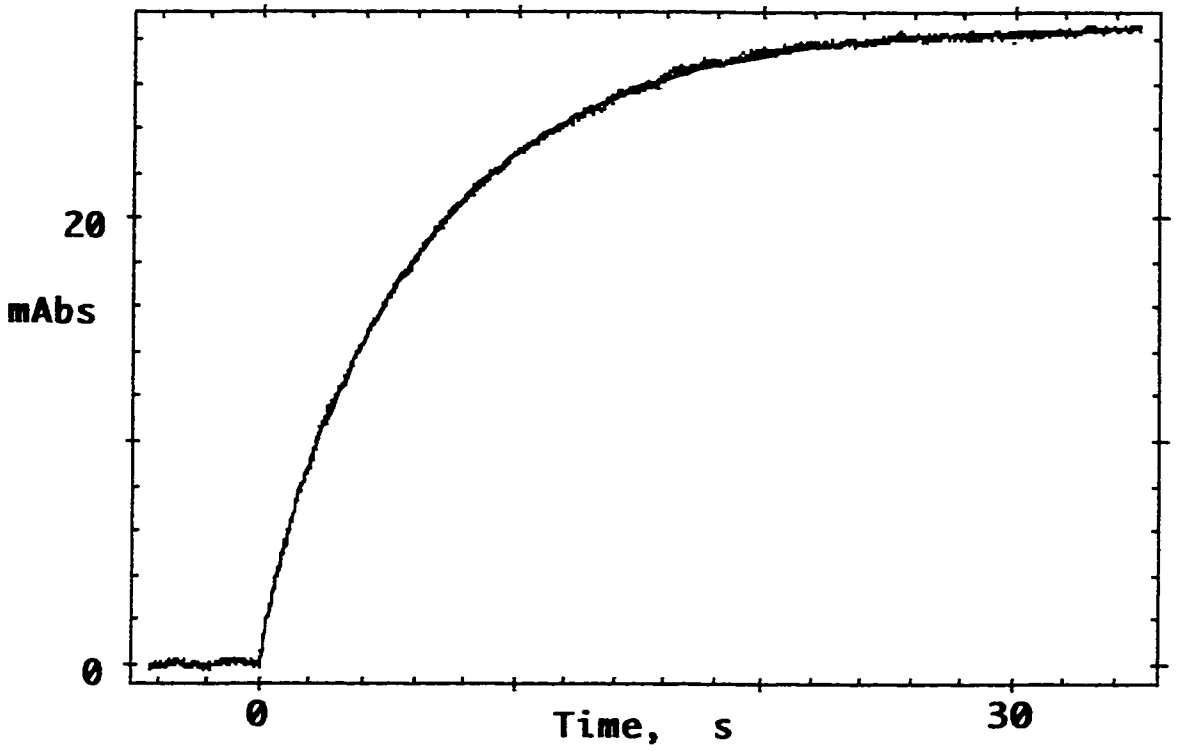

Figure 3.3 Observed absorbance change at 421 nm vs time following pulse radiolysis of 2 μM a_5Ru^{III}(His48)—Fe^{IV}=O HHMb. Reaction was carried out in N_2O-saturated, 40 mM phosphate with 12 mM sodium formate, pH 7.0, I = 0.1 M, 25.2 °C, path length 2.0 cm. The concentration of $CO_2\bullet^-$ generated in the pulse was 0.37 μM, and the observed $\Delta\varepsilon_{409}$~ 23 due to competition from $CO_2\bullet^-$ self quenching and scavengers. The solid line shows the fit of the experimental points to first-order kinetics.

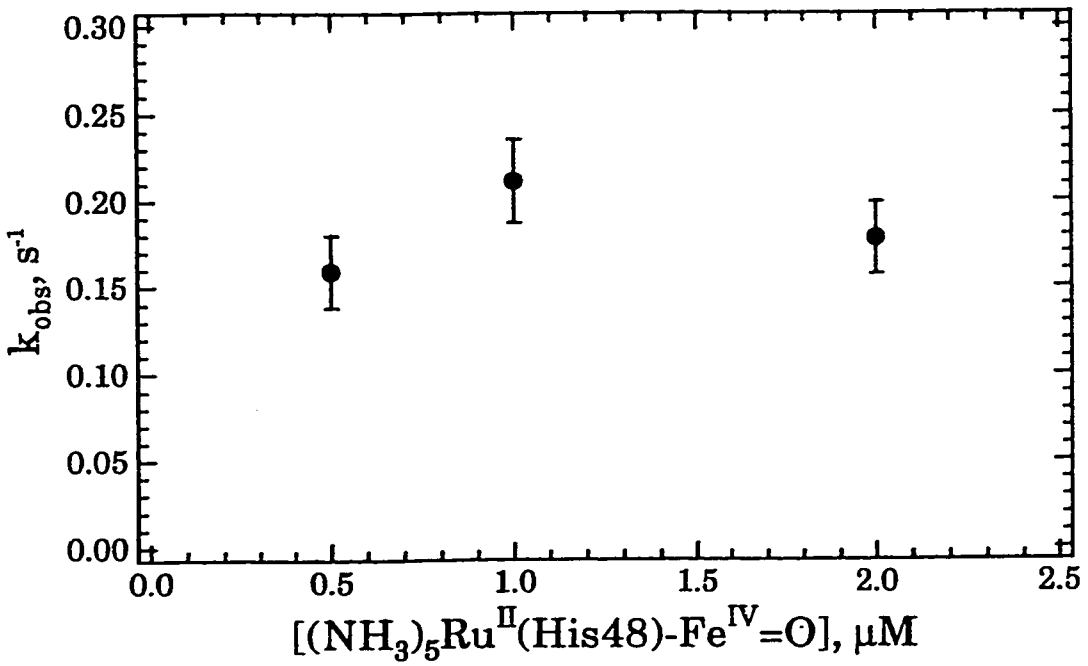

Figure 3.4 Dependence of the observed first-order rate constant k_{obs} for intramolecular ET $[a_5Ru^{II}(His48) \rightarrow Fe^{IV}=O]$ on the protein concentration.

where k_f and k_b are 7 x 10^4 and 1 x 10^5 s^{-1} at $-\Delta G^O$ values of 0.82 and 0.96 eV, respectively.[13,14] The reduction potential for $MbFe^{IV}=O \rightarrow MbFe^{III}\text{-}OH_2$ is 0.896 eV,[25] resulting in close to the same driving force (0.82 eV). Thus, over the same pathway, ET to the $Fe^{IV}=O$ of HHMb is ~ 10^6-fold slower than that to the Zn^+ porphyrin center. To ensure that reaction of $HHMbFe^{III}$ with H_2O_2, which also generates a short lived, unidentified radical,[26,27,28] did not alter the polypeptide between the Ru and heme centers, the ET rate was remeasured following reduction of the $Fe^{IV}=O$ heme. After reduction, k_{obs} (eq 3.2) was 0.063 ±0.016 s^{-1}, indicating that radical formation and decay do not retard ET. Consistent with slow *intramolecular* reduction of the $Fe^{IV}=O$ heme, the bimolecular rate constant for the reduction of unmodified $HHMbFe^{IV}=O$ by $CO_2\bullet^-$ was observed to be $<10^5$ $M^{-1}s^{-1}$, which is >3 orders of magnitude smaller than that observed for $HHMbFe^{III}\text{-}OH_2$ reduction under the same conditions.

Analysis of the temperature dependence of intramolecular $Fe^{IV}=O$ reduction is presented as an Eyring plot in Figure 3.5 and the data are presented in Table 3.1. The activation enthalpy ($\Delta H^{\ddagger}$) and entropy ($\Delta S^{\ddagger}$) for the reaction were calculated to be 11.2 ± 0.3 kcal/mol and -24.0 ± 0.9 cal/mol•deg, respectively. The $\Delta H^{\ddagger}$ is larger than that found for $Ru^{II} \rightarrow Fe^{III}$ ET in the a_5Ru(His48) derivative of SWMb (7.4 ± 0.5 kcal/mol),[12] revealing larger activation barrier for $Ru^{II} \rightarrow Fe^{IV}=O$ ET. The $\Delta S^{\ddagger}$ value being < 0 indicates that the transition state complex is more ordered than the precursor complex.

Assuming the same electronic coupling term (H_{AB} = 0.01 cm^{-1})[9] in a_5Ru(His48)Mb as in the corresponding $SWMbFe^{III/II}$ reaction, yields a reorganizational energy (λ) of 3.0 eV for reaction 3, compared to λ ~ 1.3 eV for the Zn-Mbs modified at His48.[9,14] For

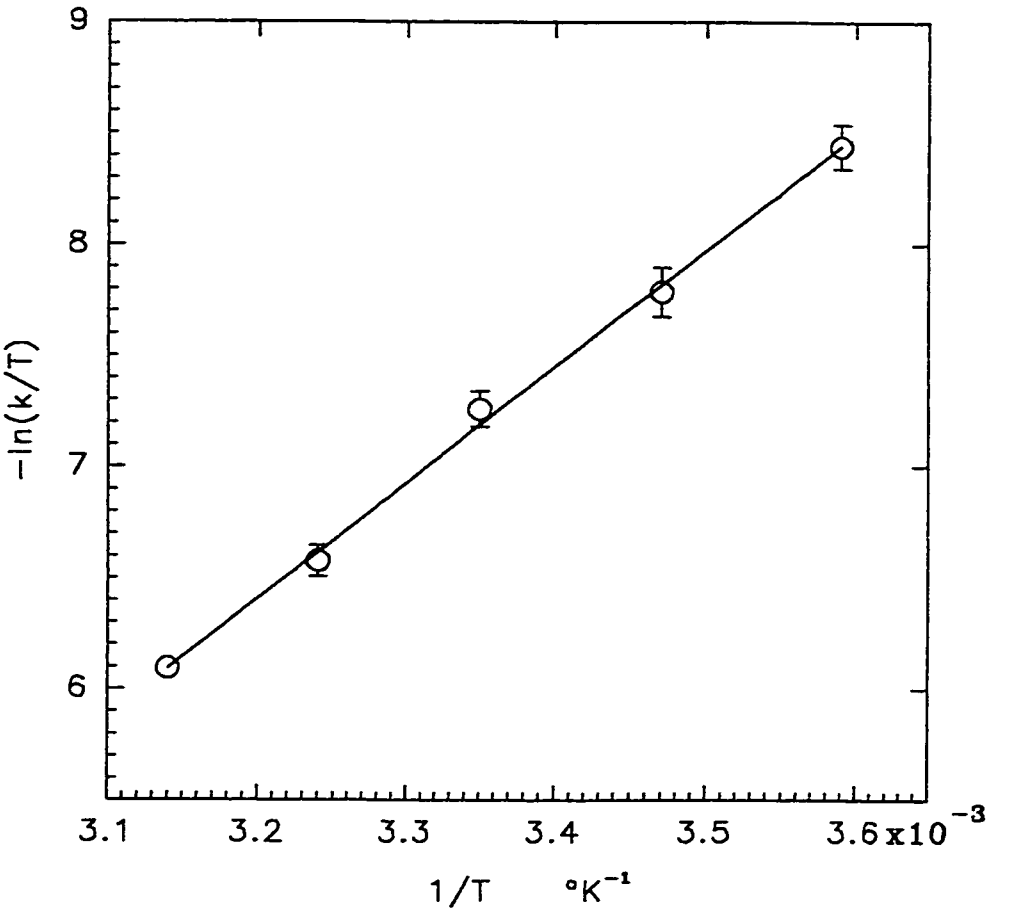

Figure 3.5 Eyring plot (ln k/T vs 1/T) for the observed first-order rate constant k_{obs} for intramolecular $Ru^{II} \rightarrow Fe^{IV}$=O ET in a_5RuHis48Mb. Experiments were performed from 5 to 35 °C in the same buffer system as in Figure 3.3 (pH 7.0, I = 0.1 M) .

Table 3.1 Temperature dependence of the observed intramolecular rate constants (k_{obs}) for $Ru^{II} \rightarrow Fe^{IV}$=O ET in a_5RuHis48Mb.

°C	k_{obs}
5.6	0.06 ± .02[a]
15.3	0.12 ± .02
25.1	0.21 ± .01
35.1	0.43 ± .01
45.2	0.72 ± .01

[a] k_{obs} are the average values from 4-7 independent pulse radiolysis experiments.

a_5Ru^{II}(His)CCP(Fe^{IV}=O) the predicted k_{obs} for ET over 12.7 Å can be calculated from the value (3.2 s^{-1}) over 21.8 Å,[16] and the Marcus equation (eq 1.6) with $H_{AB} = H^{\circ}_{AB} \exp[-^1/_2 \beta(d-d^{\circ})]$. This assumes that the electronic coupling strength (H_{AB}) decays exponentially with distance d, and H°_{AB} is the electronic coupling at van der Waals contact ($d^{\circ} \sim 3$ Å). Using a distance decay factor (β) of 1.4 $Å^{-1}$ as in Mb,[9] the predicted k_{obs} for ET over 12.7 Å would be 10^6 s^{-1}. However, the value calculated for k_{obs} depends strongly on the value used for β; for example, if β were 1.0 $Å^{-1}$ in CCP, k_{obs} at 12.7 Å would still be large (~ 10^4 s^{-1}) in CCP.[29] These rates suggest a small λ for CCP(Fe^{IV}=O) as in the Zn-Mbs.[14] However, the surprisingly slow intra- and bimolecular reduction of the Fe^{IV}=O heme in

HHMb suggests that ET may not be rate-limiting in this case. A possible explanation is that protonation of the oxene ligand precedes ET to Fe^{IV}=O. Thus, a lack of proton donors in the hydrophobic Mb heme pocket, unlike in the CCP pocket, would give rise to rate-limiting protonation in the former and rate-limiting ET in the latter (as in the Zn-Mbs). Experiments (driving force and pH/D dependence, and H/D isotope effects) to determine the nature of the rate-limiting step for reaction 3.3 will be discussed in Chapter 4.

References

1. George, P.; Irvine, D.H. *Biochem. J.* **1952**, *52*, 511.
2. George, P.; Irvine, D.H. *J. Colloid Sci.* **1956**, *11*, 327.
3. Fox, J.R., Jr.; Nicolas, R.A.; Ackerman, S.A.; Swift, C.E. *Biochemistry* **1974**, *13*, 5178.
4. King, N.K.; Winfield, M.E. *J. Biol. Chem.* **1963**, *238*, 1520.
5. King, N.K.; Looney, F.D.; Winfield, M.E. *Biochim. Biophys. Acta* **1967**, *133*, 65.
6. Winkler, J.R.; Nocera, D.G.; Yocum, K.M.; Bordignon, E.; Gray, H.B. *J. Am. Chem. Soc.* **1982**, *104*, 5798-5800.
7. Nocera, D.G.; Winkler, J.R.; Yocum, K.M.; Bordignon, E.; Gray, H.B. *J. Am. Chem. Soc.* **1984**, *106*, 5145-5150.
8. Isied, S.S.; Worosila, G.; Atherton, S.J. *J. Am. Chem. Soc.* **1982**, *104*, 7659.
9. Winkler, J.R.; Gray, H.B. *Chem. Rev.* **1992**, *92*, 369-379.

10. Bolton, J.R.; Archer, M.D. In *Advances in Chemistry Series CSC Symposium Series 2, Electron Transfer in Inorganic, Organic, and Biological Systems*, Bolton, J.R.; Mataga, N.; McLendon, G. Eds.; ACS Washington, **1991**, 8-23.

11. Lieber, C.M.; Karas, J.L.; Gray, H.B. *J. Am. Chem. Soc.* **1987**, *109*, 3778-3779.

12. Crutchley, R.J.; Ellis, W.R. Jr.; Gray, H.B. *J. Am. Chem. Soc.* **1985**, *107*, 5002.

13. Axup, A.W.; Albin, M.; Mayo, S.L.; Crutchley, R.J.; Gray, H.B. *J. Am. Chem. Soc.* **1988**, *110*, 435.

14. Casimiro, D.R.; Wong, L.-L.; Colon, J.L.; Zewert, T.E.; Richards, J.H.; Chang, I.-J.; Winkler, J.R.; Gray, H.B. *J. Am. Chem. Soc.* **1993**, *115*, 1485.

15. Tamura, M.; Woodrow, G.V.; Yonetani, T. *Biochim. Biophys. Acta* **1973**, *317*, 34.

16. Fox, T.; Hazzard, J.T.; Edwards, S.L.; English, A.M.; Poulos, T.L.; Tollin, G.; *J. Am. Chem. Soc.* **1990**, *112*, 7426-7428.

17. Uyeda, M.; Peisach, J. *Biochemistry* **1981**, *20*, 2028.

18. Evans, S.V.; Brayer, G.D. *J. Mol. Biol.* **1990**, *213*, 885.

19. Bard, A.; Faulkner, L.R. In *Electrochemistry Methods*; John Wiley & Sons: New York, **1980**; p194.

20. Tamura, M.; Asakura, T.; Yonetani, T. *Biochim. Biophys. Acta* **1973**, *295*, 467.

21. Taniguchi, I.; Watanabe, K.; Tominaga, M. *J. Electroanal. Chem.* **1992**, *333*, 331.

22. Lieber, C.M.; Karas, J.L.; Gray, H.B. *J. Am. Chem. Soc.* **1987**, *109*, 3778.

23. The $Fe^{III/II}$ and $a_5Ru^{III/II}$(His48) potential for SWMb are 58.8 and 85.5 mV, respectively.

24. Taniguchi, I.; Watanabe, K.; Tominaga, M. *J. Electroanal. Chem.* **1992**, *333*, 331.

25. He, B.; Sinclair, R.; Copeland, B.R.; Makino, R.; Powers, L.S.; Yamazaki, I. *Biochemistry* **1996**, *35*, 2413.

26. Davies, M.J. *Biochim. Biophys. Acta* **1991**, *1077*, 86.

27. Newman, E.S.R.; Rice-Evans, C.A.; Davies, M.J. *Biochem. Biophys. Res. Commun.* **1991**, *174*, 1414.

28. Catalano, C.E.; Choe, Y.S.; Ortiz de Montellano, P.R. *J. Biol. Chem.* **1989**, *264*, 10534.

29. Beratan, D.N.; Betts, J.N.; Onuchic, J.N. *Science* **1991**, *252*, 1285.

4.0 pH and Driving Force Dependence of Intramolecular Oxyferryl Heme Reduction in Myoglobin

4.1 Introduction

In recent years it has been suggested that all heme enzymes involved in redox catalysis use an oxyferryl (Fe^{IV}=O) heme in their catalytic cycles.[1,2] Fe^{IV}=O centers have oxidizing potentials close to 1 V and their reduction *in vivo* is coupled to a multitude of reactions.[2] Despite the importance and scope of heme enzymes, relatively little is known about what factors control the reactivity of Fe^{IV}=O centers in proteins. These centers are best characterized in heme peroxidases[2] where they are generated on the rapid reaction ($\geq 10^7$ M^{-1} s^{-1}) of the ferric enzymes (Fe^{III},P) with H_2O_2 :

$$Fe^{III},P + H_2O_2 \longrightarrow Fe^{IV}{=}O,P^{\bullet+} + H_2O \qquad (4.1a)$$

$$Fe^{IV}{=}O,P^{\bullet+} + 1e^- \longrightarrow Fe^{IV}{=}O,P \qquad (4.1b)$$

$$Fe^{IV}{=}O,P + 1e^- + 2H^+ \longrightarrow Fe^{III},P + H_2O \qquad (4.1c)$$

Myoglobin (Mb) is a small (MW ~17 kDa), stable heme protein designed to reversibly bind dioxygen.[3] When exposed to H_2O_2, it reacts slowly (~10^2 M^{-1} s^{-1})[4] to form a stable Fe^{IV}=O heme and a protein radical that decays quickly[4,5] without causing detectable modification to the polypeptide (Chapter 2).[6] Oxyferryl Mb ($MbFe^{IV}$=O) has been extensively characterized;[4,5,7] hence, the study of $MbFe^{IV}$=O reactivity is informative

since there are obvious structural differences between Mb and heme peroxidases. In particular, the solvent-isolated, hydrophobic heme pocket of Mb[8a] contrasts sharply with the peroxidase active site, which contains a number of H_2O molecules and is linked by a hydrated channel to the solvent.[8b] This water bridge can provide a source of protons to facilitate the rapid reduction of the oxene ligand (eq 4.1c), which appears to be the rate-limiting step in peroxidase turnover.[9]

The goal of this work is to probe the electron-transfer (ET) reactivity of the Fe^{IV}=O heme center in horse heart Mb (HHMb). The reaction of interest is the following:

$$MbFe^{IV}=O + 1e^- + 2H^+ \rightarrow MbFe^{III}\text{-}OH_2 \qquad (4.2)$$

Reaction 4.2 differs from that in 4.1c in that the H_2O generated on reductive protonation of the oxene ligand remains bound to the Fe^{III} center in Mb. To eliminate the uncertainties associated with bimolecular ET reactions, intramolecular reduction was performed by modifying the surface His48 of HHMb with redox-active Ru complexes following well-established protocols.[10-13] ET rates have been extensively studied in Fe^{II}, Fe^{III} and metalloderivatives of sperm whale Mb (SWMb) using this methodology.[10,11] We have reported previously that $a_5Ru^{II} \rightarrow Fe^{IV}$=O ET in HHMb is surprisingly slow.[14] To gain further insight into the mechanism of this latter reaction, the ligands of the bound Ru complex were changed to determine the effects of varying the driving force for ET on the observed rates. The reactions were also carried out in H_2O and D_2O as a function of pH/pD to investigate the mechanism of proton involvement in the reductive protonation

of Fe^{IV}=O to Fe^{III}-OH_2 (eq 4.2).

4.2 Materials

Horse heart Myoglobin (HHMb) and bovine liver catalase were purchased from Sigma, and modified sequencing-grade trypsin from Boehringer Mannhein. Chemicals were obtained from the following suppliers: chloropentaammineruthenium(III) chloride $(a_5Ru^{III}Cl)Cl_2$ (Johnson Matthey); $CoCl_2 \cdot 6H_2O$, pyridine, isonicotinamide, 4,4'bipyridine and 1,10 phenanthroline monohydrate (Aldrich); KCN (BDH Chemicals); buffer salts, 30% H_2O_2 (Fisher); 99.8% D_2O (Brookhaven). Chlorotetraamminepyridineruthenium(III) chloride $(a_4Ru^{III}PyrCl)Cl_2$, chlorotetraammineisonicotinamideruthenium(III) chloride $(a_4Ru^{III}IsnCl)Cl_2$,[15a-c] and tris(1,10-phenanthroline)cobalt(III) chloride $[Co(phen)_3^{3+}]$[15d] were synthesized by the literature procedures, as were the a_4LRuHis model complexes.[16] Zinc amalgam was prepared by adding acid (1 mM HCl) washed Zn granules (Fisher) to a saturated solution of mercuric chloride (Mallinckrodt), stirring over low heat for 10 min, washing with distilled water and air drying. Sephadex G-25 gel-filtration resin was purchased from Pharmacia, and a stirred ultrafiltration cell and YM 5 membranes (5000 MW cutoff) from Amicon.

4.3 Methods

Derivatization of the surface histidines of HHMb with the Ru complexes was performed using the published procedures[10] with slight modifications. Solutions containing 1 mM HHMb and 30 mM $a_4LRu^{III}Cl$ (L= NH_3, pyridine or isonicotinamide)

in 50 mM Tris buffer (pH 7.0) were separately degassed under a constant flow of argon for 1 h. Freshly prepared Zn amalgam was added to the $a_4LRu^{III}Cl$ solution and the $a_4LRu^{II}H_2O$, which formed under argon in ~1.5 h, was transferred by gas-tight syringe to the Mb sample. The resulting solution, which contained 11 mM Ru^{II} complex and 0.6 mM Mb, was left standing for 1 h at room temperature, and excess Ru complex was removed by gel filtration on a G-25 column (25 x 40 cm) under anaerobic conditions. The protein was eluted first as a dark red band, the Fe^{II} and Ru^{II} centers were immediately oxidized with $Co(phen)_3^{3+}$, and the oxidant was removed by ultrafiltration with 50 mM NaPi buffer (pH 6.0). The Mb derivatives were separated on a cation-exchange column (Mono S HR 10/10, Pharmacia) fitted to a Pharmacia FPLC system.

The FPLC-separated Mb derivatives were characterized by UV/vis spectroscopy and electrospray mass spectrometry (ES-MS). For UV/vis analysis, a 1-μM $a_4LRu^{III}MbFe^{III}$ solution was reacted with excess KCN to form the Fe^{III}-CN complex, and sufficient sodium ascorbate was added to reduce the Ru^{III} but not the Fe^{III}-CN center. The a_4LRu^{III} minus a_4LRu^{II} difference spectra were recorded on a Beckman DU 650 spectrophotometer, and compared to those of the free $a_4LRuHis$ complexes to identify the FPLC bands containing native, singly- and multiply-modified Mb.

Prior to ES-MS, 2 μg of FPLC-purified Mb derivative was desalted on a Vydac C18 HPLC column (4.6 x 250 mm) using a linear (10-60%) CH_3CN gradient in 0.1% TFA over 15 min at a flow rate of 1 mL/min. ApoMb was eluted at ~50% CH_3CN, lyophilized, resuspended in 1:1 methanol:water with 0.5% acetic acid, and infused at 2 μL/min into the ES source of a Finnigan SSQ 7000 mass spectrometer.

The site of Ru attachment in the singly-modified Mb derivatives was identified by tryptic digestion followed by on-line LC-MS. ApoMb (10 μM) was digested with 1:50 (w/w) trypsin in 0.1 M $NaHCO_3$ at 37 °C for 4 h, and digestion was stopped by lowering the pH to 2 with acetic acid. A 5-μL aliquot was loaded on a Vydac C18 microbore column (1 x 250 mm) fitted to a HP 1090 HPLC system, and the tryptic peptides separated using a linear (0 - 60%) CH_3CN gradient in 0.05% TFA over 60 min at a flow rate of 40 μL/min. The effluent was fed directly into the mass spectrometer to identify the peptides with a bound a_4LRu group.

Reduction potentials ($E^{o'}$) of the Mb-bound Ru^{III} complexes were determined by differential pulse voltammetry (DPV) using a BAS 100A potentiostat. A 1-mL solution containing 50 μM $a_4LRu^{III}Mb$ and 10 mM 4,4'-bipyridine in 50 mM NaPi (pH 7.0) was degassed under N_2 for 15 min in a sealed electrochemical cell with a gold working electrode, Ag/AgCl reference electrode (BAS) and Pt wire (Fisher) auxiliary electrode before measurements were taken. Addition of 4,4'-bipyridine promoted heterogenous ET between the gold electrode and Mb, and minimized irreversible protein adsorption on the electrode.[17]

ET was initiated by electron pulse radiolysis with a 2-MeV Van de Graaff accelerator at Brookhaven as previously described.[14,18] Derivatized Mb samples (0.5-2 μM) were prepared in 40 mM NaPi buffer containing 12 mM HCOONa and saturated with N_2O gas. The formate ion reacts with radiolytically-generated $OH^{\bullet}$ to give $CO_2^{\bullet-}$:

$$H_2O \text{ -}\!\!\wwvy\!\!\rightarrow e^-_{aq} + OH^{\bullet} + H^+ \qquad (4.3a)$$

$$e^-_{aq} + N_2O + H_2O \rightarrow N_2 + OH^{\bullet} + OH^- \qquad (4.3b)$$

$$OH^{\bullet} + HCO_2^- \rightarrow CO_2^{\bullet-} + H_2O \qquad (4.3c)$$

$CO_2^{\bullet-}$ is a strong reductant (E° = 1.90 V vs NHE)[19] that reduces the metal centers without damaging the protein. The electron dose in each pulse was chosen to generate sufficient $CO_2^{\bullet-}$ to reduce ≤10% of the protein[14] in 2.0- or 6.1-cm pathlength cells at 25 °C. Ru^{II} → heme ET was followed by monitoring changes in the Soret band of Mb (Fe^{IV}=O, ε_{421} = 123; Fe^{III}-H_2O, ε_{409} = 188; Fe^{II}, ε_{434} = 135 $mM^{-1}cm^{-1}$).[78]

Fe^{IV}=O samples were prepared by reacting 200-400 μM $MbFe^{III}$-H_2O with 5-fold excess H_2O_2 in argon degassed reaction buffer at pH 7.0. When $MbFe^{IV}$=O was fully formed (as determined spectrophotometrically), a catalytic amount of catalase was added to remove excess H_2O_2, and an aliquot transferred by gas-tight syringe to the pulse radiolysis cell containing N_2O-saturated reaction buffer. The pH was adjusted by adding stock $MbFe^{IV}$=O at pH 7.0 to a buffer of lower or higher pH in the cell, and the pH of pulsed and unpulsed samples was monitored to assure sufficient buffering during the kinetic measurements. Samples in D_2O were equilibrated overnight before use to allow complete H/D exchange at room temperature. The pD (= pH + 0.4)[20] was controlled in the same way as the pH, and extreme care was taken to minimize introduction of H^+. Kinetic measurements were performed immediately after $MbFe^{IV}$=O formation since this species spontaneously decays back to $MbFe^{III}$-OH_2 ($t_{1/2}$ ~ 66 min at pH 6.5 and 16 min at pH 5.6; Table 2.6).

4.4 Results

Purification of the ruthenation reaction mixtures by cation-exchange FPLC (Figure

4.1) allowed isolation and separation of the singly-modified HHMb derivatives as previously reported for SWMb.[10] Native HHMb was eluted first from the Mono S column, followed by singly- and multiply-modified samples. The number of ruthenium complexes attached to the modified samples was determined by taking the difference (Ru^{II} - Ru^{III}) spectra in a_4LRuMbFe^{III}-CN (Figure 4.2A and B). Figure 4.2B shows the Ru^{II} - Ru^{III} difference spectra in 3 singly- and 1 doubly- modified Mb sample. Derivatives singly-modified at the surface histidines (48, 81 and 116) were obtained in 8-15% yield. His48-modified HHMb was the last of the singly-modified derivatives to be eluted from the FPLC column for each Ru complex.

ES-MS confirmed the UV/vis results that singly-modified derivatives with covalently-bound a_4LRu had been prepared. The deconvoluted mass spectrum of a_4IsnRuHis48Mb is shown in Figure 4.3, with the major peak at 17,237 corresponding to that of the apo form, since the heme dissociates from the globin under the acidic ES-MS conditions.[21] A phosphate adduct of a_4IsnRuHis48Mb is observed at 17,335 and adduct dissociation occurs at higher voltages. The spray voltage in the ES source was maintained at <3.7 kV, otherwise fragmentation of the bound Ru complex occurred during ionization. Even under the soft ionization conditions used, peaks corresponding to apoMb and apoMb + Ru are evident in Figure 4.3.

On-line LC-MS peptide mass mapping of tryptic digested a_4IsnRuHis48Mb is shown in Figure 4.4. The a_4IsnRu-modified His48 peptide is indicated with an arrow, whereas all other peaks represent native Mb peptides. The mass spectrum of the modified peptide is shown in Figure 4.5, revealing m/z values of 397.3 and 498.2 for the native and

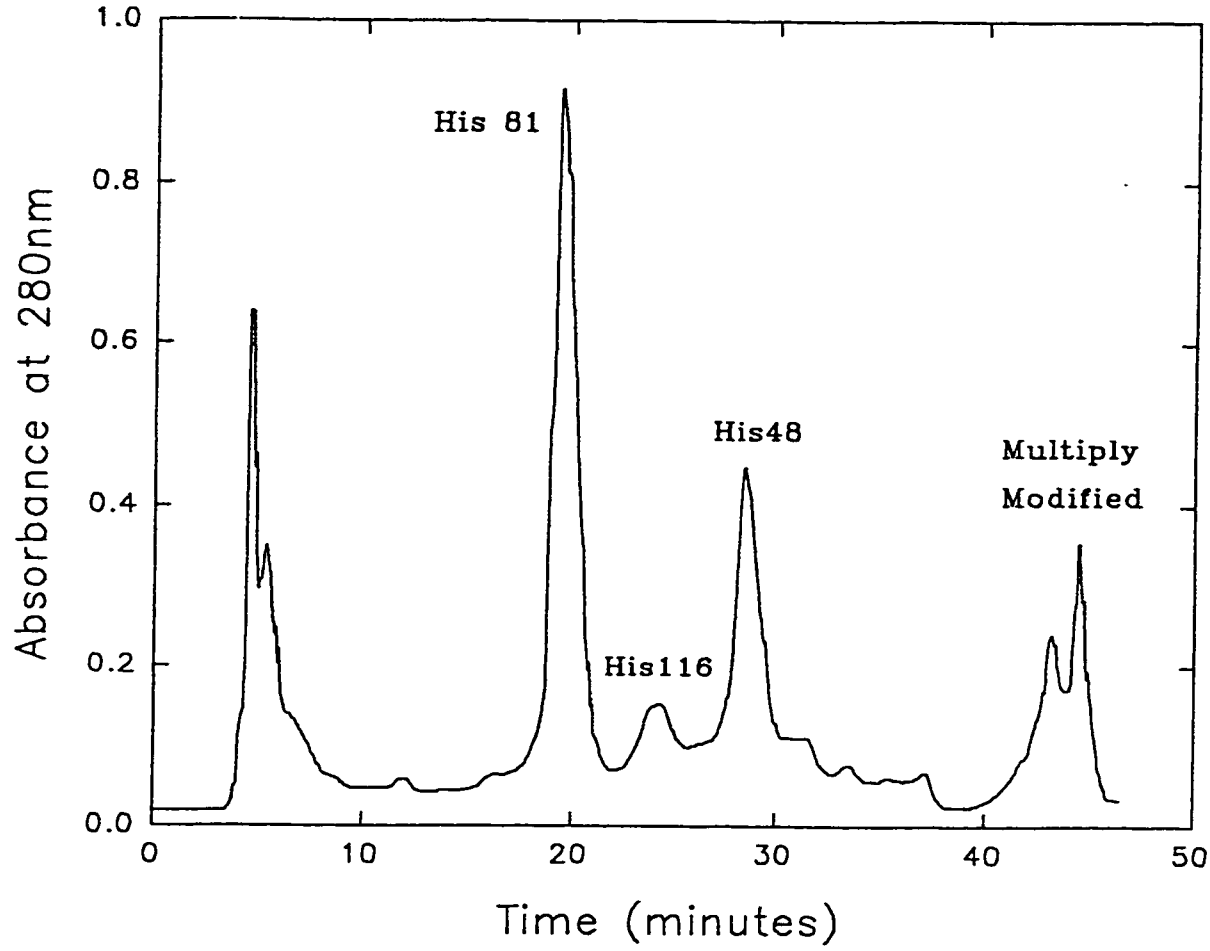

Figure 4.1 Separation of a_4IsnRuMb derivatives by cation-exchange FPLC. The Mono S HR 10/10 column was equilibrated with 50 mM NaPi, pH 7.0, and ~500 µL of 1 mM (17 mg/ml) Mb was loaded on the column and the components separated using a linear gradient NaCl (0 to 200 mM) in 50 mM NaPi, pH 7.0, with a flow rate of 0.6 ml/min, fraction size 0.5 ml. The elution was monitored at 280 nm and each peak was collected and saved for analysis. The peaks containing Mb singly-derivatized at the three surface histidines are labelled.

Figure 4.2 UV-vis spectra of 1 μM $a_4IsnRu^{III}MbFe^{III}$-CN and $a_4IsnRu^{II}MbFe^{III}$-CN (a) and the difference (Ru^{II} - Ru^{III}) spectra (b). The latter were compared to Ru^{II} -Ru^{III} spectra of the model compounds and used to identify the number of ruthenium complexes bound to Mb. a_4IsnRu^{III} was reduced to a_4IsnRu^{II} with a small excess of ascorbate and the $MbFe^{III}$ heme remained redox insensitive due to the bound cyanide. Samples were in 50 mM Pi, (pH 7.0).

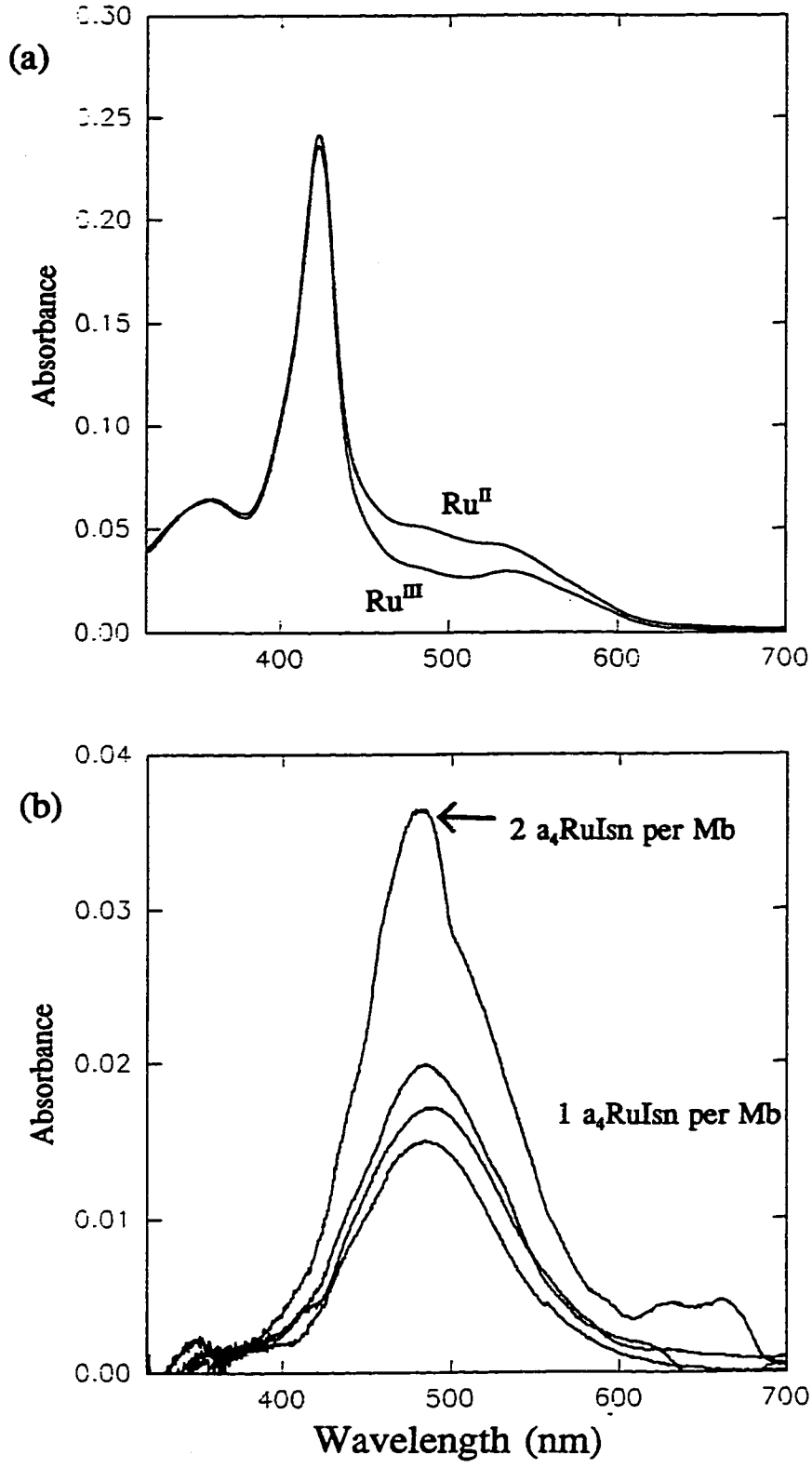
(a)
0.30
0.25
0.20
0.15
0.10
0.05
0.00
Absorbance
400
500
600
700
Ru^II
Ru^III
(b)
0.04
0.03
0.02
0.01
0.00
Absorbance
2 a4RuIsn per Mb
1 a4RuIsn per Mb
400
500
600
700
Wavelength (nm)

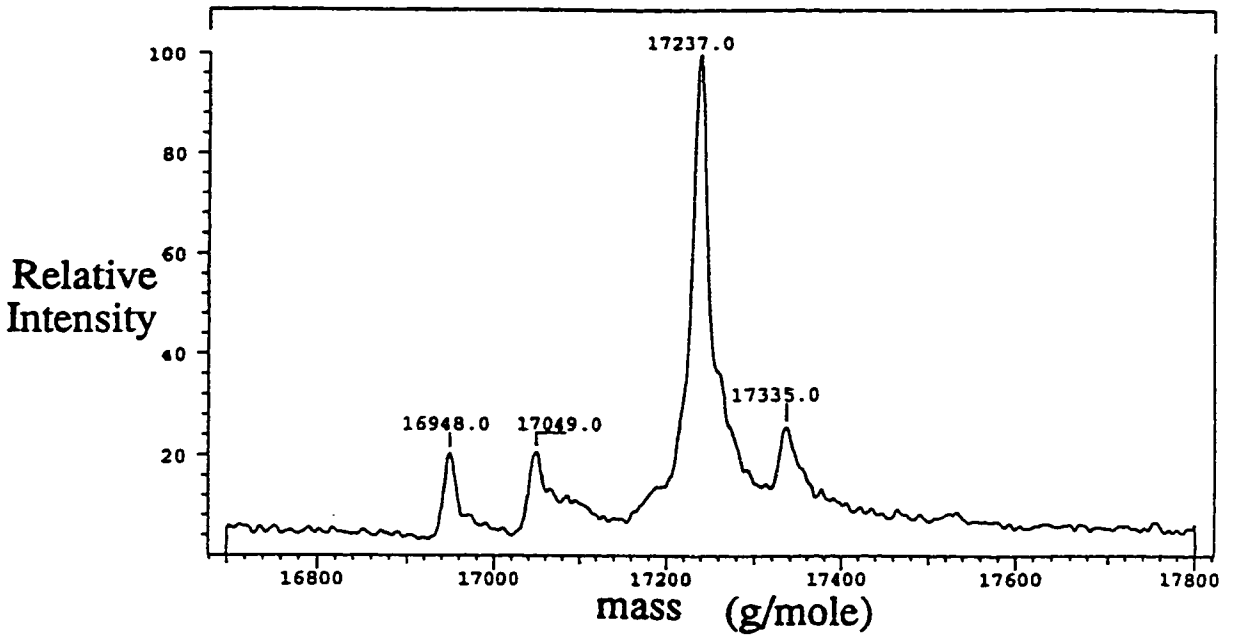

Figure 4.3 Deconvoluted ES mass spectrum of a_4IsnRuHis48Mb. The lyophilized sample (< 1 μg) dissolved in 50 μL methanol:H_2O with 0.5% acetic acid was infused into the ES source at a flow rate of 2 μL/min. The spray voltage was maintained at 3.7 kV to avoid dissociation of the Ru complex (see text). The peaks at mass 17,237 and 17,335 correspond to the heme-free form of a_4IsnRuHis48Mb and a phosphate adduct, and those at 16,948.0 and 17,049.0 to apoMb and apoMb plus Ru.

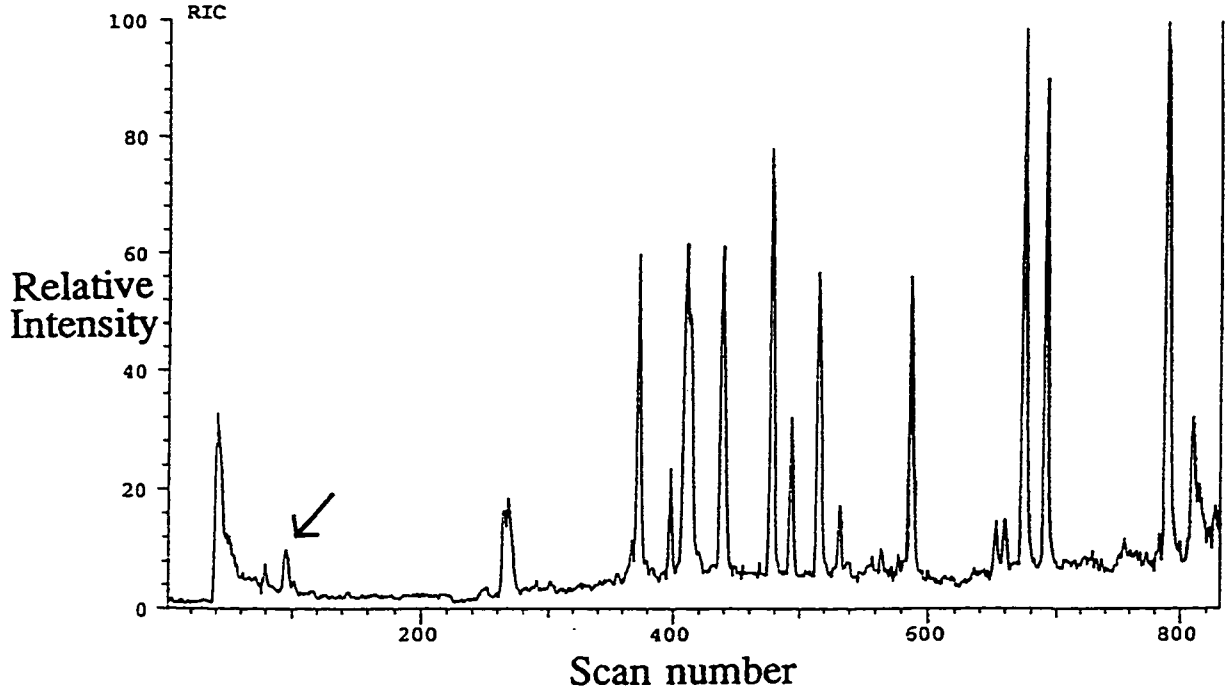

Figure 4.4 Separation of a_4IsnRuHis48Mb tryptic peptides by HPLC with on-line ES-MS analysis. A 5-μL aliquot was loaded on a Vydac reversed phase C18 microbore column, and the tryptic peptides separated using a linear (0 - 60%) CH_3CN gradient in 0.05% TFA over 60 min at a flow rate of 40 μL/min. The arrow indicates the a_4IsnRu modified His48 peptide.

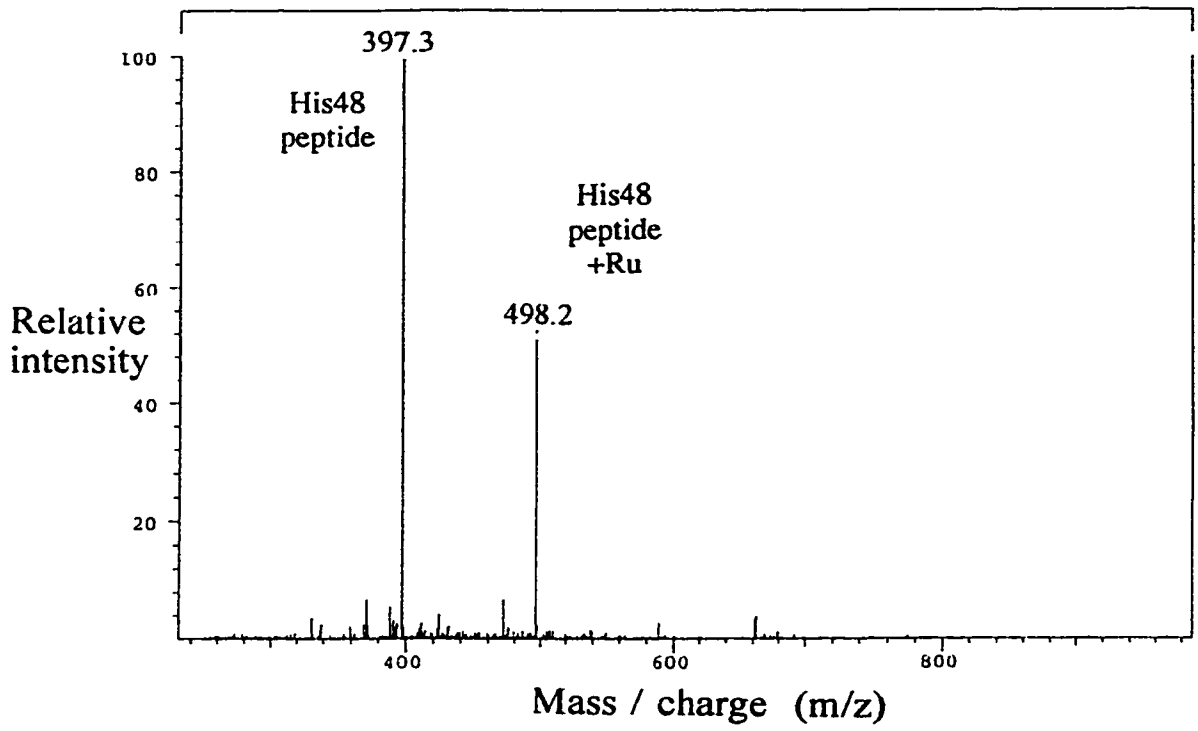

Figure 4.5 Mass spectrum of the a_4IsnRu-modified His48 peptide. The spectrum was recorded during the LC-MS run (scan number 96) shown in Figure 4.4. Fragmentation during the ionization process results in the loss both of individual Ru ligands and the whole Ru complex from the His48 peptide. The 498.2-Da peak represents the His48 peptide (397 Da) + Ru (101 Da).

Ru bound peptide, respectively. As with the whole-protein mass spectrum (Figure 4.3), fragmentation of the bound Ru complex occurred during ionization.

Reduction potentials for the HHMb-bound $a_4LRu^{III}His$ groups (structures given in Figure 4.6) were determined since the protein environment is known to shift the E°'s of the Ru complexes from those measured for the corresponding free complexes.[22] Peak potentials (E_p) were measured at several different pulse amplitudes (ΔE) for each Mb derivative, and E°' values were determined from:[23]

$$E_p = E^{\circ\prime} - \frac{\Delta E}{2} \qquad (4.4)$$

Slopes of E_p vs ΔE plots (Figure 4.7) were close to the predicted value of -0.5, and the

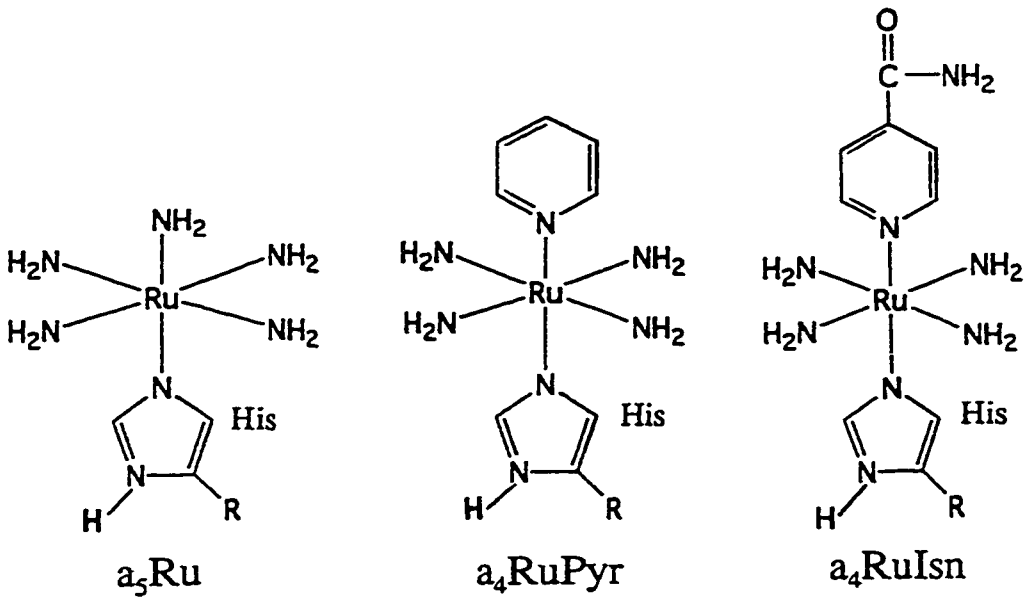

Figure 4.6 Structures of the three ruthenium complexes coordinated to His48 of HHMb.

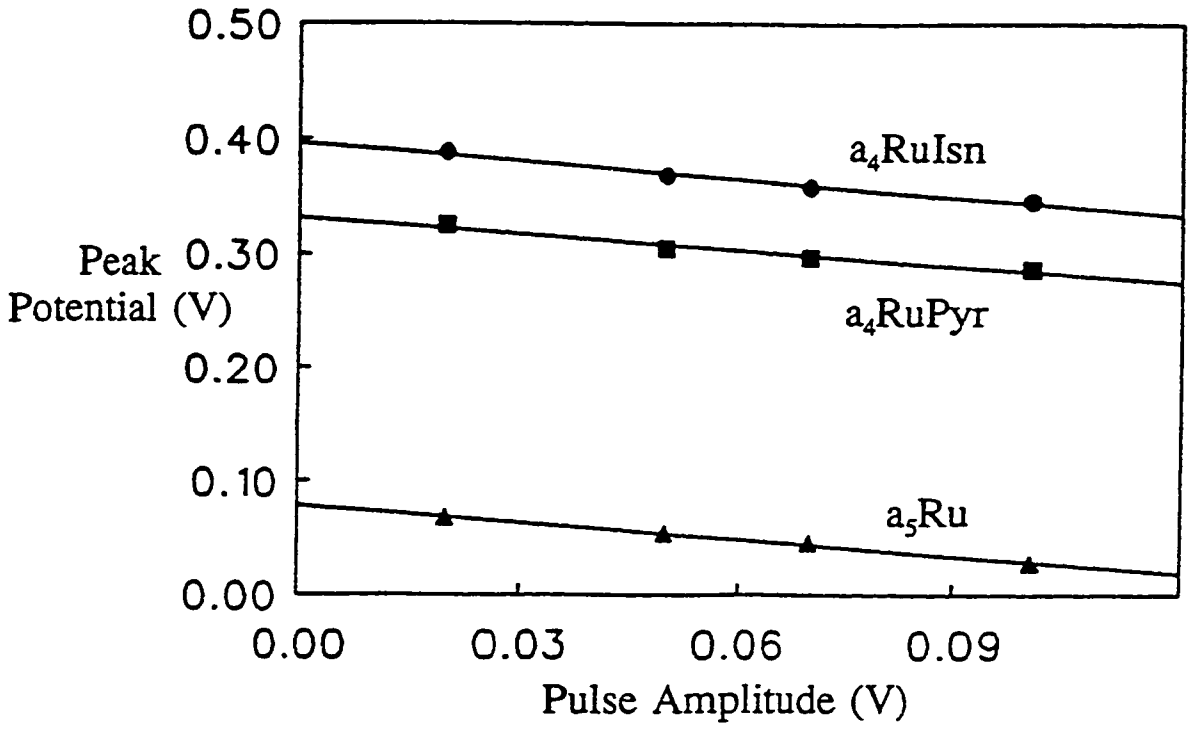

Figure 4.7 Differential pulse voltammetry of the Ru^{III} center of a_4LRuHis48Mb (40 - 100 μM) in N_2-saturated 50 mM NaPi (pH 7.0) containing 10 mM 4,4'-bipyridine. The potential of the gold working electrode (vs Ag/AgCl) was scanned at 5 mV/s, and the data points represent peak potentials of $Ru^{III/II}$ (vs NHE) at different pulse amplitudes. The E°' values were calculated from eq 4.4 in the text.

Table 4.1 Reduction Potentials (mV vs NHE) for $Ru^{III/II}$ in Free and Protein-Bound a_4LRuHis Complexes[a]

a_4LRu group	Model complex[b]	HHMb[b] His48	SWMb[c] His48	Ck Cyt c[d] His39	HH Cytc[d] His33
a_5Ru	71 ± 2	77 ± 1	85	95	128
a_4PyrRu	309 ± 3	330 ± 3	340	-	370
a_4IsnRu	388 ± 3	400 ± 2	420	400	434

[a] Phosphate buffer (pH 7.0) with 10 mM 4,4'-bipyridine

[b] This work (see Figure 4.7)

[c] Sperm whale Mb data from Refs 10a and 10e

[d] *Candida krusei* and horse heart cyts c data from Ref 52

y- intercepts yielded E°'s of 77, 330 and 400 mV for a_5RuHis48Mb, a_4PyrRuHis48Mb, and a_4IsnRuHis48Mb, respectively. These values are compared in Table 4.1 to those found for the free model complexes and to literature values for other heme proteins. Interestingly, the E°'s for the Ru^{III} centers bound to His48 of HHMb are 8-20 mV lower than those bound to His48 of SWMb.

Following the electron pulse, the $CO_2^{\bullet-}$ radical rapidly ($k > 10^9$ M^{-1} s^{-1}) and preferentially (>95%) reduced the Ru centers of $a_4LRu^{III}MbFe^{IV}=O$.[24] $Ru^{II} \rightarrow Fe^{IV}=O$ ET

was readily followed on the second timescale by monitoring the absorbance increase at 409 nm on $MbFe^{III}$-OH_2 formation, or the decrease at 421 nm on $MbFe^{IV}$=O decay. The rate data were analyzed by fitting the absorbance changes by competing first- and second-order processes. At pH ≤ 7, the amplitude of the second-order process was negligible at the low concentration of protein used and the data are well fit by the first-order process alone (Figure 4.8), which is attributed to:

$$a_4LRu^{II}His48—Fe^{IV}=O + 2H^+ \xrightarrow{k_{obs1}} a_4LRu^{III}His48—Fe^{III}\text{-}OH_2 \qquad (4.5)$$

The k_{obs1} values were independent of the initial $a_4LRu^{II}His48MbFe^{IV}$=O concentration (0.5-2.0 μM), indicating that Fe^{IV}=O reduction occurs via intramolecular ET as indicated in eq 4.5, and as previously reported for $a_5Ru^{II}His48MbFe^{IV}$=O.[14] Above pH 7.5 the second-order process has significant amplitude, and dominates at pH 8 where k_{obs1} values are ≤0.01 s^{-1}.

Figure 4.9 shows k_{obs1}-pH and k_{obs1}-pD plots for $a_5Ru^{II}His48MbFe^{IV}$=O, and the k_{obs1}-pH plot for the a_4LRu derivatives; the k_{obs1} values are also listed in Table 4.2. The kinetics of $a_5Ru^{II}His48—Fe^{III}$-OH_2 ⇌ $a_5Ru^{III}His48—Fe^{II}$ + H_2O in HHMb were also examined at pH 7.0 and pH 5.4, and k_{obs} values of 0.059 ± 0.003 and 0.063 ± 0.005 s^{-1}, respectively, were obtained as discussed in Section 3.3. Since ET to the Fe^{III} heme is not a proton-coupled process, the pH independence of k_{obs1} suggests that the electronic coupling between the Ru^{II} and heme centers is also pH independent over the same range.

Figure 4.8 Observed absorbance change at 409 nm (Fe^{III}-OH_2 formation) and 421 nm (Fe^{IV}=O decay) vs time following pulse radiolysis of 1 μM $a_5Ru^{III}His48MbFe^{IV}$=O in N_2O-saturated 40 mM NaPi, 12 mM HCOONa (pH 7.0) at room temperature, pathlength 2 cm. A 60-ns electron pulse was applied at t = 0 and the dose used was sufficient to reduce <10% of the Ru^{III} centers. The solid lines show the fit of the experimental points by first-order kinetics.

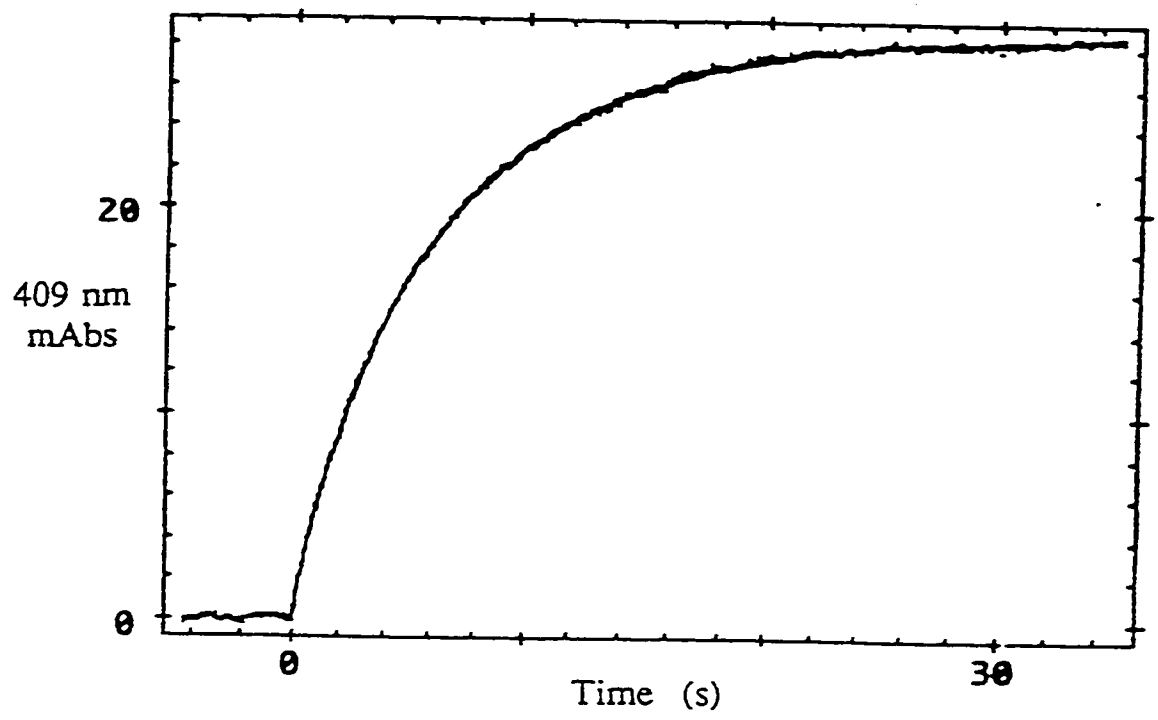
20
409 nm
mAbs
0
0
30
Time (s)

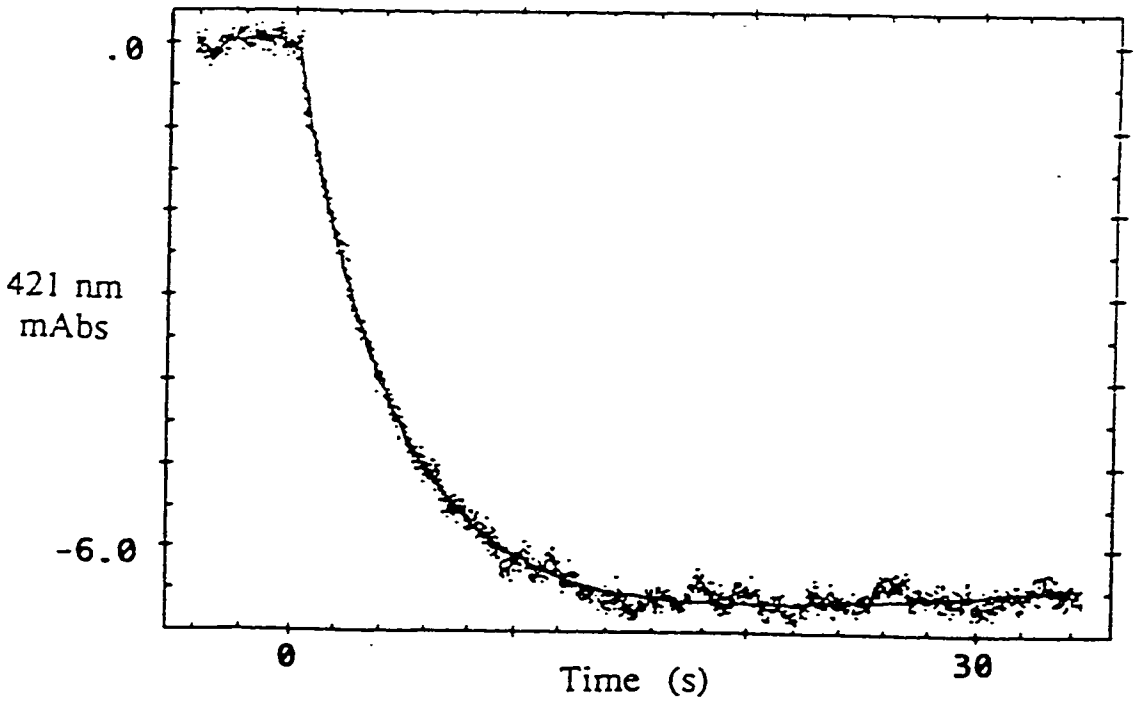
.0
421 nm
mAbs
-6.0
0
30
Time (s)

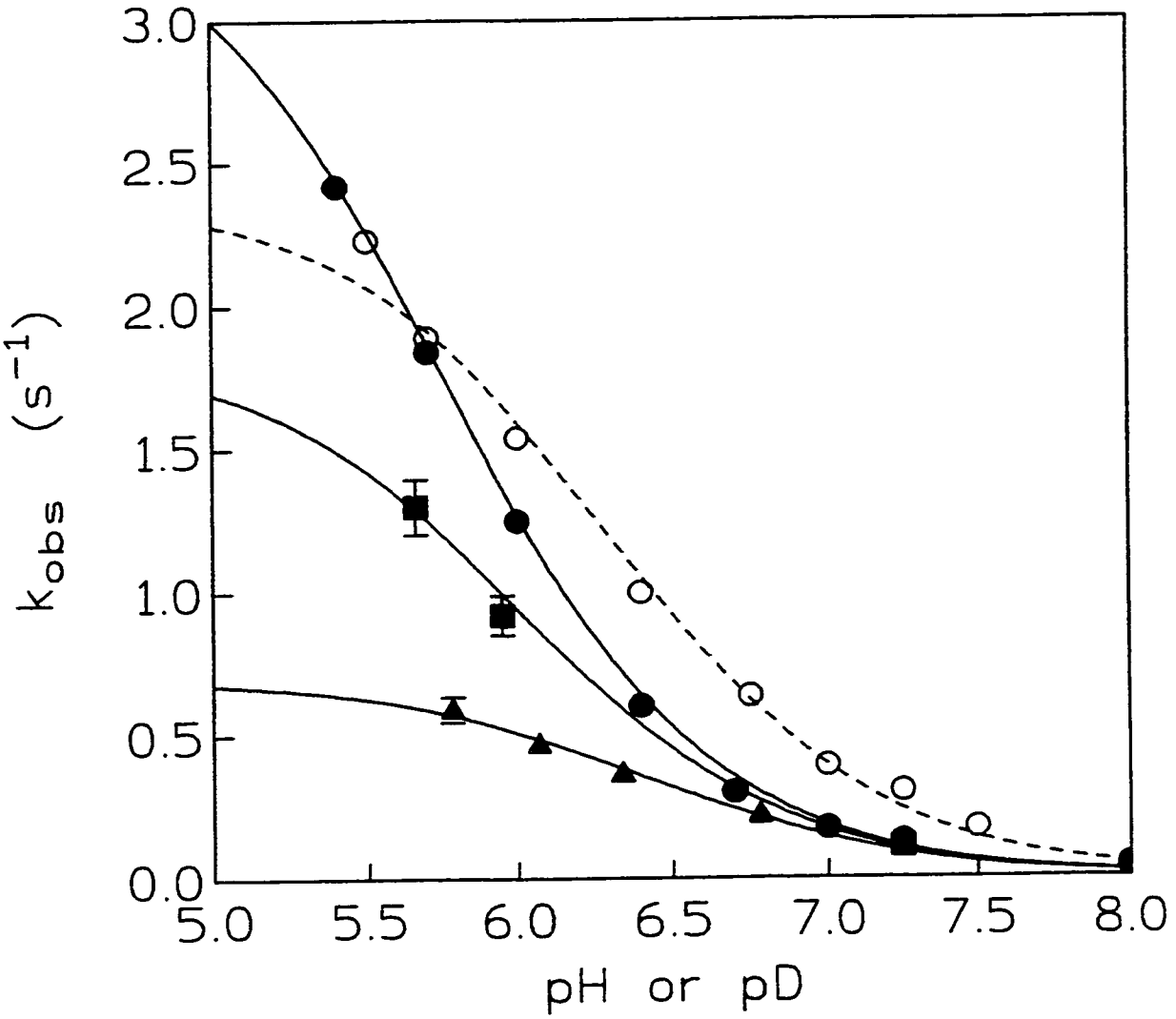

Figure 4.9: Variation of k_{obs1} with pH (pD) for the first-order reduction of Fe^{IV}=O by surface-bound Ru^{II} in a_5Ru^{II}His48MbFe^{IV}=O. Experimental conditions are given in Figure 4.8. Fit of the experimental data by eq 4.6b in the text is given by the solid lines for the pH data, and the dashed line for the pD data. The non-linear least squares analyses were carried out using MINSQ Software (MicroMath). Closed circles, a_5RuHis48Mb in H_2O; open circles, a_5RuHis48Mb in D_2O; squares, a_4PyrRuHis48Mb in H_2O; triangles, a_4IsnRuHis48Mb in H_2O. Data points are the average of 4-8 kinetic runs.

Table 4.2 First-order Rates Constants (k_{obs1}) for Intramolecular Fe^{IV}=O reduction in a_4LRuMb vs pH and pD[a]

a_5RuMb[b]		a_5RuMb		a_4PyrRuMb		a_4IsnRuMb	
pH	k_{obs1} (s^{-1})	pD	k_{obs1} (s^{-1})	pH	k_{obs1} (s^{-1})	pH	k_{obs1} (s^{-1})
5.4	2.42 ± .04	5.5	2.23 ±.021	5.66	1.3 ±.096	5.78	.59 ±.045
5.7	1.84 ±.04	5.7	1.89 ±.023	5.95	.92 ±.07	6.07	.47 ±.03
6.0	1.25 ±.03	6.0	1.54 ±.017	7.25	.11 ±.011	6.34	.367 ±.023
6.4	.604 ±.008	6.4	1.0 ±.015			6.78	.221 ±.012
6.7	.301 ±.007	6.75	.637 ±.016			7.25	.11 ±.01
7.0	.174 ±.006	7.0	.393 ±.015				
7.25	.128 ±.009	7.25	.304 ±.015				
8.0	.0306 ±.004	7.5	.174 ±.008				
		8.0	.0443 ±.005				

[a] Experimental conditions are given in Figure 4.8.

[b] k_{obs1} values are the average of 4-8 measurements.

Table 4.3 Analysis Using Eq 4.6b of k_{obs1} (s^{-1}) vs pH for Fe^{IV}=O Reduction by Surface-Bound Ru^{II} in $a_4LRu^{II}His48MbFe^{IV}$=O[a]

a_4LRu group	pK_a	k_2 (s^{-1})	$-\Delta G^o$ (eV)[b]
a_5Ru (in H_2O)	5.7	3.6	0.752
a_5Ru (in D_2O)	6.2	2.5	0.752
a_4PyrRu (in H_2O)	6.0	1.9	0.499
a_4IsnRu (in H_2O)	6.4	0.74	0.429

[a] Experimental details are given in Figure 4.7.

[b] Kinetic driving force estimated for $Ru^{II} \rightarrow Fe^{IV}$=O ET; see text.

4.5 Discussion

Mechanism of Fe^{IV}=O Reduction in a_4LRuMb. As Figure 4.9 reveals, the k_{obs1}'s for intramolecular Fe^{IV}=O reduction by Ru^{II} are greater in D_2O than H_2O for a_5RuHis48Mb between ~pH 5.8 and 7.5. This is indicative of an isotope effect arising from an acid-base equilibrium of a group on the protein, the pK_a of which will be elevated in D_2O.[20] The presence of an equilibrium isotope effect reveals that a protonated form of Mb is reactive in ET suggesting the following mechanism:

$$a_5Ru^{II}\text{—}MbFe^{IV}\text{=}O + H^+ \underset{K_a}{\rightleftharpoons} a_5Ru^{II}\text{—}H^+MbFe^{IV}\text{=}O \xrightarrow{k_2} a_5Ru^{III}\text{—}MbFe^{III}\text{-}OH_2 \quad (4.6a)$$

$$k_{obsl} = \frac{k_2 [H^+]}{K_a + [H^+]} \qquad (4.6b)$$

Fitting the k_{obsl} values in Figure 4.9 by eq 4.6b yielded pK_a and k_2 values of 5.71 and 3.60 s^{-1} in H_2O, and 6.23 and 2.53 s^{-1} in D_2O for the a_5Ru derivative (Table 4.3). A ΔpK_a of 0.52 is within the range of equilibrium isotope effects predicted for acids of pK_a 3-10,[20] and is assigned to the distal His64 of Mb since the imidazole side chain of this group interacts with heme ligands as discussed below.

The fit by eq 4.6b of the k_{obsl} vs $[H^+]$ data for the intramolecular reduction of Fe^{IV}=O in a_4PyrRuMb and a_4IsnRuMb was also carried out (Figure 4.9). The resultant k_2 values (Table 4.3) decreased as $E^O/Ru^{III/II}$ increased (Table 4.1) indicating that ET is involved in the rate-limiting step following the preequilibrium in eq 4.6a. However, K_a was also found to be sensitive to ligand substitution in a_4LRu with pK_a = 5.7, 6.0, and 6.4 for L = NH_3, Pyr, and Isn, respectively. This variation in pK_a assigned to the distal His64 with a redox group bound at the surface His48 was unexpected, and the reasons for it are not obvious at the present time. Addition of an extra term in eq 4.6b corresponding to the rate constant for ET in the unprotonated form of Mb essentially has no effect on either the pK_a or k_2 values listed in Table 4.3.

In Mb the heme sits in the hydrophobic pocket shown in Figure 4.10a. Ligand access to the pocket requires fluctuations in the polypeptide structure,[25-27] which protects the O_2 ligand from protonation[3,28] and promotes reversible O_2 binding since the distal

Figure 4.10 (a) Diagram of the heme pocket of Mb generated using the x-ray coordinates from the 1.9-Å structure of horse heart metMb.[26] (b) Heme pocket of cytochrome c peroxidase (CCP) showing the key catalytic residues. The dashed lines represent H-bonds. The diagram was generated using the x-ray coordinates from the 1.7-Å structure of CCP.[8b]

(a)

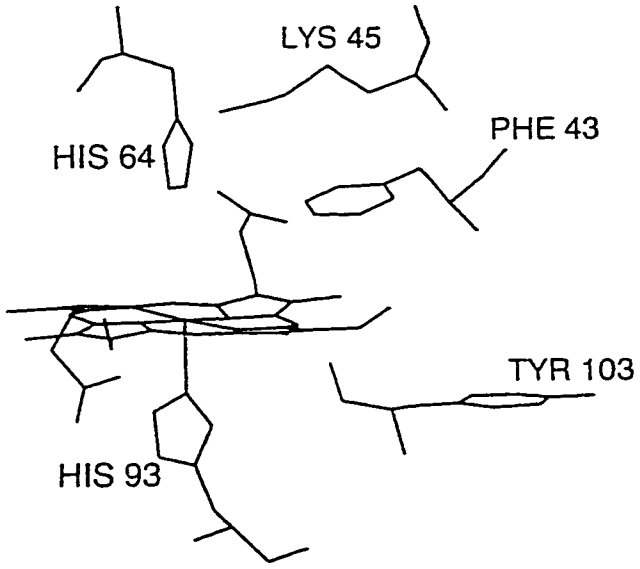

Myoglobin

(b)

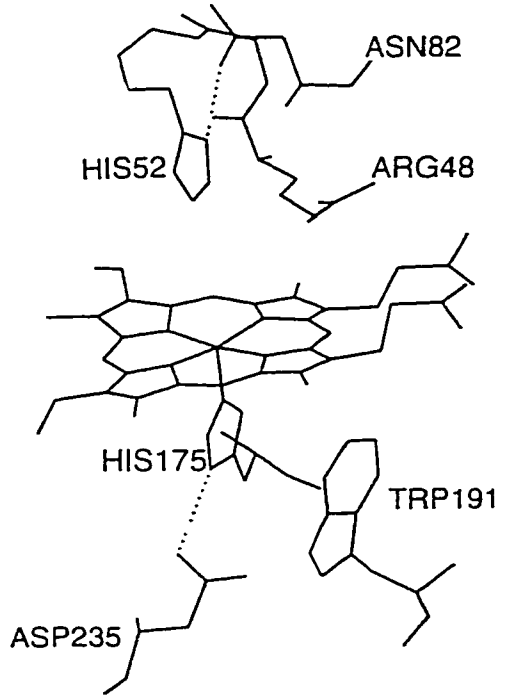

Cytochrome c peroxidase

His64 at 4.3 Å from the iron[26] forms a stabilizing H-bond with the O_2 ligand.[3] Protonation of His64 increases accessibility to the heme[29,30] because the protonated form swings out toward the solvent, leaving the heme pocket in the open conformation observed by x-ray crystallography of Mb with bulky ligands.[31] CO on- and off-rates to the Fe^{II} heme are ~10 times higher in the open- compared to the closed-pocket conformations,[30] which interconvert on protonation of His64 with a pK_a of ~6.[29] From the different Fe-C and CO stretching vibrations in the open and closed conformations,[29,30] $MbFe^{II}$-CO appears to be mainly in the closed-pocket conformation at neutral pH, but interconversion between the closed and open forms is reported to be fast (1-10 μs).[30]

A similar equilibrium may be important for Mb's physiological function since O_2 dissociation rates drastically increase ($10^{3\pm2}$ vs 13 s^{-1}) in the open- vs closed-pocket form of $MbFe^{II}$-O_2, facilitating O_2 delivery to muscle tissue at lower pH's.[30] $MbFe^{II}$-O_2 is also more susceptible to autoxidation at low pH.[28,32] The proposed mechanism for acid-catalyzed autoxidation involves proton transfer (PT) from the *protonated* distal His64 to the O_2 ligand, followed by displacement of $HO_2^{\cdot}$ by an entering H_2O molecule to form $MbFe^{III}$-OH_2.[28,32] The H-bond provided by the NE2 atom of the *neutral* His64 stabilizes the O_2 ligand, preventing both its dissociation and protonation so that PT to the O_2 ligand is efficient only in the *acid* form of $MbFe^{II}$-O_2.[28,32]

Fe^{IV}=O reduction by mechanism 4.6a can be interpreted in terms of the pH-dependent processes involving the heme pocket of Mb. Species a_4LRu^{II}—H^+MbFe^{IV}=O is assumed to be an open-pocket conformation of Mb with the distal His64 protonated. The pK_a of this residue is ~6 in the open-pocket form of $MbFe^{II}$-CO,[29] which agrees with

the pK_a values predicted by mechanism 4.6a (Table 4.3).

Kinetic vs Thermodynamic Driving Force for ET. The thermodynamic potential for $MbFe^{IV}=O$ reduction to $MbFe^{III}-OH_2$ is 0.896 eV (vs NHE) at pH 7.[33a] Equilibrium measurements of E°' vs pH reveal the uptake of two protons[33b] below the pK_a of $HHMbFe^{III}-OH_2$ (8.93).[34] Since the ET reactions were carried out at pH's below the pK_a, the observed product possessed H_2O as a ligand rather than OH^-, due to rapid PT to the latter. The $\Delta G°'$ value associated with the PT steps were calculated from:

$$-\Delta G = 0.05916(pK_a - pH) \quad eV \tag{4.7}$$

Using the average $pK_a = 6.0$ for $a_4LRu^{II}—H^+MbFe^{IV}=O$ (Table 4.3) and the literature pK_a of 8.93 for $HHMbFe^{III}-OH_2$,[34] yields $\Delta G°'$ values of 0.059 and -0.126 eV for the PT steps before and after ET, respectively. Thus, assuming the mechanism in eq 4.6a, the kinetic driving force for $H^+MbFe^{IV}=O$ reduction to $MbFe^{III}-OH^-$ is 0.829 eV, which is 0.067 eV lower than the reported thermodynamic potential of 0.896 eV.[33a] Therefore, the kinetic driving force for $Ru^{II} \rightarrow Fe^{IV}=O$ ET in eq 4.6a (Table 4.3) is also 0.067 eV lower than the thermodynamic driving force.

Reorganization Energy for $Ru^{II} \rightarrow Fe^{IV}=O$ ET. Marcus theory predicts that the rate constant for ET (k_{ET}) within a precursor complex is given by:[35]

$$k_{ET} = (4\pi^3/h^2\lambda k_B T)^{1/2}(H_{AB})\exp[-(\Delta G° + \lambda)^2/4\lambda k_B T] \tag{4.8}$$

The reorganization energy (λ) for the ET step can be calculated from eq 4.8. As has been previously stated (Chapter 3),[14] the efficiency of ET between His48 and the heme in HHMb and SWMb appears to be identical, so the tunneling matrix element (H_{AB}) reported for SWMb (0.01 cm^{-1})[10,11] is adopted here. Using the $-\Delta G^{\circ}$ values estimated in the previous section (Table 4.3), and assuming $k_{ET} = k_2$ (eq 4.6a), results in a λ = 1.8 eV for $Ru^{II} \rightarrow Fe^{IV}$=O ET in the a_4IsnRu and a_4PyrRu derivatives, but λ = 2.1 eV for the a_5Ru derivative. Since λ is not expected to vary significantly between the three Mb derivatives, the much larger value in the latter suggests that ET is strongly gated at the higher driving force. A Marcus plot of $\ln k_{ET}$ vs $-\Delta G^{\circ}$ with λ = 1.8 eV (Figure 4.11) reveals that k_{ET} for the a_5Ru complex should be over 10-fold higher than the observed k_2 values of 3.6 s^{-1} (Table 4.3).

The generation of a negatively-charged oxo ligand (Fe^{III}-O^{2-}) in the hydrophobic heme pocket of Mb is likely to be highly unfavorable; hence, the oxene ligand is expected to be partially protonated in the precursor complex for ET. FTIR, resonance Raman and kinetic studies have revealed that multiple open- and closed-pocket forms of MbFe^{II}-CO exist.[29,30,36] Thus, it is conceivable that ET is gated due to the formation of a precursor complex in which a distal group is strongly H-bonded to the oxene ligand. The positively-charged guanidinium side chain of the distal Arg48 in cytochrome c peroxidase (CCP)[37] (Figure 4.10b) or the distal Arg38 in horseradish peroxidase (HRP),[38] act as H-bond donors to the oxene ligands in these peroxidases. Furthermore, there is strong evidence that reduction of the Fe^{IV}=O center in HRP compound II (HRP-II) is rapid only when the oxene ligand is H-bonded to a distal species. Resonance Raman studies show

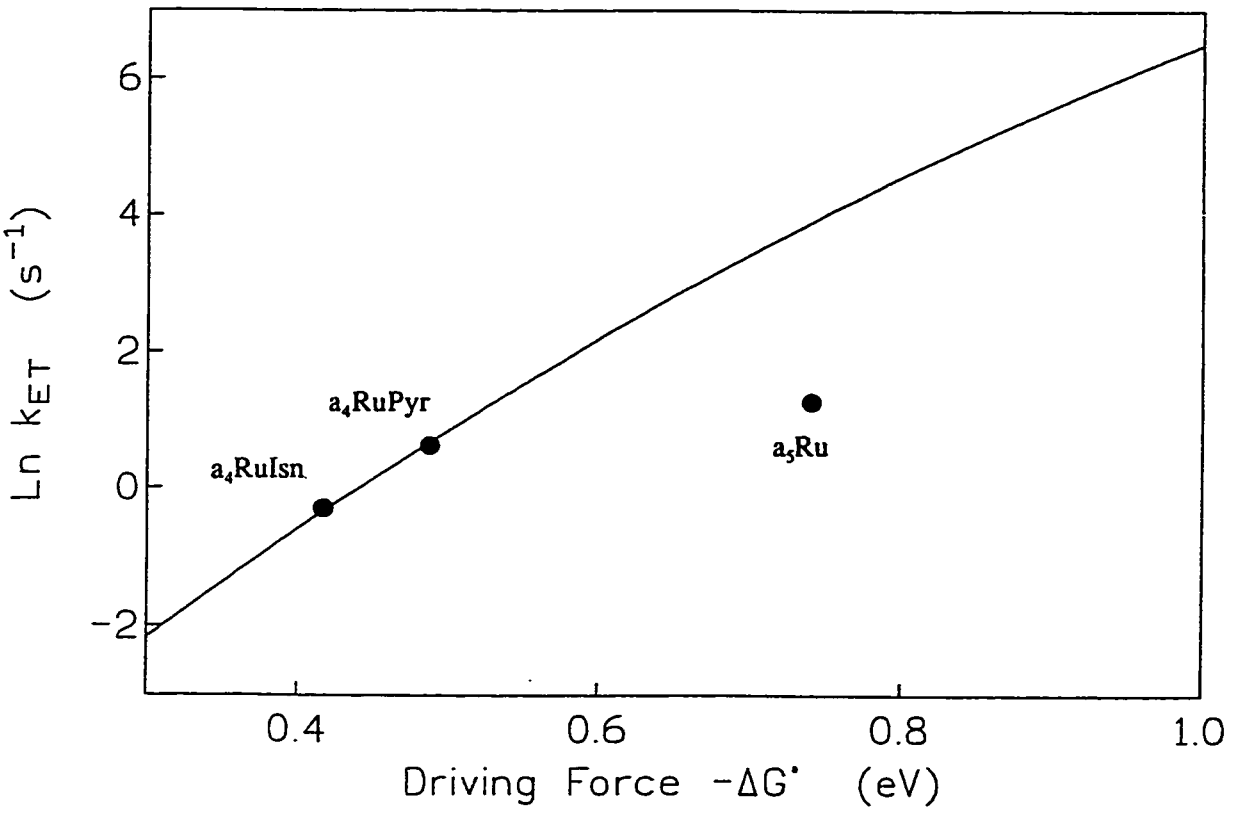

Figure 4.11 Plot of $\ln(k_{ET})$ vs $-\Delta G^{\circ}$ (eV) for a_4LRuHis48Mb. Data from Table 4.3 with $k_2 = k_{ET}$ (see text). The solid line represent the fit to the semiclassical Marcus equation for ET (eq 4.8) assuming $H_{AB} = 0.01$ cm^{-1}, and yields a reorganization energy (λ) value of 1.8 eV for ET between the Ru and heme centers.

that in HRP-II υ(Fe-O) shifts from 776 to 788 cm^{-1} at alkaline pH, with a transition midpoint at pH ~8.5.[39] The 776-cm^{-1} band has been assigned to a H-bonded Fe^{IV}=O moiety, and the 788-cm^{-1} band, being insensitive to deuterium exchange, to a non H-bonded Fe^{IV}=O group.[39] HRP-II is a kinetically competent one-electron oxidant (eq 4.1c) at low pH but not at high pH, with a transition midpoint at pH 8.6.[40] Since υ(Fe-O) of $MbFe^{IV}$=O is high (797 cm^{-1}) compared to that of the peroxidases (745 - 779 cm^{-1}),[41] and the 797-cm^{-1} band is insensitive to pH in the range 6 - 12 and to substitution of D_2O for H_2O,[42] H-bonding to the oxene ligand in $MbFe^{IV}$=O is highly unlikely.

Terminal metal oxo groups have been proposed to possess the resonance structures:[40]

$$M{=}\ddot{O}: \rightleftharpoons M^{-}{\equiv}O:^{+} \qquad (4.9)$$

The resonance can be expected to lie more to the right in $MbFe^{IV}$=O but to the left in the Fe^{IV}=O forms of the peroxidases because of the trans ligand effect of the proximal histidine. This is H-bonded to a carboxylate side chain in the peroxidases (Figure 4.10b),[2] and to a peptide carbonyl group in Mb, giving rise to a less basic oxygen atom in the latter. We propose that $MbFe^{IV}$=O resembles the nonreactive, alkaline form of HRP-II, and that a conformational change is required to generate a Mb species that corresponds to the acid or kinetically competent form of HRP-II, leading to conformational gating of ET at high driving force, which is also consistent with the low SKIE (1.4) observed for k_2 (Table 4.3).

A λ of 1.8 eV was calculated at lower driving forces for $Ru^{II} \rightarrow Fe^{IV}$=O ET in the a_4LRu derivatives where ET must be rate limited because of the sensitivity of k_{obs1} to -

ΔG° (Table 4.3 and Figure 4.11). It is of interest to compare this value with the λ (1.48 eV) reported for the intramolecular ET ($a_5Ru^{II}His48—Fe^{III}\text{-}OH_2 \rightarrow a_5Ru^{III}His48—Fe^{II} + H_2O$) in SWMb.[11] Considering that ET involves loss of the H_2O ligand and movement of the Fe with respect to the heme plane in $MbFe^{III}\text{-}OH_2$, the inner sphere λ at the heme[44] was not expected to differ considerably from that associated with the ET in eq 4.6a. However, if the large Fe-O bond length change (0.2 Å) observed by EXAFS[45] on going from the oxene to the aquo ligand is taken into consideration, as well as the spin change on reduction of LS Fe^{IV}=O (S = 1)[46] to HS $Fe^{III}\text{-}OH_2$ ($MbFe^{II}$ is also HS),[44] a ~0.3 eV higher λ might not be unreasonable.

Conclusions. The results presented here would explain why $MbFe^{IV}$=O is much less reactive towards one-electron reductants than compound II of heme peroxidases (eq 4.1c) at high $-\Delta G^\circ$. The requirement for H-bonding to the oxene ligand to generate a kinetically competent oxidant has been convincingly demonstrated for HRP-II.[39,40] The distal arginine of HRP,[38] CCP [37] (Arg 48 in Figure 4.9b) and other heme peroxidases[2] provides a strong H-bond donor to the oxene ligand. The lack of such a donor in its heme pocket under physiological conditions, requires that $MbFe^{IV}$=O must be converted to an activated form in a pH-dependent process prior to reduction. Furthermore, strong H-bonding to the proximal histidine ligand in the peroxidases (Figure 4.10b) would favor a resonance structure like that on left of eq 4.9, with a considerably more basic oxygen atom than in the form on the right. It is of interest in this context that the solvent-exposed Fe^{IV}=O center of microperoxidase is observed to be an unreactive oxidant.[47] Presumably, the oxene ligand is very weakly basic rendering the Fe^{IV}=O group unreactive

around neutral pH.

CCP mutants are currently under preparation in our laboratory to study reaction 4.5 in a peroxidase chemical context. Surface residues close to the heme are being mutated to histidine to allow rapid $Ru^{II} \rightarrow Fe^{IV}$=O ET to be examined, and thereby determine the controlling factors in Fe^{IV}=O reduction in CCP.[48] The present results on $MbFe^{IV}$=O reduction suggest that activation of the Fe^{IV}=O group is controlled by strong H-bonding to the oxene ligand and the proximal histidine. Such interactions would allow the local environment to determine the reactivity of Fe^{IV}=O catalytic intermediates in heme enzymes.

Addendum. Marcus analysis of the rate-limiting Fe^{IV}=O reduction rates (k) for the a_4LRu derivatives of Mb may not be appropriate given the gating observed in the a_5Ru derivative. Electron transfer that cannot be described by a single reaction coordinate, such as a partially gated system, should not fit a Marcus plot, nor should the apparent λ have the conventional meaning. The degree of gating will increase with the driving force for the electron transfer step so that Fe^{IV}=O reduction in the a_5Ru Mb derivative is more strongly gated than in the a_4IsnRu and a_4PyrRu Mb derivatives.[1] Analysis of the data by assigning a constant pK_a to the pre-equilibrium step may be more appropriate. However, further experimentaal data (pH/D, $-\Delta G^\circ$ dependence) are required to clarify these issues.

References

1. (a) Mueller, E.J.; Loida, P. J.; Sligar, S. G.; In *Cytochrome P450 Structure, Mechanism and Biochemistry 2nd Edn.* Ortiz de Montellano, P. R., Ed.; Plenum

Press: New York, 1995; pp 83-124; (b) Poulos, T. L.; Cupp-Vickery, J.; Li, H. In *Cytochrome P450 Structure, Mechanism and Biochemistry 2nd Edn.* Ortiz de Montellano, P. R., Ed.; Plenum Press: New York, 1995; pp 125-150; (c) Babcock, G. T.; Wilkström, M. *Nature* **1992**, *356*, 301; (d) Malmström, B. G. *Acc. Chem. Res.* **1993**, *26*, 332.

2. (a) English, A. M.; Tsaprailis, G. *Adv. Inorg. Chem.* **1995**, *43*, 79; (b) Poulos, T. L. *Adv. Inorg. Biochem.* **1987**, *7*, 1; (c) Poulos, T. L.; Fenna, R. E. In *Metal Ions in Biological Systems: Metalloenzymes Involving Amino Acid-Residue and Related Radicals*, Sigel, H.; Sigel, A., Eds.; Marcel Dekker: New York, **1994**; Vol. 30, pp 25-75.

3. Springer, B. A.; Sligar, S. G.; Olson, J. S.; Phillips G. N. Jr. *Chem. Rev.* **1994**, *94*, 699.

4. Yonetani, T.; Schleyer, H. *J. Biol. Chem.* **1967**, *242*, 1974.

5. (a) King, N. K.; Winfield, M. E. *J. Biol. Chem.* **1963**, *238*, 1520; (b) Davies, M. J. *Biochim. Biophys. Acta.* **1991**, *1077*, 86.

6. Chapter 2

7. (a) George, P.; Irvine, D. H. *Biochem. J.* **1952**, *52*, 511; (b) King, N. K.; Winfield, M. E. *Aust. J. Biol. Sci.* **1966**, *19*, 211; (c) Fox, J. B.; Nicholas, R. A.; Ackerman. S. A.; Swift, C. E. *Biochemistry* **1974**, *13*, 5178; (d) Wittenberg, J. B. *J. Biol. Chem.* **1978**, *253*, 5694; (e) Peisach, J.; Uyeda, M. *Biochemistry* **1981**, *20*, 2028; (f) Foote, N.; Gadsby, P. M. A.; Greenwood, C.; Thomson, A. J. *Biochem. J.* **1989**, *261*, 515.; (g) Tamura, M.; Asakura, T.; Yonetani, T. *Biochim. Biophys.*

Acta **1973**, *295*, 467-479.

8. (a) Quillin, M. L.; Arduini, R. M.; Olson, J. S.; Phillips, G. N., Jr. *J. Mol. Biol.* **1993**, *234*, 140; (b) Finzel, B. C.; Poulos, T. L.; Kraut, J. *J. Biol. Chem.* **1984**, *259*, 13027.

9. (a) Miller, M. A.; Vitello, L.; Erman, J. E. *Biochemistry* **1995**, *34*, 12048; (b) Farhangrazi, Z. S.; Fossett, M. E.; Powers, L. S.; Ellis, W. R. Jr.; *Biochemistry* **1995**, *34*, 2866; (c) Hahm, S.; Miller, M. A.; Geren, L.; Kraut, J.; Durham, B.; Millett, F. *Biochemistry* **1994**, *33*, 1473; (d) Hasinoff, B. B.; Dunford, H. B *Biochemistry* **1970**, *9*, 4930.

10. (a) Crutchley, R. J.; Ellis, W. R. Jr.; Gray, H. B. *J. Am. Chem. Soc.* **1985**, *107*, 5002; (b) Lieber, C. M.; Karas, J. L.; Gray, H. B. *J. Am. Chem. Soc.* **1987**, *109*, 3778; (c) Axup, A. W.; Albin, M.; Mayo, S. L.; Crutchley, R. J.; Gray, H. B. *J. Am. Chem. Soc.* **1988**, *110*, 435; (d) Karas, J. L.; Lieber, C. M.; Gray, H. B. *J. Am. Chem. Soc.* **1988**, *110*, 599; (e) Karas, J. L. PhD Thesis, California Institute of Technology, **1989**.

11. Winkler, J. R.; Gray, H. B. *Chem. Rev.* **1992**, *92*, 369.

12. Isied, S. S. In *Electron Transfer in Inorganic, Organic and Biological Systems*, Bolton, J. R.; Mataga, N.; McLendon, G., Eds.; Advances in Chemistry Series No. 228; American Chemical Society: Washington, DC, 1991; pp 229-245.

13. Sykes, A. G. *Chemistry in Britain, June*, **1988**, 551.

14. Fenwick, C.; Marmor, S.; Govindaraju, K.; English, A. M; Wishart, J. F.; Sun, J. *J. Am. Chem. Soc.* **1994**, *116*, 3169.

15. (a) Vogt, L. H. Jr.; Katz, J. L.; Wiberley, S. E. *Inorg. Chem.* **1965**, *4*, 1157; (b) Curtis, J. C.; Sullivan, B. P.; Meyer, T. J. *Inorg. Chem.* **1983**, *22*, 224; (c) Marchant, J. A.; Matsubara, T.; Ford, P. C. *Inorg. Chem.* **1977**, *16*, 2160; (d) Schlit, A. A.; Taylor, R. C. Russ. *J. Inorg. Chem.* (Engl. Transl.) **1959**, *9*, 211.

16. Sundberg, R. J.; Gupta, G. *Bioinorg. Chem.* **1973**, *3*, 39.

17. (a) Eddowes, M. J.; Hill, H. A. O. *J. Chem. Soc. Chem. Commun.* **1977**, 771; (b) Eddowes, M. J.; Hill, H. A. O.; Uosaki, K. *Bioelectrochem. Bioenerg.* **1980**, *7*, 527.

18. Sun, J.; Su, C.; Wishart, J. F. *Inorg. Chem.* **1996**, *35*, 0000.

19. Schwartz, H. A.; Dodson, R. W. *J. Phys. Chem.* **1989**, *93*, 409.

20. Schowen, K. B. J. In *Transition States of Biochemical Processes*; Gandour, R. D.; Schowen, R. L., Eds.; Plenum Press: New York, 1978; pp 225-283.

21. Feng, R.; Konishi, Y. *Am. Soc. Mass. Spec.* **1993**, *4*, 638.

22. Bowler, B. E.; Raphael, A. L.; Gray, H. B. *Prog. Inorg. Chem.* **1990**, *38*, 259.

23. Bard, A. J.; Faulkner, L. R. In *Electrochemical Methods*, John Wiley & Sons: New York, **1980**; p 194.

24. The ratio of the rates for $CO_2^{\bullet-}$ radical reacting with the R^{III} and Fe^{IV}=O centers was estimated from the absorbance growth at 409 nm due to Fe^{III}-OH_2 formation on millisecond (direct reduction by $CO_2^{\bullet-}$) and second (intramolecular ET from Ru^{II}) time scales.

25. (a) Takano, T. *J. Mol. Biol.* **1977**, *110*, 569; (b) Phillips, S. V. E. *J. Mol. Biol.* **1980**, *142*, 531; (c) Kuriyan. J.; Wilz, S.; Karplus, M.; Petsko, G. A. *J. Mol. Biol.*

1986, *192*, 133.

26. Evans, S. V.; Brayer, G. D. *J. Mol. Biol.* **1990**, *213*, 885.

27. Lambright, D. G.; Balasubramanian, S.; Decatur, S. M.; Boxer, S. G. *Biochemistry* **1994**, *33*, 5518.

28. Shikama, K. *Coord. Chem. Rev.* **1988**, *83*, 73.

29. Morikis, D.; Champion, M. P.; Springer, B. A.; Sligar, S. G. *Biochemistry* **1989**, *28*, 4791.

30. Tian, W. D.; Sage, J. T.; Champion, P. M. *J. Mol. Biol.* **1993**, *233*, 155.

31. Johnson, K. A.; Olson, J. S.; Phillips, G. N. Jr. *J. Mol. Biol.* **1989**, *207*, 459.

32. Brantley, R. E., Jr; Smerdon, S. J.; Wilkinson, A. J.; Singleton, E. W.; Olson, J. S. *J. Biol. Chem.* **1993**, *268*, 6995.

33. (a) He, B.; Sinclair, R.; Copeland, B.R.; Makino, R.; Powers, L.S.; Yamazaki, I. *Biochemistry* **1996**, *35*, 2413; (b) George, P.; Irvine, D.H. *Biochem. J.* **1954**, *58*, 188.

34. George, P.; Hanania, G. I. H. *Biochem. J.* **1952**, *52*, 517.

35. Marcus, R.A.; Sutin, N. *Biochim. Biophys. Acta* **1985**, *811*, 265.

36. (a) Hong, M. K.; Braunstein, D.; Cowen, B. R.; Frauenfelder, H.; Iben, I. E. T.; Mourant, J. R.; Ormos, P.; Scholl, R.; Schulte, A.; Steinbach, P. J.; Xie, A.; Young, R. D. *Biophys. J.* **1990**, *58*, 429; (b) Doster, W.; Beece, D.; Bowne, S. F.; DiIorio, E. E.; Eisenstein, L.; Frauenfelder, H.; Reinisch, L.; Shyamsunder, E.; Winterhalter, K. H.; Yue, K. T. *Biochemistry* **1982**, *21*, 4831.

37. (a) Fülöp, V.; Phizackerley, R. P.; Soltis, S. M.; Clifton, I. J.; Wakatsuki, S.;

Erman, J.; Edwards, S. L. *Structure* **1994**, *2*, 201; (b) Miller, M. A.; Shaw, A.; Kraut, J. *Nature Struct. Biol.* **1994**, *1*, 524.

38. Holzbaur, I. E.; English, A. M.; Ismail, A. A. *J. Am. Chem. Soc.* **1996**, *118*, 3354.

39. Sitter, A. J.; Shifflett, J. R.; Terner, J. *J. Biol. Chem.* **1988**, *263*, 13032.

40. (a) Critchlow, J. E.; Dunford, H. B. *J. Biol, Chem.* **1972**, *247*, 3714; (b) Dunford, H. B.; Stillman, J. S. *Coord. Chem. Rev.* **1976**, *19*, 187.

41. Reczek, C. M.; Sitter, A. J.; Terner, J. *J. Mol. Struct.* **1989**, *214*, 27.

42. Sitter, A. J.; Reczek, C. M.; Terner, J. *SPIE.* **1989**, *1055*, 271.

43. Kramarz, K.W.; Norton, J.R. *Prog. Inorg. Chem.* **1994**, *42*, 1.

44. Tsukahara, K. *J. Am. Chem. Soc.* **1989**, *111*, 2040.

45. Chance, M.; Powers, L.; Kumar, C.; Chance, B. *Biochemistry* **1986**, *25*, 1259.

46. (a) Schulz, C.E.; Rutter, R.; Sage, J.T.; Debrunner, P.G.; Hager, L.P. *Biochemistry* **1984**, *23*, 4743; (b) Schulz, C.E.; Devaney, P. W.; Winkler, H.; Debrunner, P.G.; Doan, N.; Chiang, R.; Rutter, R.; Hager, L.P. *FEBS Let* **1979**, *103*, 102.

47. Low, D. W.; Winkler, J. R.; Gray, H. B. *J. Am. Chem. Soc.* **1996**, *118*, 117.

48. English, A.M.; Fox, T.; Tsaprailis, G.; Fenwick, C.W.; Wishart, J. F.; Hazzard, J.T.; Tollin, G. In *Photochemistry and Radiation Chemistry: Complementary Methods for the Study of Electron Transfer*, Wishart, J. F.; Nocera, D. G., Eds; Advances in Chemistry Series No.x; American Chemical Society: Washington, DC

49. Sun, J.; Wishart, J.F.; Gardineer, M.B.; Cho, M.P.; Isied, S.S. *Inorg. Chem.* **1995**, *34*, 3301.

50. Agmon, N.; Hopfield, J.J.; *J. Chem. Phys.* **1983**, *78*, 6947.

5.0 Study of the Protein-Based Radical Centers Formed in the $MbFe^{III}/H_2O_2$ Reaction

5.1 Introduction

Free radicals have been found to be important highly reactive species in biological systems. Radicals are involved in the catalytic cycle of enzymes[1] such as ribonucleotide reductase,[2,3] where a tyrosyl radical reduction is coupled to ribonucleotide C-H bond cleavage in deoxyribonucleotide synthesis. Some enzymes are suspected of using radicals as a means of self-inactivation as in prostaglandin H synthase.[4] Uncontrolled radicals in cells can have damaging effects[5,6] and lead to the onset of diseases such as cancer and amyotrophic lateral sclerosis (Lou Gehrig's disease).[7] The current method of choice in the study of free radicals is EPR. While the unpaired electron can be detected directly by EPR, spectroscopic observation of radicals is often limited by short lifetimes and low concentrations. Spin traps are frequently used to stabilize the paramagnetic nature of the radical species and the EPR spectra of the spin adducts can provide additional structural information.[8] Techniques such as HPLC-EPR have been used in the analysis of radical mixtures[9,10,11,12] and GC-MS for radicals trapped on small molecule.[13] However, interpretation of the EPR signals from protein-based radicals can be difficult due to environmental effects and the multitude of potential radical sites in a protein matrix. One way of determining the location of a protein-based radical is to prepare site-directed mutants. Substitution of the radical-forming residue with one that is more difficult to oxidize should alter the EPR spectrum of the mutant protein, and this approach was used to locate the primary protein radical in CCP.[14] Although effective, this procedure requires

expression of the recombinant proteins of interest and suffers from the fact that suitable mutants may not have similar properties as their wild types.

Metmyoglobin ($MbFe^{III}$) reacts with H_2O_2 to form an oxyferryl (Fe^{IV}=O) heme and unstable protein radical species (Chapters 1 and 2). Although the latter have been under investigation for over 40 years, there is still debate as to the sites of radical formation. Both the free radicals formed and their spin adducts have been detected by EPR,[15,16,17] but the signals have not been unambiguously assigned to specific residues.[15,16] Since protein radicals appear to play key roles in redox catalysis and redox signaling,[18,19] we are investigating the use of MS analysis for the localization of spin adducts and hence the sites of radical formation. $MbFe^{III}$ was reacted with H_2O_2 in the presence of the spin trap, 2-methyl-2-nitrosopropane (MNP; Figure 1.4). Tryptic digestion of the MNP-Mb spin adducts was performed, followed by on-line peptide mass mapping to locate the MNP modified peptides. ESI-MS was then used to carry out collisionally induced dissociation (CID) to sequence the modified peptides and identify the radical-forming residues. Since Tyr103 is reported to be the major site of radical formation in the $MbFe^{III}/H_2O_2$ reaction, iodination of this residue was carried out to alter its redox properties. Radical formation in the $MbFe^{III}/H_2O_2$ reaction was also investigated at pH 5 since different protein radical signals appear in the EPR spectra at low pH.[20]

5.2 Materials and Methods

A 1 mM stock horse heart $MbFe^{III}$ (Sigma) solution was prepared in 50 mM Pi buffer (pH 7.4) treated with Chelex resin (BioRad) followed by the addition of the

chelating agent diethylentriamine-N,N,N',N",N"-pentaacetic acid (DETPA; ICN) to a final concentration of 50 μM. A stock solution (23 mM) of the spin trap 2-methyl-2-nitrosopropane (MNP; Aldrich) was prepared from the MNP dimer in the same buffer by stirring the solution in the dark at 45 °C for 1 h, as described previously.[11] The stocks were mixed under normoxic conditions to give a solution of 200 μM $MbFe^{III}$ and 18.4 mM MNP in 50 mM Pi buffer (pH 7.4). The Mb + MNP solution was reacted with 1-10 molar equivalents (1-10x) of H_2O_2 (Fisher) for 5 min and excess H_2O_2 removed with a catalytic amount of bovine catalase (Sigma).

The MNP-Mb spin adducts were reduced with excess sodium ascorbate (~1 mM) for ~ 1 h and then acidified with HCl to pH 2. The products for the $MbFe^{III}/H_2O_2$/MNP reaction performed at pH 5.0 were treated as above, except that after reduction the heme group was extracted using HCl/acetone.[21]

Prior to MS analysis samples were desalted on a HPLC column. The reaction mixture (~20 μg of protein) was injected onto a Hamilton PRP-∞ HPLC column (4.6 x 30 mm) and the protein separated from heme and buffer salts with a 20-65% CH_3CN gradient in 0.1% TFA at 2 mL/min over 10 min. The protein peak was lyophilized and <1 μg resuspended in 50 μL of 1:1 methanol/H_2O with 0.5% acetic acid and infused into the ES source of a Finnigan SSQ 7000 mass spectrometer at a flow rate of 1-2 μL/min. MS analysis of the whole protein allowed for the identification of samples that contained a MNP-Mb spin adduct.

The apoMb (~ 20μg) samples were digested with 1:50 (w/w) trypsin at 25 °C for 8 h in 50 mM Tris buffer, pH 8.0. The digests were acidified to pH 2 with HCl, and 2-4

μg was separated on a Vydac microbore C18 column (1 x 300 mm) with a 3-55% CH_3CN gradient in 0.05% TFA at 40 μL/min over 120 min. The peptide maps of the digested apoMb samples identified peptides that were modified with the spin adduct.

Collision induced dissociation (CID) was performed to sequence the modified peptides and identify the site of modification. Peptides to be sequenced were purified from the tryptic digests by HPLC using a Vydac 4.6- x 300-mm C18 RP-HPLC column, lyophilized, resuspended in 1:1 methanol/H_2O + 0.05% acetic acid, and directly infused at ~1.5 μL/min into the ES source of either a Finnigan TSQ 7000 triple quadrupole MS or a Finnigan SSQ 7000 single quadrupole MS. For TSQ analysis, the +3 ion at *m/z* 653.2 was selected with Q1 and fragmented by CID in the collision cell (Q2) with Ar gas at 2.5 mTorr and a collision offset voltage of -22 eV (laboratory frame of reference). The fragment ions were analyzed in Q3. CID on the SSQ was performed in the capillary/skimmer region with the capillary at 90 mV and the tube lens at 145 mV. The +1, +2, and +3 ions simultaneously fragmented in this region and were analyzed in Q1.

Tryptic peptides that could not be unambiguously sequenced through the modification site were purified by HPLC and lyophilized. Digestion of peptide 32-47 was performed with 1:50 (w/w) V8 endoproteinase Glu-C (Sigma) at 25 °C for 4 h in 50 mM NH_3HCO_3, pH 7.8. Digestion of peptide 64-77 was performed with 1:50 (w/w) pepsin (Sigma) in 3 mM HCl (pH 2) at 25 °C for 4 h. The V8 and pepsin digests were separated by HPLC and sequenced by CID as before.

Iodination of Tyr103 was performed by titrating a 200 μM Mb solution in 0.1 M sodium borate (pH 9.0) with 5 mM ICl as reported previously.[22] The extent of iodination

was monitored by on-line LC-MS analysis (Section 2.3.4). Samples that were ~ 90% iodinated were digested with trypsin and peptide mass mapping was performed to ensure that Tyr103 was the major site of iodination.

Denaturation studies of $MbFe^{III}$ (2 μM) in guanidine-HCl (G-HCl; 8 M stock solution) were carried out in 100 mM Pi buffer at pH 7.4. $MbFe^{III}$ was incubated for 1 h at the desired concentration of G-HCl before the protein steady-state fluorescence was measured on a Shimadzu RF 5000 spectrophotofluorometer. Fluorescence intensities are expressed relative to a 2 μM apoMb solution.

5.3 Results and Discussion

The UV/vis absorbance spectra of the $MbFe^{III}/H_2O_2$ reaction products (data not shown) were identical in the presence and absence of excess MNP, indicating that the latter does not react with the Fe^{IV}=O heme center. MS analysis of the desalted $MbFe^{III}/H_2O_2$/MNP pH 7.4 reaction products by direct infusion into the ES source showed that a major species with a mass of 16950 Da and a minor species with a mass of 17036 Da were present (Figure 5.1a). The 17036-Da species has an increased mass of 86 Da over untreated Mb, corresponding to the formation of MNP spin adducts. Mb treated with 1 and 2 molar equivalents of H_2O_2 was 10-15% and 20-30% modified with MNP as monitored by MS. However, tryptic digests of the MNP-Mb samples contained exclusively native Mb peptides (Figure 5.2A and B), indicating that the spin adducts are unstable under the peptide mapping conditions. The stability of the spin adduct(s) during whole-protein MS analysis may be due to shielding of the MNP adduct(s) by the

Figure 5.1 Deconvoluted ES mass spectra of the $MbFe^{III}/H_2O_2$/MNP reaction products (A) before and (B) after ascorbate reduction and acidification. The 16950-Da peaks correspond to apoMb while the 17036-Da peak in (A) corresponds to the MNP-Mb spin adduct (+86), and the 17021-Da peak in (B) to the reduced (R-MNP-Mb) adducts (+71).

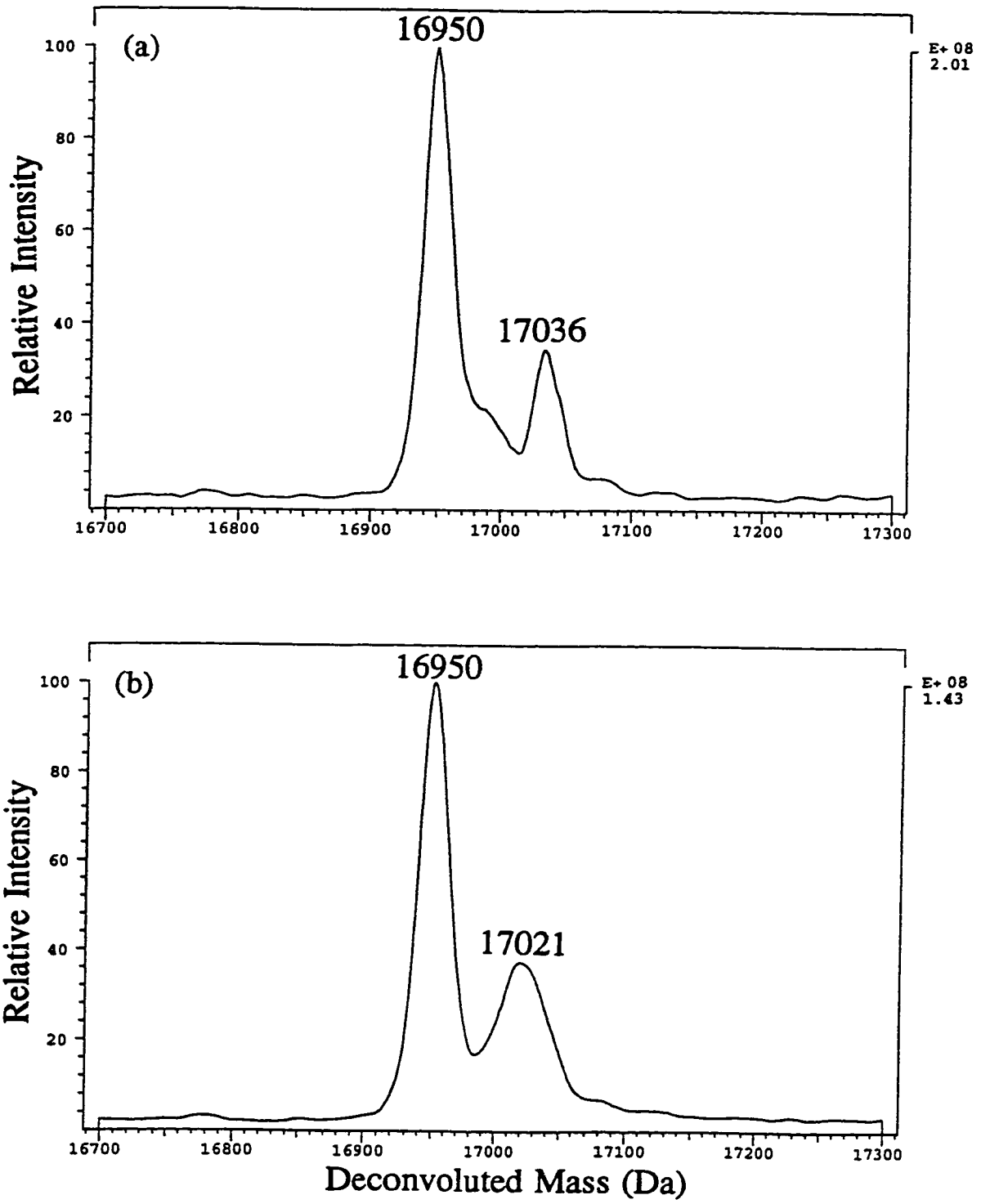
(a)
16950
17036
100
80
60
40
20
Relative Intensity
E+ 08
2.01
16700
16800
16900
17000
17100
17200
17300
(b)
16950
17021
100
80
60
40
20
Relative Intensity
E+ 08
1.43
16700
16800
16900
17000
17100
17200
17300
Deconvoluted Mass (Da)

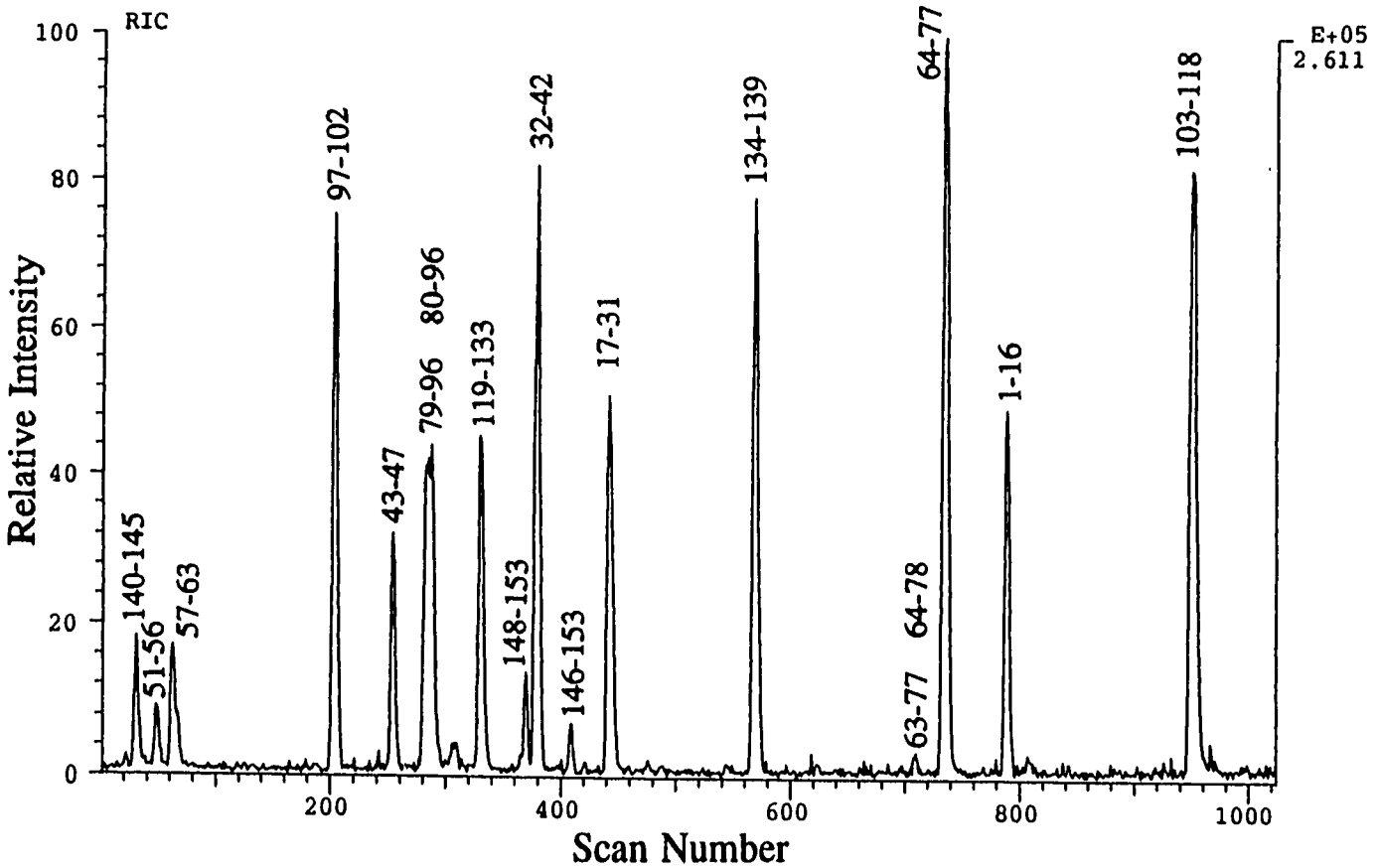

Figure 5.2 (A) Peptide mass map of the $MbFe^{III}/H_2O_2$/MNP reaction products. The Mb sample was not reduced with ascorbate and yielded only native Mb peptides.

Gly_{1}-Leu-Ser-Asp-Gly-Glu-Trp-Gln-Gln-Val-Leu-Asn-Val-Trp-Gly-Lys_{16} ||

Val_{17}-Glu-Ala-Asp-Ile-Ala-Gly-His-Gly-Gln-Glu-Val-Leu-Ile-Arg_{31} ||

Leu_{32}-Phe-Thr-Gly-His-Pro-Glu-Thr-Leu-Glu-Lys_{42} || Phe_{43}-Asp-Lys_{45} || Phe_{46}-Lys_{47} ||

His_{48}-Leu-Lys_{50} || Thr_{51}-Glu-Ala-Glu-Met-Lys_{56} || Ala_{57}-Ser-Glu-Asp-Leu-Lys_{62} ||

Lys_{63} || His_{64}-Gly-Thr-Val-Val-Leu-Thr-Ala-Leu-Gly-Gly-Ile-Leu-Lys_{77} || Lys_{78} || Lys_{79} ||

Gly_{80}-His-His-Glu-Ala-Glu-Leu-Lys-Pro-Leu-Ala-Gln-Ser-His-Ala-Thr-Lys_{96} ||

His_{97}-Lys_{98} || Ile_{99}-Pro-Ile-Lys_{102} ||

Tyr_{103}-Leu-Glu-Phe-Ile-Ser-Asp-Ala-Ile-Ile-His-Val-Leu-His-Ser-Lys_{118} ||

His_{119}-Pro-Gly-Asn-Phe-Gly-Ala-Asp-Ala-Gln-Gly-Ala-Met-Thr-Lys_{133} ||

Ala_{134}-Leu-Glu-Leu-Phe-Arg_{139} || Asn_{140}-Asp-Ile-Ala-Ala-Lys_{145} || Tyr_{146}-Lys_{147} ||

Glu_{148}-Leu-Gly-Phe-Gln-Gly_{153} ||

Figure 5.2 (B) Tryptic map of horse heart myoglobin

polypeptide.

In order to stabilize the spin adducts, the Fe^{IV}=O heme and radicals were reduced with excess ascorbate. The products were acidified to pH 2 with HCl and separated by RP-HPLC. The mass spectrum of the protein peak revealed that the reduced MNP adducts (R-MNP-Mb) have an increased mass of + 71 Da (vs +86 Da for the MNP-Mb spin adducts) over untreated Mb (16950 Da) (Figure 5.1a and b). The reduction step with ascorbate had to be carried out for ≥ 1 h to ensure full conversion to the +71-Da form. The R-MNP-Mb derivatives yielded modified peptides which were identified when the following controls and samples were subjected to tryptic digestion and on-line LC-MS analysis: (1) Mb, (2) Mb + 5x H_2O_2, (3) Mb + MNP, (4) Mb + 1x H_2O_2 + MNP, (5) Mb + 2x H_2O_2 + MNP, (6) Mb + 5x H_2O_2 + MNP, (7) Mb + 10x H_2O_2 + MNP. The controls (1-3) yielded only native tryptic peptides (Figure 5.2 and 5.3A), while samples 4-7 possessed a new peak (denoted by an asterisk in Figure 5.3B) corresponding to peptide 103-118 plus 71 Da. The intensity of this peak leveled off at 5x H_2O_2, and sequencing by CID[23] (Figure 5.4) revealed Tyr103 to be the site of modification. The mass spectrum shows that the R-MNP adduct is fragmented during CID; however, the modified peptide remains +15 Da higher in mass than the native peptide. The peptide fragments containing the +15 Da adduct are marked by $b^{\ddagger}$ and $a^{\ddagger}$ ions (Figure 5.4) and identify the adduct forming residue to be Tyr103. Two minor peaks (denoted by a circled asterisk in Figure 5.3B) were also present in the LC-MS spectra of samples 4-7 but not in the controls. CID provided partial sequences, allowing the peaks to be assigned to peptides 32-45 and 32-47. Peptide 32-47 was further digested with V8 protease, and CID

Figure 5.3 Peptide mass maps of horse heart myoglobin. (A) Tryptic digestion following incubation of metMb with 18.4 mM MNP (pH 7.4) in the absence of H_2O_2 yields only native Mb peptides. (B) Reaction of metMb with 2x H_2O_2 and 18.4 mM MNP (pH 7.4) followed by ascorbate reduction gives rise to ~30% peptide 103-118 with an increased mass of 71 Da (*) (*m/z* 1955) and to peptides 32-45 and 32-47 with decreased masses of 17 Da (circled asterisk) (*m/z* 1645 and 1919). (C) Iodination of Mb prior to reaction with 2x H_2O_2 and 18.4 mM MNP (pH 7.4) results in loss of MNP-modified peptide 103-118 (*), and MNP-modified peptides 32-45 and 32-47 (circled asterisk) appear slightly more prominent. The new peaks above scan number 1170 contain iodinated peptide 103-118. (D) Same reaction as in (B) carried out at pH 5.0. Approximately 30% of peptide 64-77 has increased in mass by 40 Da (▾) (*m/z* 1419), and R-MNP-modified peptides 103-118 (*), and 32-45 and 32-47 (circled asterisk) are also seen in the map.

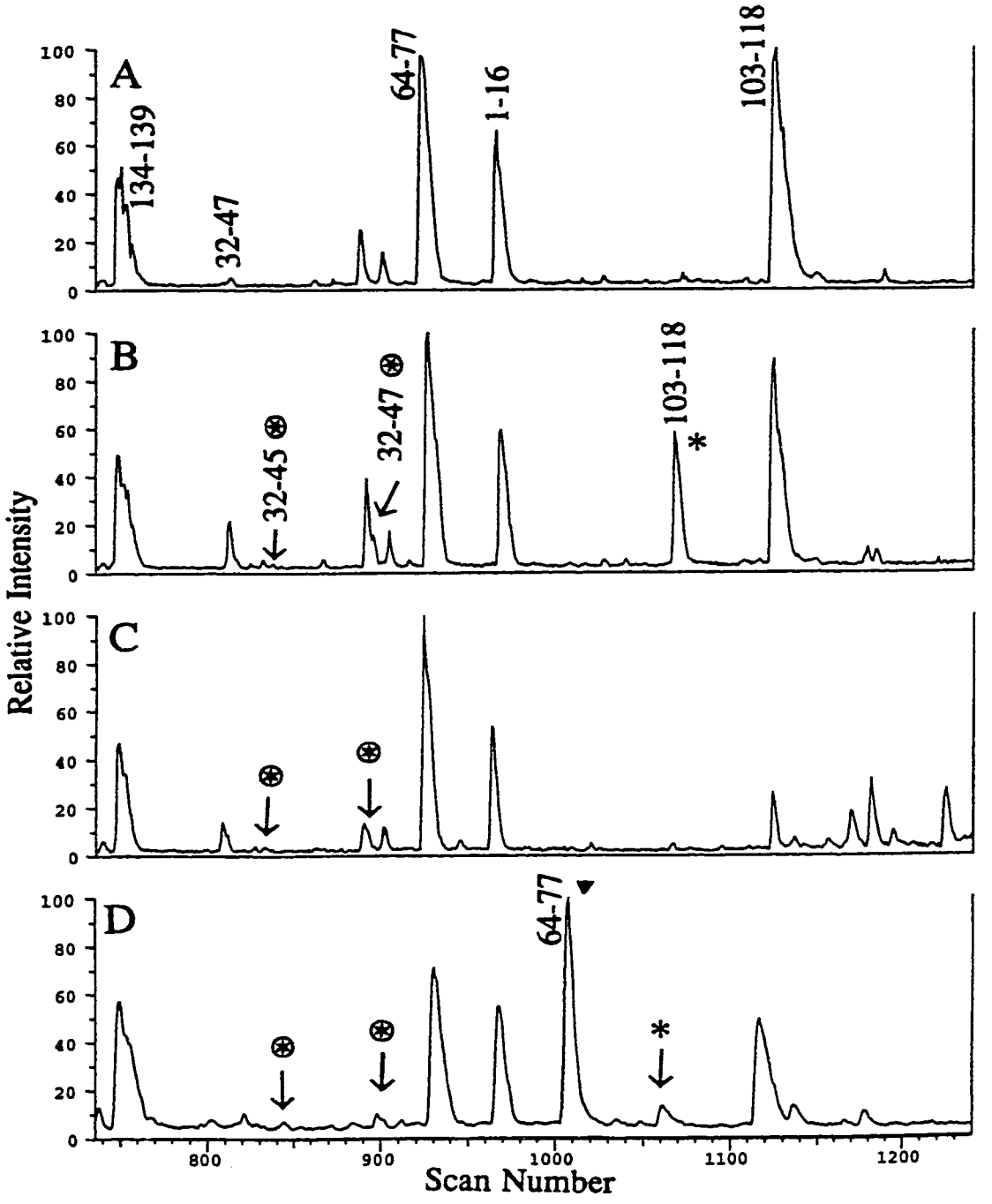
A
B
C
D
134-139
32-47
64-77
1-16
103-118
32-45 ⊛
32-47 ⊛
103-118
*
64-77
Relative Intensity
Scan Number
100
80
60
40
20
0
800
900
1000
1100
1200

Figure 5.4 CID sequencing of MNP-modified peptide 103-118. The peptide was purified from the tryptic digest, lyophilized, resuspended in 1:1 methanol/H_2O + 0.05% acetic acid, and directly infused at ~1.5 µL/min into the ES source of a Finnigan TSQ 7000 triple quadrupole MS. The +3 ion at *m/z* 653.2 was selected with Q1 and fragmented by CID in the collision cell (Q2) with Ar gas at 2.5 mTorr and a collision offset voltage of -22 eV (laboratory frame of reference). The fragment ions were analyzed in Q3. Masses of the major a, b, and $y/_2$ (doubly-charged) fragment ions are given. The R-MNP-Tyr moiety is cleaved during CID, and fragment ions containing the altered Tyr103 residue (+15 Da) are denoted by a double dagger.

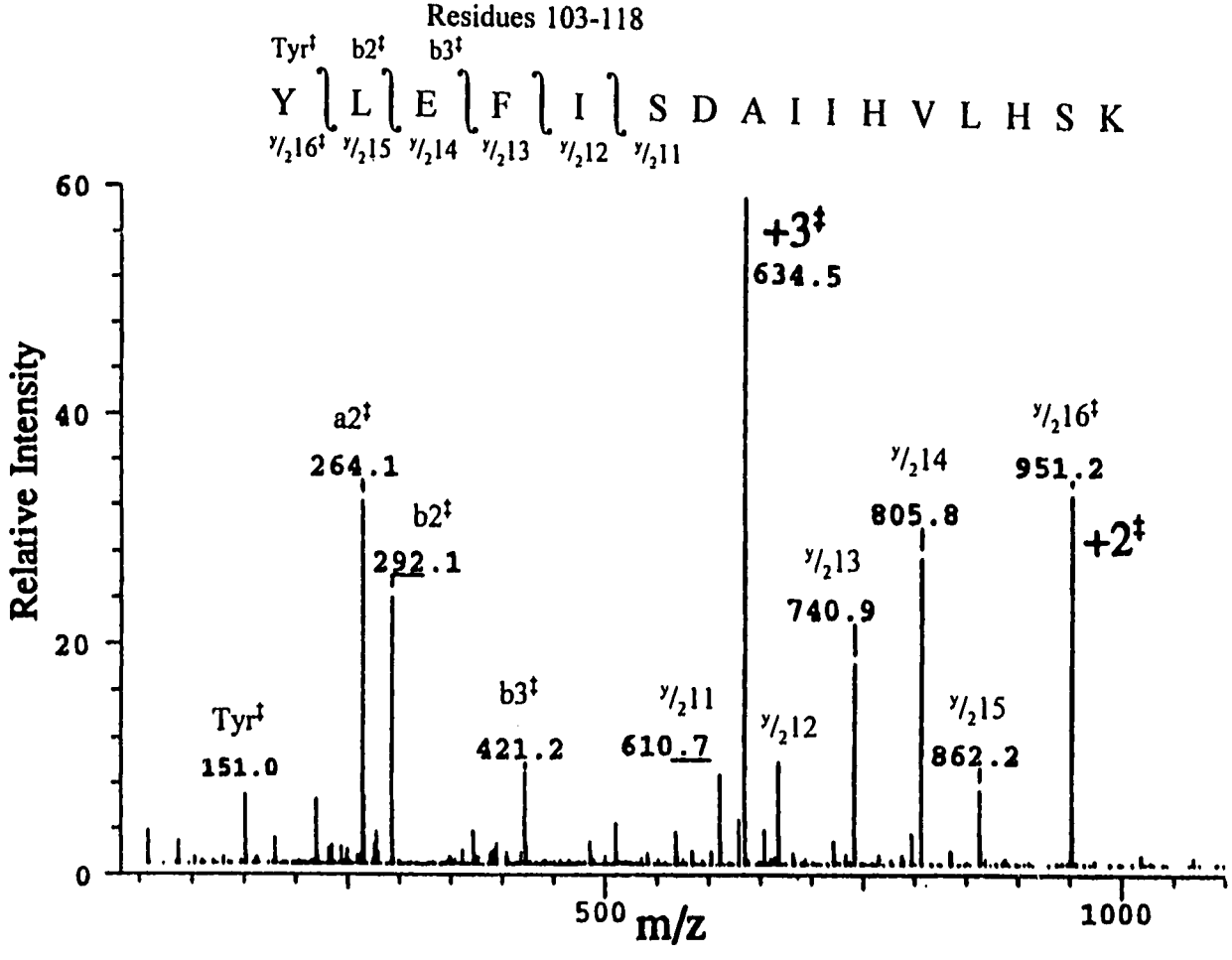
Residues 103-118
Tyr‡ b2‡ b3‡
Y L E F I S D A I I H V L H S K
y/2 16‡ y/2 15 y/2 14 y/2 13 y/2 12 y/2 11
Relative Intensity
60
40
20
0
+3‡
634.5
a2‡
264.1
b2‡
292.1
y/2 16‡
951.2
y/2 14
805.8
+2‡
y/2 13
740.9
Tyr‡
151.0
b3‡
421.2
y/2 11
610.7
y/2 12
y/2 15
862.2
500
m/z
1000

of one of the resulting peptides (residues 42-47) showed that residue 42 (Lys) was 17 Da lighter than in untreated Mb (Figure 5.5).

Iodination of Mb at Tyr103 was reported to alter the radical signal observed by EPR.[16] Hence, following iodination[22] the species trapped by MNP were determined by peptide mass mapping (Figure 5.3C). A radical was no longer found to be trapped at Tyr103, but peaks containing modified peptides 32-45 and 32-47 were consistently 30-40% more abundant in the iodinated samples. Figure 5.3C shows that Tyr103 was singly and doubly iodinated with little unmodified Tyr103 remaining.

MNP spin trapping experiments were also carried out at pH 5.0, since the radical formed in the $MbFe^{III}/H_2O_2$ reaction exhibited different EPR and absorption spectra at acidic pH values.[24,25] Modification of Tyr103 and Lys42 was again observed, and an additional intense peak (▾) appeared in the map (Figure 5.3D), which was shown to be peptide 64-77 with an increased mass of +40 Da by CID sequencing. The high intensity of the modified peptide 64-77 was due to its efficient charging by ESI-MS as compared to the unmodified peptides since a UV-vis trace of the peptide map (data not shown) showed that the modified 14-residue peptide 64-77 (▾) had similar 210-nm absorbance as the modified 16-residue peptide 103-118 (*). CID sequencing was inconclusive, so peptide 64-77 was further digested with pepsin, and CID of peptide 64-69 unambiguously demonstrated that His64 was modified (Figure 5.6). The modified His64 peptide was not observed when either MNP or acid/acetone extraction was omitted from the reaction procedure.

In addition, the $MbFe^{III}/H_2O_2$/MNP reaction was carried out in the presence of 0.8

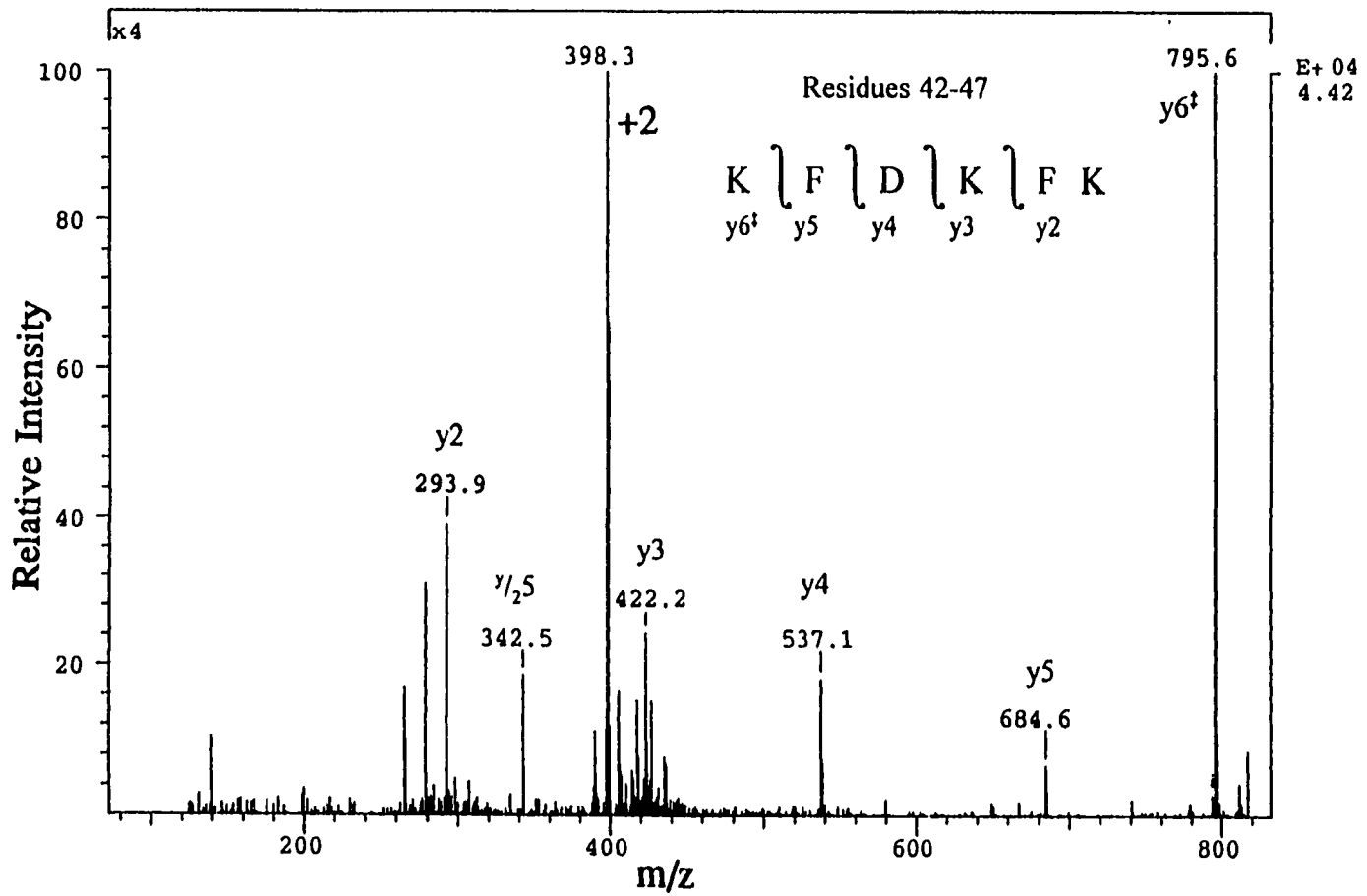

Figure 5.5 CID sequencing R-MNP-modified V8 peptide 42-47. The R-MNP-modified tryptic peptide 32-47 (1919 Da) was digested with V8 protease in 50 mM NH_4HCO_3 (pH 7.8) at 25 °C for 4 h. CID was performed on the SSQ as described in Figure 5.4.

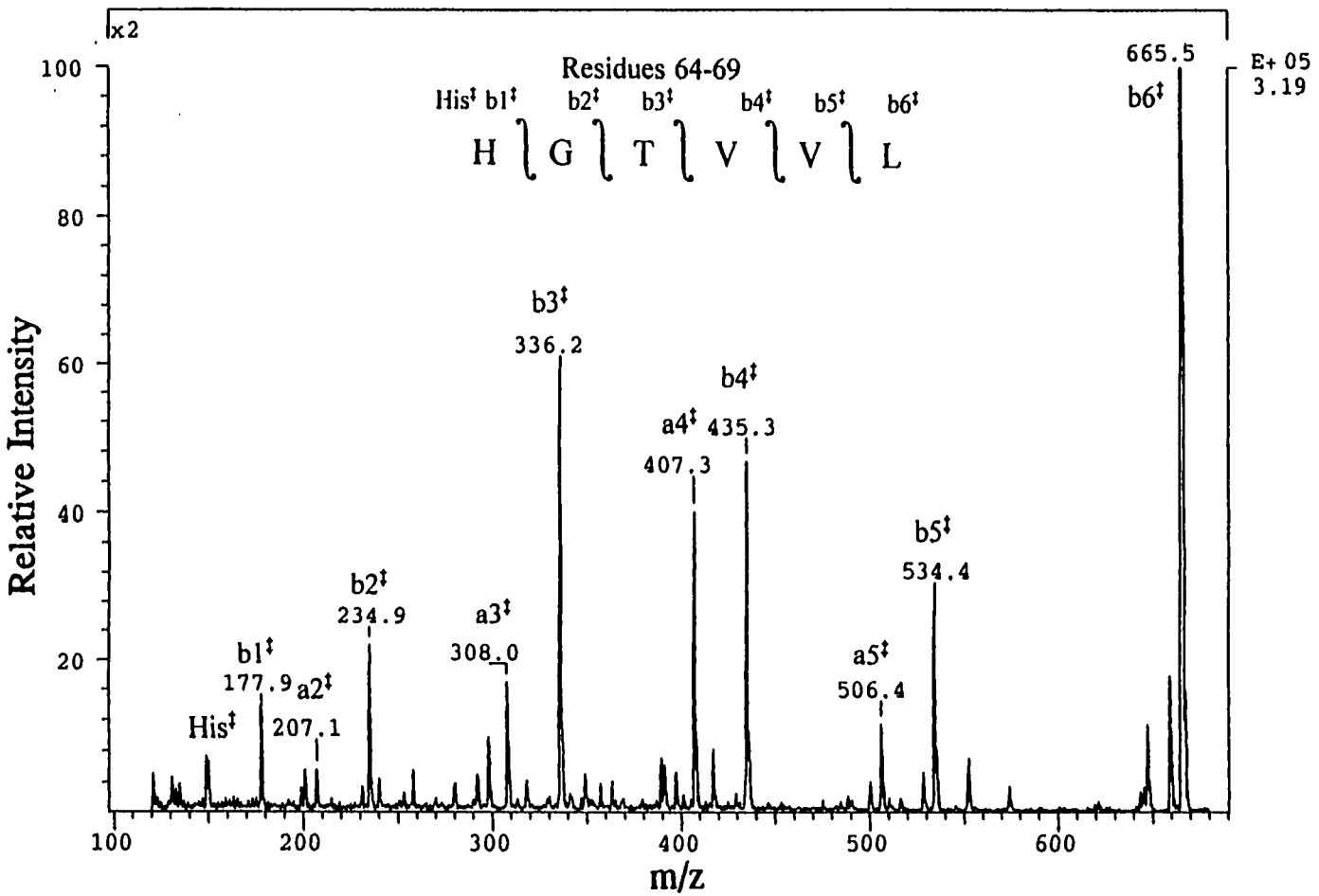

Figure 5.6 CID sequencing of R-MNP-modified peptic peptide 64-69. The R-MNP-modified tryptic peptide 64-77 (1419 Da) was digested with pepsin in 3 mM HCl (~ pH 2) at 25 °C for 4 h. CID was performed on the SSQ as described in Figure 5.4.

M guanidine-HCl (G-HCl) at pH 7.4. The unfolding of Mb in different concentration of G-HCl, a chaotropic agent, was monitored by steady-state fluorescence (Figure 5.7). Fluorescence is quenched in folded Mb by the heme, and Mb unfolding results in an increase in fluorescence.[26,27] The fluorescence-monitored unfolding curve of $MbFe^{III}$ in G-HCl relative to apoMb has an unfolding midpoint at 1.6 M G-HCl. From Figure 5.7, $MbFe^{III}$ is expected to have a slightly looser conformation in the presence of 0.8 M G-HCl than in 0 M G-HCl. Thus, any buried radicals should be more accessible to the MNP spin trap in 0.8 M G-HCl. Upon tryptic digestion of the MNP-Mb sample formed in G-HCl, no modified peptides were found aside from the Tyr103- and Lys42- containing peptides. Therefore, it is possible that loosening of the globin was insufficient at 0.8 M G-HCl to allow MNP to form spin adducts with buried radicals, or G-HCl quenched some radicals, or the only major sites of radical formation are those trapped in both 0 and 0.8 M G-HCl.

The chemical nature of the R-MNP-Mb adducts is of interest. The mass increase in the MNP-Mb spin adducts, as determined by MS of the undigested samples, was +86 Da, which corresponds to the mass of the MNP monomer ($C_4H_{10}NO$). However, the modified tryptic peptides isolated from the R-MNP-Mb samples exhibited mass changes that depended upon the residues modified. Since MNP is primarily a carbon-based spin trap,[8] structures for the reduced adducts can be proposed based on (1) the carbon likely to be the site of radical formation and (2) the observed mass change in the modified peptide. The mass increase of the Tyr103 adduct is +71 Da, which corresponds to the MNP spin adduct (86 Da) minus 16 Da. Loss of the nitroxide oxygen from MNP would

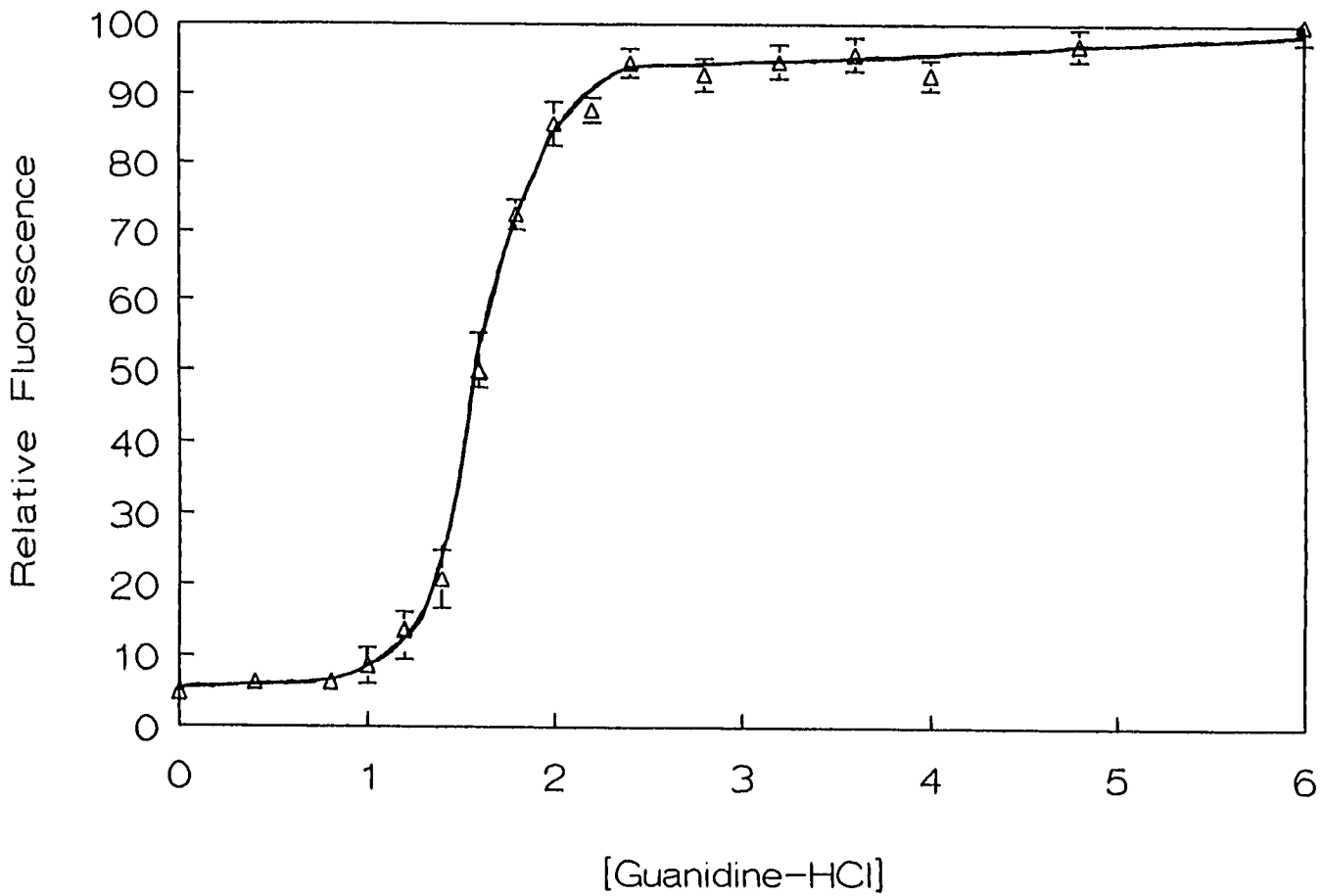

Figure 5.7 Steady-state protein fluorescence of $MbFe^{III}$ at different concentrations of G-HCl in 100 mM Pi buffer (pH 7.4) at 25 °C. The excitation and emission wavelengths were 280 and 350 nm, and the slits 5 nm.

give the proposed structure shown in Figure 5.8A. Adduct formation at Lys42 results in a mass loss of 17 Da. A possible explanation for this is that the spin adduct was attached to carbon-6 in Lys42 and upon reduction, the MNP adduct and the terminal amino group dissociate (Figure 5.8B). The mass of the adduct attached to His64 was +40 Da. Since formation of a stable adduct on His64 required exposure to acetone at low pH, it is proposed that the His64-MNP adduct reacts with acetone to give the product shown in Figure 5.8C. If MNP modification at a given amino acid residue consistently results in the same mass change, identification of modified residues would be simplified since peptide mass mapping would allow the modified sites to be readily recognized, and obviate the need for sequencing in most cases.

The $MbFe^{III}/H_2O_2$ reaction is >99% complete within 20 s in the presence of 10x (2 mM) peroxide ($k \approx 200\ M^{-1}s^{-1}$),[28] but the maximum MNP-Mb spin adduct yield estimated from the MS data was ~50% at pH 7.4. Extrapolation of the EPR signal intensity to time zero indicated that the radical concentration was ~50% that of the globin,[29] suggesting that MNP efficiently traps the EPR-detectable protein-based radicals generated in the $MbFe^{III}/H_2O_2$ reaction. Figure 5.9 shows the location of the radical species identified by LC-MS. Tyr103 is in van der Waals contact with the heme edge and solvent exposed, so trapping a radical on Tyr103 should be facile. Lys42 is also solvent exposed and adjacent to Tyr103. A note of interest concerning Tyr103 and Lys42 is that although these residues are conserved in virtually all vertebrate Mbs,[30] their mutation has shown to have no effect on either O_2 or CO binding in the ferrous protein.[31] Efficient spin trapping at the distal His64 at pH 5.0, which gives rise to the intense peak (▾) in

Figure 5.8 Proposed structures for the (A) Tyr103, (B) Lys42 and (C) His64 MNP spin adducts and their reduced forms detected by LC-MS.

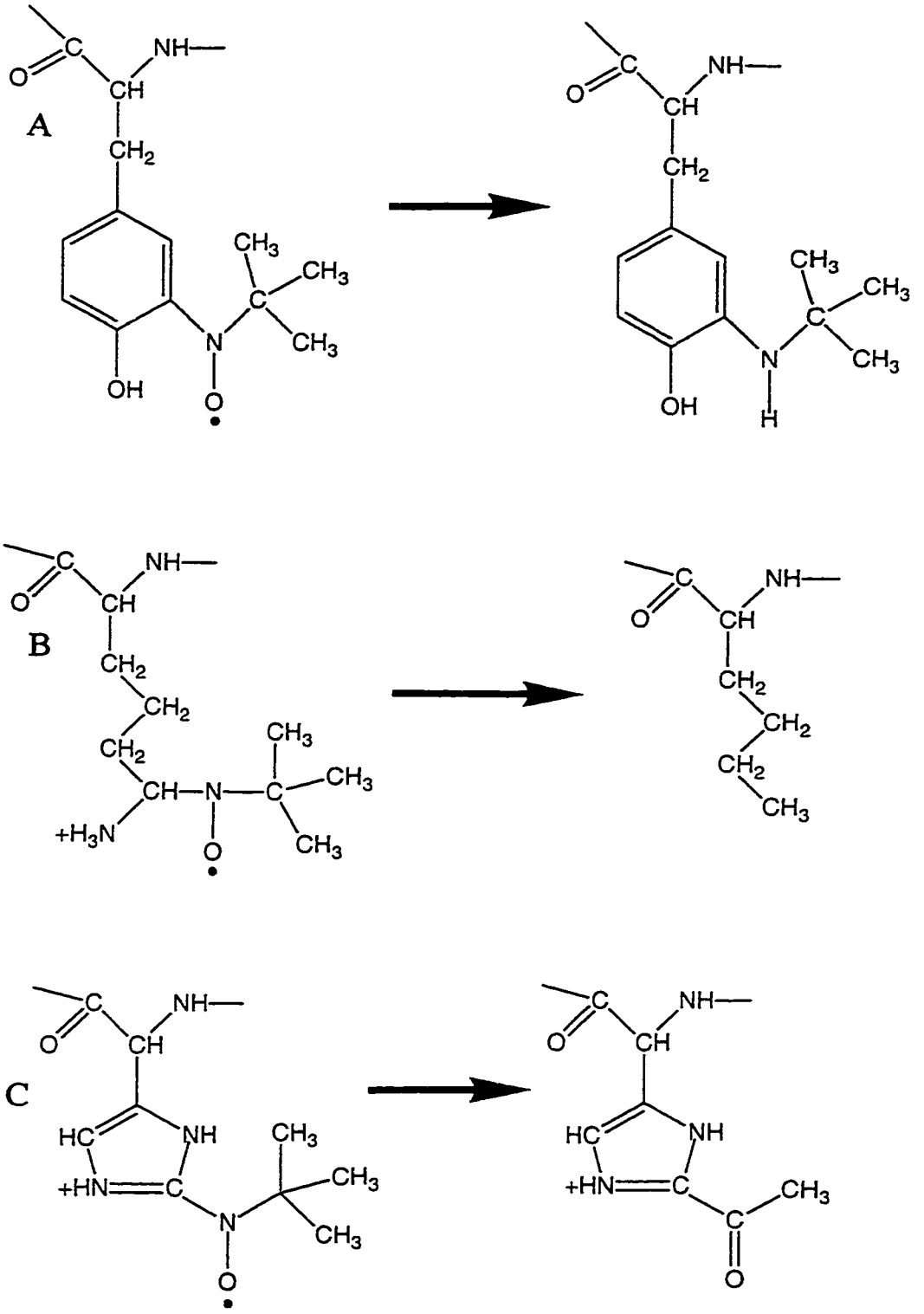
A
B
C

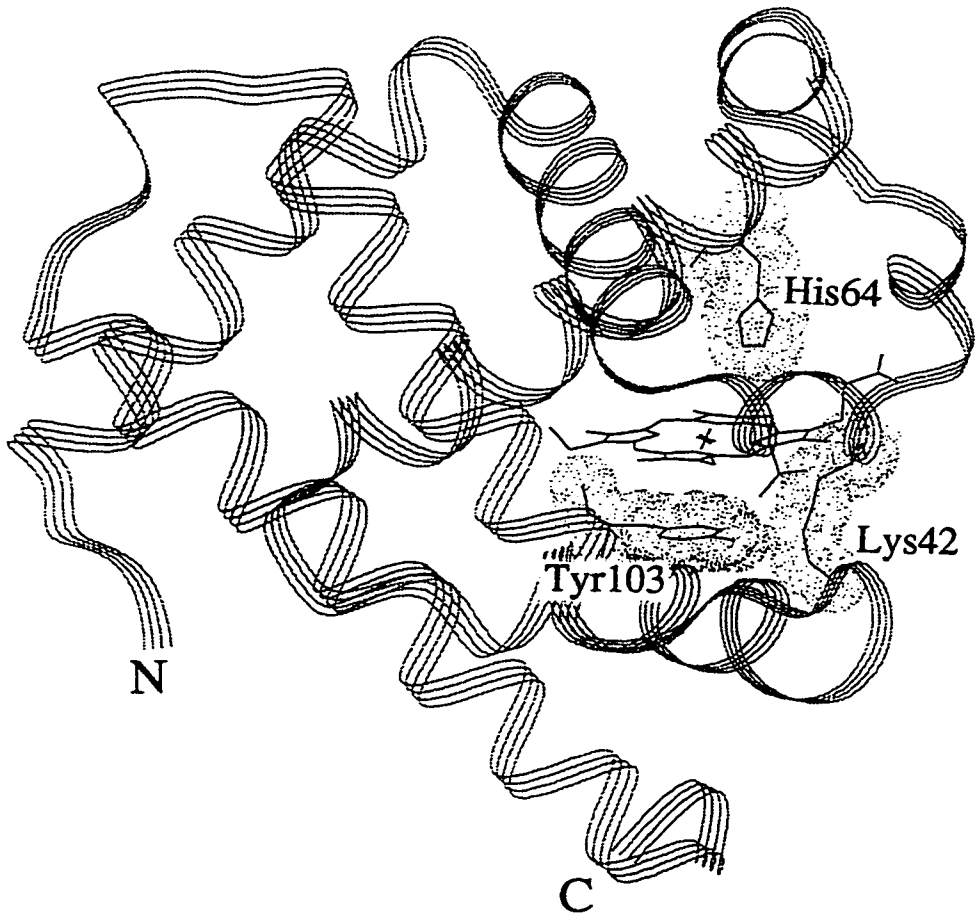

Figure 5.9 Sites of MNP spin adduct formation (depicted by their van der Waals radii) in horse heart Mb and the heme superimposed on the Cα backbone.[32] Tyr103 and Lys42, the sites of radical trapping at pH 7.4, are solvent exposed and form a triangle with the heme edge. The distal His64 above the heme is a site of radical trapping at pH 5.0.

Figure 5.3D, may be due to opening of the heme pocket at low pH,[33] allowing MNP better access to the distal cavity.

The present trapping results are consistent with the assignment of the EPR signals to radicals centered on Tyr103 and additional residues.[16] Furthermore, radical formation on non-Tyr residues has been confirmed, since sperm whale $MbFe^{III}$ mutants devoid of Tyr exhibit EPR signals arising from protein-based radicals on oxidation with H_2O_2.[17] The LC-MS data in Figure 5.3 are, however, inconsistent with the proposed[15] MNP spin adduct formation at Trp7 and/or Trp14 of horse heart Mb, since peptide 1-16 is not modified under the conditions examined here. More recent analysis of the EPR data reveal that MNP spin adducts are more likely formed on Tyr residues in both Mb and cytochrome c.[34] It has also been proposed that Tyr103 is crosslinked to the heme in H_2O_2-oxidized horse heart $MbFe^{III}$,[21] as discussed in Chapter 2.

Whole-protein EPR data acquired in the presence or absence of spin traps cannot provide unambiguous assignments of protein radical signals.[15,16,17] However, conversion of the spin adducts to more stable diamagnetic species permits peptide mass mapping and the identification of each of the spin-trapped species. A further advantage of coupling spin trapping with LC-MS is that picomole quantities of sample can be analyzed. With the biological roles of redox-active amino acid residues becoming more apparent,[18,19] the identification of protein-based radicals is of increased importance and interest.

References

1. Pedersen, J.Z.; Finazzi-Agrò, A. *FEBS* **1993**, *325*, 53.
2. Sjöberg, B.M.; Reichard, P.; Gräslund, A.; Ehrenberg, A. *J. Biol. Chem.* **1977**, *252*, 536.
3. Stubbe, J. *J. Biol. Chem.* **1990**, *265*, 5329.
4. Smith, W.L.; Marnett, L.J. *Biochim. Biophys. Acta* **1991**, *1083*, 1-17.
5. McNamara, J.O.; Fridovich, I. *Nature* **1993**, *362*, 20.
6. Hanan, T.; Shaklai, N. *Eur. J. Biochem.* **1995**, *233*, 930.
7. Rosen, D.R.; Siddique, T.; Patterson, D.; Figlewicz, D.A.;Brown, R.H.Jr. *Nature* **1993**, *362*, 59.
8. Perkins, M.J. *Adv. Phys. Org. Chem.* **1980**, *17*, 1.
9. Kominami, S.; Rokushika, S.; Hatano, H. *Int. J. Radiat. Biol.* **1976**, *30*, 525.
10. Moriya, F.;Iguchi, N.; Makino, K. Rokushika, S.;Hatano, H. *Can. J. Chem.* **1984**, *62*, 2206-2216.
11. Makino, K.;Moriya, F.;Hatano, Hiroyuki, H. *J. Chromatogr.* **1985**, *332*, 71-106.
12. Nozaki, K.; Naito, A.; Hatano, H.;Okazaki, S. *J. Chem. Soc. Perkin Trans.* **1990**, 113-119.
13. Iwahashi, H.;Albro, P.W.;McGown, S.R.;Tomer, K.B.;Mason, R.P. *Arch. Biochem. Biophys.* **1991**, *285*, 172-180.
14. Scholes, C.P.; Liu, Y.; Fishel, L.A.; Farnum, M.F.; Mauro, J.M.; Kraut, J. *Isr. J. Chem.* **1989**, *29*, 85.
15. Gunther, M.R.; Kelman, D.J.; Corbett, J.T.; Mason, R.P. *J. Biol. Chem.* **1995**, *270*, 16075.

16. Davies, M.J. *Biochim. Biophys. Acta* **1991**, *1077*, 86.

17. Wilks, A.; Ortiz de Montellano, P.R. *J. Biol. Chem.* **1992**, *267*, 8827.

18. Poulos, T.L.; Fenna, R.E. In *Metal ions in Biological Systems: Vol. 30, Metalloenzymes Involving Amino Acid-Residue and Related Radicals*; Sigel, H., Sigel, A., Eds.; Marcel Dekker: New York, 1994, pp 25-75.

19. Sundaresan, M.; Yu, Z.-X.; Ferrans, V.J.; Irani, K.; Finkel, T. *Science* **1995**, *270*, 296.

20. King, N.K.; Looney, F.D.; Winfield, M.E. *Biochim. Biophys. Acta* **1967**, *133*, 65.

21. Cantalano, C.E.; Choe, Y.S.; Ortiz de Montellano, P.R. *J. Biol. Chem.* **1989**, *264*, 10534.

22. Parker, C.W. *Methods Enzymol.* **1990**, *182*, 729.

23. Biemann, K. *Method Enzymol.* **1990**, *193*, 455.

24. King, N.K.; Winfield, M.E. *Aust. J. Biol. Sci.* **1966**, *19*, 211.

25. Kelso, N.; Looney, F.D.; Winfield, M.E. *Biochim. Biophys. Acta* **1967**, *133*, 65.

26. Tsong, T.W. *J. Biol. Chem.* **1974**, *249*, 1988.

27. Myer, Y.P.; MacDonald, L.H.; Verma, B.C.; Pande, A. *Biochemistry* **1980**, *19*, 199.

28. Yonetani, T.; Scheyer, H. *J. Biol. Chem.* **1967**, *242*, 1974.

29. King, N.K.; Winfield, M.E. *J. Biol. Chem.* **1963**, *238*, 1520.

30. Twenty sequences in the Swiss Protein Data Bank were examined.

31. Huang, X.; Boxer, S.G. *Struc. Biol.* **1994**, *1*, 226.

32. X-ray coordinates: Evans, S.V.; Brayer, G.D. *J. Mol. Biol.* **1990**, *213*, 885.

33. Tian, W.D.; Sage, J.T.; Champion, P.M. *J. Mol. Biol.* **1993**, *233*, 155.

34. Barr, D.P.; Gunther, M.R.; Deterding, L.J.; Tomer, K.B.; Mason, R.P. *J. Biol. Chem.* **1996**, *271*, 15498.

6.0 Conclusions and Suggestions for Further Study

Chapter 2

The stoichiometry of the reaction of $MbFe^{III}$ with H_2O_2 showed that ~2 molar equivalents of H_2O_2 are needed for complete formation of $MbFe^{IV}$=O at pH 7.0. Analysis of the $MbFe^{III}/H_2O_2$ reaction (1:10 molar equivalents) by two concurrent first-order processes gives a bimolecular rate constant of ~195 $M^{-1}s^{-1}$ for the Fe^{IV}=O forming reaction, and a slower reaction was attributed to H_2O_2-linked oxidation which causes porphyrin oxidation and/or heme dissociation from the globin. The rate constants for the $MbFe^{IV}$=O forming reaction were found to be unchanged between pH 7.0 and 5.4 (Table 2.2).

Oxidative damage in Mb on exposure to H_2O_2 was shown to be minimal when the $MbFe^{III}/H_2O_2$ reaction products were reduced with ascorbate (sample 1). This indicates that Fe^{IV}=O formation and decay of the protein-based radicals do not cause chemical modification to Mb. However, significant amounts of chemically modified heme and globin were present following Fe^{IV}=O autoreduction (sample 2 and 3), especially at low pH. The autoreduction process of fully formed $MbFe^{IV}$=O (Section 2.4.9) was found to be pH dependent with a faster rate of $MbFe^{IV}$=O autoreduction observed in samples still containing $MbFe^{III}$. However, for the purpose of electron transfer studies the half-life of $MbFe^{IV}$=O (Table 2.6) is sufficiently long to probe its redox reactivity when $MbFe^{III}$ is fully converted to $MbFe^{IV}$=O.

ESI-MS analysis of samples 2 and 3 revealed that although unmodified globin was the major species in these samples, minor species, corresponding to globin (16950 Da) + oxygen (16 Da) and globin (16950 Da) + heme (616 Da) + oxygen (16 Da), were also

present. Since the MS analysis was performed under acidic conditions where the heme dissociates from the polypeptide, it is reasonable to assume that the heme is crosslinked to the globin in the 17583-Da species. However, tryptic digestion did not reveal the sites of modification since the crosslinked species were not susceptible to tryptic attack.

The $MbFe^{III}/H_2O_2$ reaction was found to consume 2 molar equivalents of H_2O_2 at the same rate as $MbFe^{IV}=O$ formation at neutral pH without the release of O_2. Hence, the side reactions on the globin must account for consumption of some of the H_2O_2 oxidizing equivalents by Mb.

The FTIR investigations of the amide I' and II bands reveal little secondary structure changes in Mb under the conditions studied. The pH-dependent movement of His64, shown by the change in $\upsilon(CO)$ for $MbFe^{II}$-CO, is attributed to a localized conformational change.

Chapters 3 and 4

Intramolecular $Fe^{IV}=O$ reduction by Ru^{II} in a_4RuLHis48Mb was found to be dependent on protonation of a group on the protein that was assigned to distal His64. The ET competent species a_4LRu^{II}—$H^+MbFe^{IV}=O$ is assumed to be an open-pocket conformation of Mb with the distal His64 protonated.

The rate limiting step in $MbFe^{IV}=O$ intramolecular reduction by surface-bound a_5Ru^{II}, a_4PyrRu^{II} and a_4IsnRu^{II} (k_2) was analyzed using the Marcus equation. Assuming $k_2 = k_{ET}$, the reorganization energy (λ) for the ET step results in a $\lambda = 1.8$ eV for $Ru^{II} \rightarrow Fe^{IV}=O$ ET in the a_4IsnRu and a_4PyrRu derivatives, but $\lambda = 2.1$ eV for the a_5Ru

derivative. The much larger value in the latter suggests that ET is strongly gated at the higher driving force. The difference between the λ = 1.8 eV for Fe^{IV}=O reduction vs λ 1.48 eV reported for the intramolecular ET (a_5Ru^{II}His48—Fe^{III}-OH_2 $\rightleftharpoons$ a_5Ru^{III}His48—Fe^{II} + H_2O) in SWMb is attributed to the large Fe-O bond length change (0.2 Å) observed by EXAFS on going from the oxene to the aquo ligand, as well as the spin change on reduction of LS Fe^{IV}=O (S = 1) to HS Fe^{III}-OH_2 ($MbFe^{II}$ is also HS).

The generation of a negatively-charged oxo ligand (Fe^{III}-O^{2-}) in the hydrophobic heme pocket of Mb is likely to be highly unfavorable; hence, the oxene ligand is expected to be partially protonated in the precursor complex for ET. We conclude that a conformational change is required to generate a Mb species with a H-bond donor to the oxene ligand, which leads to conformational gating of ET at the higher driving force in the a_5Ru derivatives.

Chapter 5

The identification of the sites of protein-based radical formation were carried out using spin trapping and LC-MS techniques. Collisionally induced dissociation of MNP modified peptides was effective in determining that the radicals formed in the $MbFe^{III}/H_2O_2$ reaction at neutral pH are Tyr103 and Lys42; at pH 5 MNP trapped an additional radical on His64. The observed mass change of the peptides bearing the reduced-MNP-adducts was found to vary depending on which residue was modified. Hence, the mass of the a MNP-adduct could be very useful in identifying the specific amino acid residue modified if the changes observed here are consistently observed for

other proteins.

A note of interest concerning Tyr103 and Lys42 is that these residues are conserved in virtually all vertebrate Mbs but their mutation has shown to have no effect on O_2 or CO binding in the ferrous protein. This may indicate a specific role (perhaps related to radical formation) for these residues *in vivo*.

Suggestions for Further Study

1. Analysis of the intramolecular ET rates in a_4RuLHis48Mb at high salt concentration could be performed since these conditions have been shown by NMR to disrupt the H-bond between Lys45 and a heme propionate.[1] This H-bond has been shown by site-directed mutagenesis to be involved in the movement of His64, and is also part of the strongly-coupled ET pathway between His48 and the heme (Figure 3.1)

2. ET studies in a_4LRuHis48Mb could also be performed in the Mb (L89D) mutant which forms a strong H-bond with proximal His93. EXAFS studies have shown that this mutant has porphyrin Fe-N bond lengths similar to heme peroxidases (~1.9 Å) and has mainly a 5-coordinate heme.[2] ET studies in this mutant would reveal the effects of strong H-bonding to the proximal histidine on the Fe^{IV}=O redox activity.

3. CCP mutants could be engineered with surface histidines in close proximity to the heme to allow rapid $Ru^{II} \rightarrow Fe^{IV}$=O ET to be examined, and thereby determine the controlling factors in Fe^{IV}=O reduction in CCP.

4. Investigations could be carried out on protein-radical formation in the $MbFe^{III}/H_2O_2$

reaction with Mb mutants that lack the Tyr103 and Lys42 residues. For example, the Mb (Y103F/K102Q) mutant has been prepared previously.[3]

5. Spin trapping of the $MbFe^{III}/H_2O_2$ reaction products could be performed in the presence of meclofenamic acid or adriamycin. LC-MS investigation of the reaction products may reveal how these drugs interact with Mb to stimulate lipid oxidation.[4,5]

References

1. Morishima, I.; Iizuka, T. *Biochim. Biophys. Acta* **1975**, *386*, 542.
2. Sinclair, R.; Hallam, S.; Chen, M.; Chance, B.; Powers, L. *Biochemistry* **1996**, *35*, 15120.
3. Wilks, A.; Ortiz de Montellano, P.R. *J. Biol. Chem.* **1992**, *267*, 8827.
4. Evans, P.J.; Akanmu, D.; Halliwel, B. *Biochem. Pharmacol.* **1994**, *48*, 2173.
5. Trost, L.C.; Wallace, K.B. *Biochem. Biophys. Res. Comm.***1994**, *204*, 30-37.